1993

Synthesis, Isolation, Characterization and Homogeneous Catalytic Reactions of Racemic- And Meso-Metal Binucleating Tetraphosphine Complexes.

Booker Washington ochieng Juma
Louisiana State University and Agricultural & Mechanical College

Order Number 9401542

Synthesis, isolation, characterization and homogeneous catalytic reactions of racemic- and meso-metal binucleating tetraphosphine complexes

Juma, Booker Washington Ochieng, Ph.D.

The Louisiana State University and Agricultural and Mechanical Col., 1993

U·M·I
300 N. Zeeb Rd.
Ann Arbor, MI 48106

SYNTHESIS, ISOLATION, CHARACTERIZATION AND HOMOGENEOUS CATALYTIC REACTIONS OF RACEMIC- AND MESO-METAL BINUCLEATING TETRAPHOSPHINE COMPLEXES

A Dissertation

Submitted to the Graduate Faculty of the
Louisiana State University and
Agricultural and Mechanical College
in partial fulfillment of the
requirements for the degree of
Doctor of Philosophy

in

The Department of Chemistry

by
Booker Washington Ochieng Juma
B.Sc. (1st Class Honors) University of Nairobi, Kenya, 1986
May, 1993

To my father and mother.

Acknowledgments

I thank Dr. George G. Stanley for his leadership, teaching, support and encouragement. His friendship, patience, concern and assistance when needed made working enjoyable and rewarding.

I thank all the committee members for their time spent reading this dissertation: Dr. Frank K. Cartlege, Dr. Les Butler, Dr. Andrew Maverick, and Dr. Mark McLaughlin and Dr. Ralph Pike. I also thank Dr. Nikolaus Fischer, Dr. Richard Gandour, Dr. Steven Watkins, and Dr. Robert Hammer for their helpful suggestions and discussions.

In addition, I would like to thank Dr. Frank R. Fronczek who did all the X-ray structural studies; Mr. Marcus Nauman for his assistance on NMR spectroscopy; Spencer Train for technical assistance in catalytic runs; Melanie Broussard whose chromatographic skills proved invaluable; Dr. Weijun Peng and Dr. Kris Tesh for helpful suggestions and interesting discussions; Cindy Lamberty, Donna Johnson, and Pia Alburquerque for the many "helping hands" given.

I would further like to thank Dr. & Mrs. M. Clyde Day Jr. for their friendship and unwavering concern and support as my "Host Family"; Mr. & Mrs. Michael Fuller for their friendship; my parents, brothers and sisters for their love, unfailing confidence and loyalty during my study leave.

Special thanks to my wife Linda for her unconditional love, unselfish devotion, practical help and patience throughout the endeavor.

I wish to acknowledge financial support from The Department of Chemistry, Louisiana State University; Hoechst-Celanese Corporation; The National Science Foundation; and the Louisiana Educational Quality Support Fund through the span of this research.

Moi University, Kenya, gave me study leave to undertake this work.

Table of Contents

List of Tables

List of Figures

List of Schemes

List of Abbreviations

AIBN	2,2'-Azobis(isobutyronitrile)
CH_2Cl_2	dichloromethane
d	doublet (NMR)
dd	doublet of doublets (NMR)
DMF	dimethylformaldehyde
et,ph-P4	$Et_2PCH_2CH_2P(Ph)CH_2P(Ph)CH_2CH_2PEt_2$
Et	ethyl, $-CH_2CH_3$
EtOH	ethanol
Hz	Hertz, sec^{-1}
HPLC	high performance liquid chromatography
I.D.	internal diameter (HPLC)
nbd	norbornadiene
m	multiplet (NMR)
NMR	nuclear magnetic resonance
Ph	Phenyl, $-C_6H_5$
rpm	revolutions per minute
s	singlet (NMR)
t	triplet (NMR)
THF	tetrahydrofuran

Abstract

The tetraphosphine ligand $Et_2PCH_2CH_2P(Ph)CH_2P(Ph)CH_2CH_2PEt_2$ (to be referred to as et,ph-P4) was designed to both bridge and chelate two metal centers and hold them in general proximity to investigate bimetallic cooperativity in homogeneous catalysis. The internal phosphines of et,ph-P4 are chiral, thereby generating a pair of diastereomers: the *racemic*, and the *meso*. These are produced in approximately equal amounts from the ligand synthesis.

This project has concentrated on the separation and isolation of diastereomerically pure forms of et,ph-P4 to determine individual hydroformylation catalytic activity of each bimetallic complex. Complexes of $Ni(NCS)_2$ with et,ph-P4 were effective in accomplishing this separation by utilizing solubility differences between the two diastereomeric nickel complexes.

The reaction of one equivalent of $Ni(NCS)_2$ with et,ph-P4 in EtOH precipitates pure *meso*-[Ni(NCS)(η^3-et,ph-P4)](NCS) leaving *racemic*-[Ni(NCS)(η^3-et,ph-P4)](NCS) in solution. The *meso*-[Ni(NCS)(η^3-et,ph-P4)](NCS) readily crystallizes in $CHCl_3$/EtOH solution. Two equivalents of $Ni(NCS)_2$ reacts with et,ph-P4 to produce dimeric *racemic*- and *meso*-$Ni_2(NCS)_4$(et,ph-P4). The pure *racemic*- and *meso*-et,ph-P4 ligands were decomplexed from the metal complexes by refluxing with excess NaCN in a heptane/water solvent mixture.

Pure *meso* et,ph-P4 converts to a mixture of both diastereomers when heated close to 150 °C for 20 minutes. This can provide additional yields for the *racemic* diastereomer if desired.

Catalytic results for the hydroformylation of 1-hexene using the bimetallic rhodium complexes *racemic*- and *meso*-$[Rh_2(nbd)_2$(et,ph-P4)$](BF_4)_2$ support our molecular modeling predictions that the *racemic*-$[Rh_2(nbd)_2$(et,ph-P4)$](BF_4)_2$ catalyst system is the more active species. Molecular modeling studies further indicated a distinct energy difference between the two faces of a pro-chiral alkene coordinating to

the (*S,S*) or (*R,R*)-bimetallic catalyst. The *racemic*- et,ph-P4 was then separated into individual (*S,S*) and (*R,R*)-et,ph-P4 enantiomers by chiral-column HPLC. Chiral rhodium catalysts of each enantiomer afforded asymmetric hydroformylation of vinyl acetate to give the appropriate optically active 2-acetoxypropanal with high enantiomeric excess and regioselectivity. Both chiral catalysts have been isolated and each gives enantioselective hydroformylation of vinyl acetate to the opposite chiral product.

Model reaction of $Ni(NCS)_2$ with crude $Et_2PCH_2CH_2PPh_2$ in EtOH yields two products, $Ni(NCS)_2(Et_2PCH_2CH_2PPh_2)$ and $Ni(NCS)_2[Ph_2PCH_2CH_2P(Et)$-$CH_2CH_2PPh_2]$ which have different solubilities in heptane, acetone and acetonitrile. X-ray crystal structure analyses of $Ni(NCS)_2(Et_2PCH_2CH_2PPh_2)$, $Ni(NCS)_2[Ph_2PCH_2CH_2P(Et)CH_2CH_2PPh_2]$, *meso*-$[Ni(NCS)(\eta^3$-et,ph-P4)](NCS), *meso*-$Ni_2(NCS)_4$(et,ph-P4),and dimethylammonium [hydrogen-μ-oxo-bis{phenylphosphinate}] are presented.

Chapter 1 Introduction

Virtually all homogeneous catalytic processes to date are based on monometallic catalysts. Several groups have reported dimer and cluster catalysis, but none of these polymetallic catalysts combine high product regioselectivities with high reaction rates and few, if any, of them compare favorably to the best known monometallic catalyst systems.[1]

Of the many homogeneous catalytic processes, we decided to study hydroformylation catalysis with the goal to demonstrate that two (or more) metal centers can cooperate in a homogeneous catalytic process to produce a better catalyst compared to monometallic systems. Monometallic rhodium triphenylphosphine catalysts dominate the industry, particularly for C_3 through C_6 1-alkenes, where regioselectivity in making the more valuable linear aldehyde products is critical.

1.1 Hydroformylation

Hydroformylation (also called "oxo") refers to the chemical reaction of alkenes with hydrogen and carbon monoxide to give either linear or branched aldehydes, with one more carbon atom than the alkene substrate [Eq. (1)]. Rhodium or cobalt carbonyl hydride complexes are the most commonly used catalysts for hydroformylation.

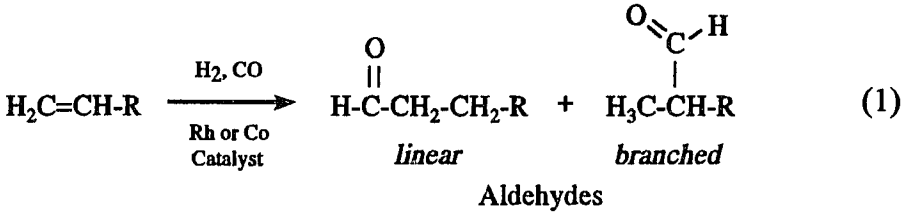

(1)

It is also the world's largest industrial homogeneous catalytic process producing over 10 billion pounds of aldehydes and derivatives annually. Because unsaturated hydrocarbons, especially C_2-C_4 alkenes, are important building blocks in the petrochemical industry, and oxygenated products such as alcohols and carboxylic acids

are industrially important chemicals, hydroformylation has continued to be the subject of intensive investigation.

1.2 Industrial Applications

The product aldehydes themselves have minimum utility. They can, however, be used to provide useful derivatives such as alcohols and carboxylic acids. The alcohols are formed either by direct hydrogenation [Eq. (2)], or by aldol condensation followed by hydrogenation [Eq. (3)].

$$RCH_2CHO \xrightarrow{H_2} RCH_2CH_2OH \qquad (2)$$

$$2RCH_2CHO \xrightarrow{base} RCH_2C(OH)HC(R)HCHO \xrightarrow{-H_2O} RCH_2CH{=}C(R)CHO \xrightarrow{H_2} RCH_2CH_2C(R)HCH_2OH \qquad (3)$$

Among alcohols produced by hydroformylation, *n*-butanol is mainly used in solvent applications. 2-ethylhexanol is also derived from butanal [Eq. (3), R = Et] with over 5 billion pounds produced annually. It is esterified with phthalic anhydride to form dioctyl phthalate (DOP), a plasticizer for polyvinyl chloride resins. Some detergents are made from alcohols of higher chain length, principally C_{13}-C_{15}, which are also made from aldehydes produced by hydroformylation.

Other derivatives formed from the aldehydes are acids and amines. These are produced by oxidation and reductive amination, respectively [Eqs. (4) and (5)].

$$RCH_2CHO \xrightarrow{[O]} RCH_2COOH \qquad (4)$$

$$RCH_2CHO + H_2 + NH_3 \longrightarrow RCH_2CH_2NH_2 \qquad (5)$$

1.3 Reaction Mechanisms

The mechanism of hydroformylation catalysis is relatively well understood and the core mechanism for the commercial monometallic Rh/PPh_3 catalyst system is shown in Scheme **1**. Alkene substrate is added to the square planar rhodium complex to form a five-coordinate 18 electron species. The alkene inserts into the Rh-H bond generating a square planar 16 electron rhodium alkyl species. This is considered the regioselectivity step.[2] When the hydride adds to the internal carbon of alkene, the rhodium bonds to the terminal carbon of that alkene to give a linear rhodium-alkyl species. A branched rhodium-alkyl is produced when the hydrogen adds to the terminal carbon of the alkene.

Addition of carbon monoxide followed by carbonyl insertion (or alkyl migration) gives a square planar four-coordinate rhodium acyl. This species undergoes an oxidative addition in the presence of molecular hydrogen to give a six-coordinate 18 electron acyl dihydride species. One hydride is *cis* to the acyl group favoring reductive elimination of aldehyde, regenerating the original catalyst. One equivalent of alkene, in the presence of one equivalent of carbon monoxide and hydrogen generates one equivalent of aldehyde. One loop through the catalytic cycle is referred to as a turnover, and the rate of catalysis is generally measured in terms of turnovers per unit time (usually per hour for hydroformylation).

Although hydroformylation is generally thought of as a monometallically catalyzed process, in 1961 Heck and Breslow[3] proposed that one could potentially also have a bimetallic mechanism involving an intermolecular hydride transfer (Scheme **2**). The first series of proposed steps are analogous to the rhodium catalyzed process described above, until one reaches the tetracarbonylcobalt-acyl stage. Heck then proposed that another $HCo(CO)_4$ could intermolecularly transfer a hydride to an acyl-tricarbonyl species to generate an aldehyde and $Co_2(CO)_7$. For a number of years it was believed that the bimetallic cycle was the major mechanistic route for

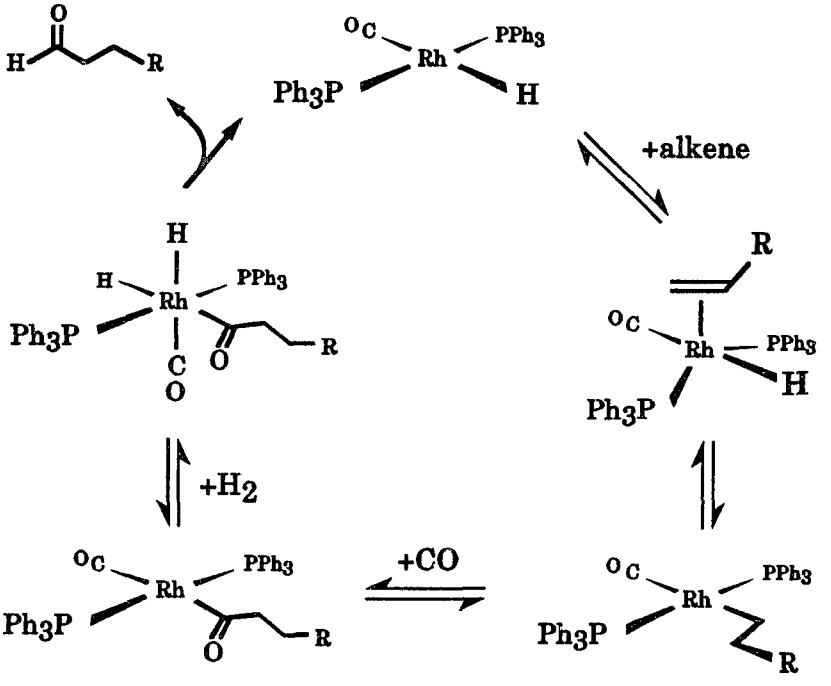

Scheme 1: Proposed mechanism for hydroformylation using commercial Rh/PPh_3 catalyst

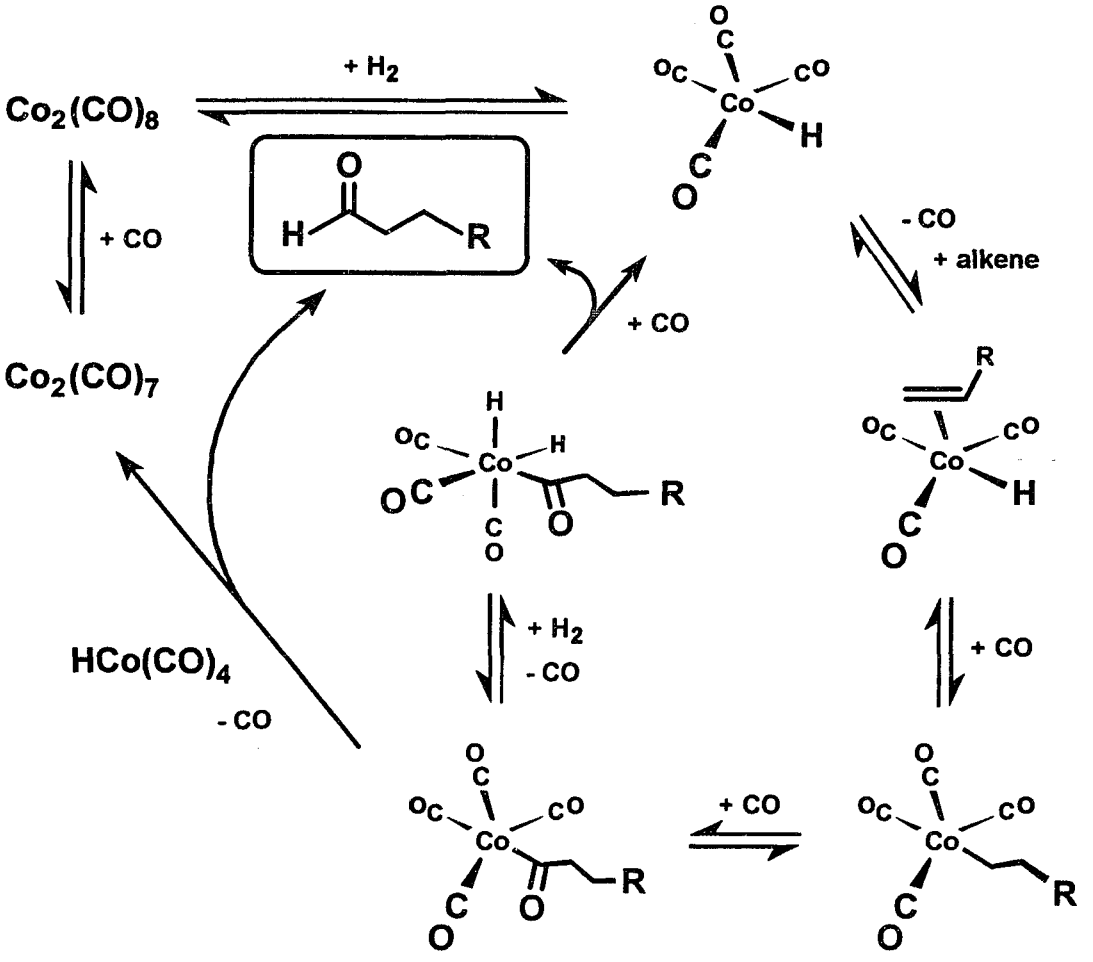

Scheme 2: Heck-Breslow mechanism for hydroformylation catalyzed by $HCo(CO)_4$

$HCo(CO)_4$-catalyzed hydroformylation. Recently, however, careful high-pressure FT-IR studies have provided strong evidence that the monometallic cycle dominates under commercial reaction conditions.[4] In spite of this, Bergman,[5] Halpern,[6] Norton[7] and Marko[8] have all demonstrated that intermolecular hydride transfers can occur in stoichiometric reactions between metal hydrides and metal-acyl complexes.

Thus a bimetallic route was envisaged, in contrast to the more traditional monometallic route. It has also been demonstrated that stoichiometric $HCo(CO)_4$ hydroformylation is indeed bimetallic. This was our primary motivation for studying the effectiveness of the bimetallic complexes for hydroformylation activity.

1.4 Bimetallic Systems

In the literature there are numerous examples where phosphine ligands have been used in studies of coordination chemistry and homogeneous catalysis.[9] These phosphines generally act as σ-donors in metal complexes, and their electron donating tendencies increase considerably by changing the substituent groups from alkoxide, to aryl, to more electron-rich alkyl groups. Similarly, the reactivity of the metal is often significantly altered by changes in the electron density on the metal, and sometimes can be optimized by steric and electronic tuning of the ligand system. Phosphines are quite versatile, especially in stabilizing low-valent, late transition metal complexes. Bisphosphines, like bis(diphenylphosphino)ethane, $Ph_2PCH_2CH_2PPh_2$ (dppe), are capable of forming five-membered chelate rings to further stabilize coordination to the metal center relative to monodentate phosphines.

In addition, bridging phosphine ligands have been used to maintain close M-M proximity. For example, bis(diphenylphosphino)methane, $Ph_2PCH_2PPh_2$, is capable of bridging two metals and there are hundreds of bimetallic complexes bridged by such phosphines in the literature.[10]

The vast majority of bimetallic phosphine complexes, however, have two *trans* oriented bis(phosphino)methane-type ligands. These *trans* doubly-bridged bimetallic

complexes are commonly called A-frame dimer systems. In spite of the large number of A-frame dimer complexes known, none have catalytic activities or selectivities that even come close to monometallic catalyst systems. One potential reason for the poor catalytic behavior could be the rigidity of the A-frame unit.

A specially designed bridging ligand template composed of bridging, chelating, and strongly binding electron-rich phosphines should eliminate problems commonly associated with the fragmentation of polymetallic complexes. Such a ligand can coordinate two metal centers and keep them in general proximity allowing M-M bond breakage and reformation, while the electron-rich, strongly coordinating phosphines inhibit dissociation and fragmentation of the overall polymetallic complex.

The tetraphosphine ligand $Et_2PCH_2CH_2P(Ph)CH_2P(Ph)CH_2CH_2PEt_2$, (et,ph-P4) was synthesized in 1988 by Laneman and Stanley in these laboratories.[11] It is less sterically demanding, has bridging phosphines (Figure 1) for keeping the two metal centers in general proximity, and chelation of each metal for added stability. Its electron-rich alkylated phosphines will coordinate strongly to transition metal centers and should be far more effective at inhibiting ligand dissociation and dimer fragmentation than the A-frame dimer systems. In this way, it behaves as a strong binucleating tetraphosphine ligand.

The internal phosphines of et,ph-P4 are chiral, thereby generating a pair of diastereomers: the *racemic* (*R,R; S,S*) diastereomer is formed when the chelating arms occupy positions anti to each other, while the *meso* (*R,S*) diastereomer is formed when the chelating arms are syn to each other. The two diastereomers are produced in approximately equal amounts from the ligand synthesis.

The diastereomeric mixture of et,ph-P4 was used to synthesize a bimetallic catalyst precursor $Rh_2(nbd)_2(et,ph\text{-}P4)^{2+}$ as shown in Scheme **3**.[12] This had been shown to be a good hydroformylation catalyst.[13] However, it was not clear which of the bimetallic diastereomers was the active catalyst species. Thus, a key experiment in

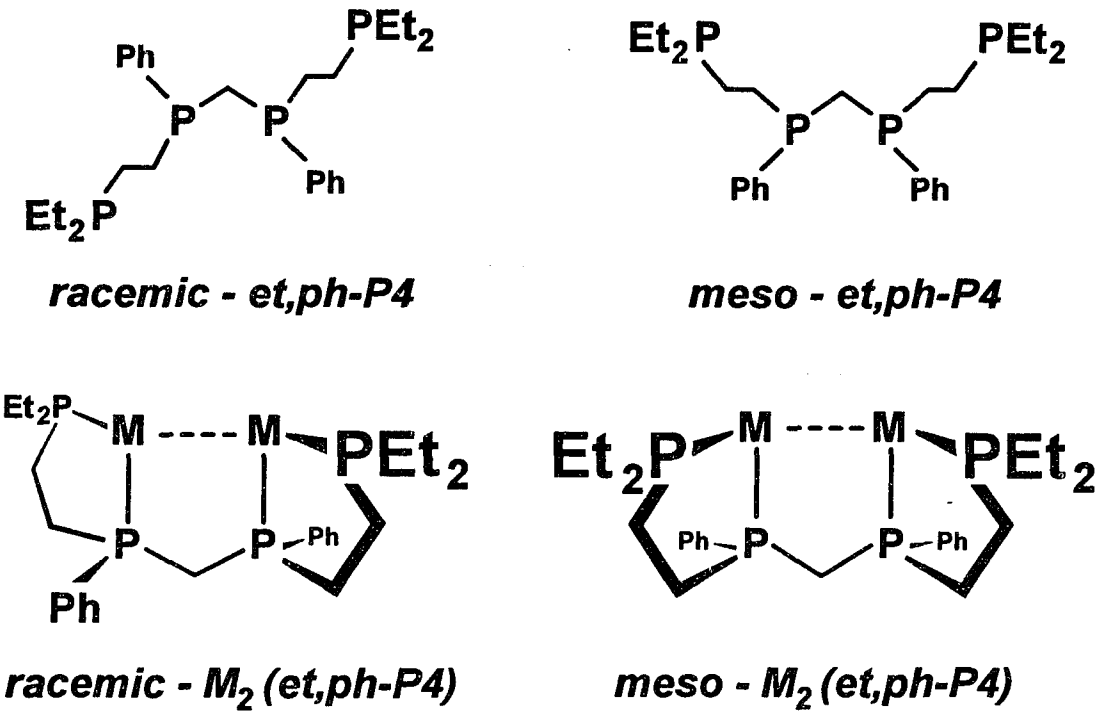

Figure 1: et,ph-P4 ligand system and hypothetical bimetallic complexes.

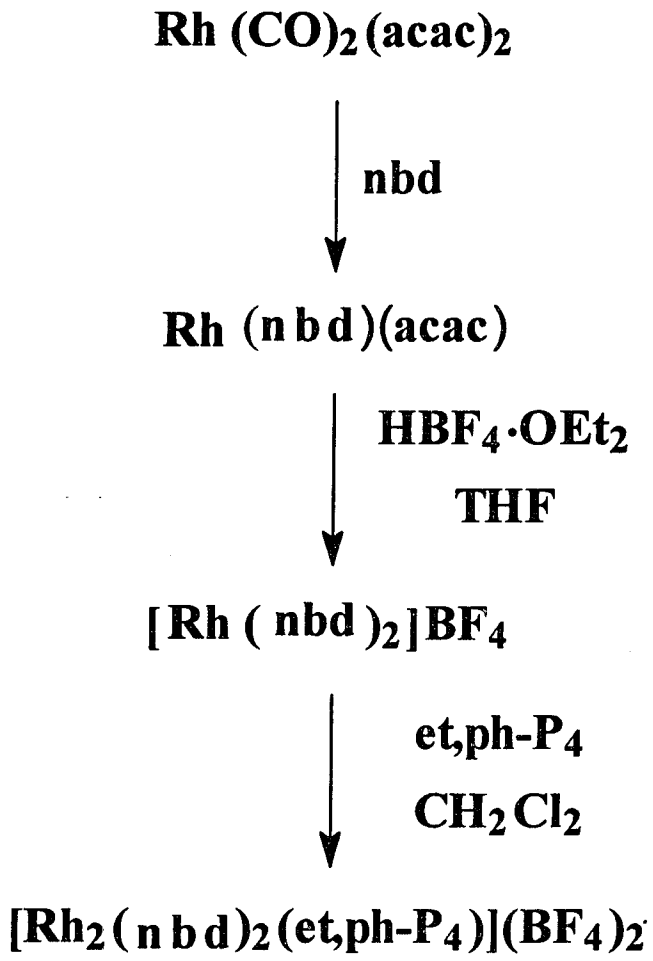

Scheme 3: Synthesis of $[Rh_2(nbd)_2(et,ph\text{-}P4)](BF_4)_2$.[12]

studying this system was to find a way to separate and readily isolate diastereomerically *pure* et,ph-P4 ligand so that the individual performance of *meso*- and *racemic*-et,ph-P4 dirhodium catalysts could be evaluated. After successful separation of pure *racemic*-et,ph-P4, the (*S,S*) and (*R,R*) enantiomers of the *racemic* ligand could be further separated to study asymmetric hydroformylation. Based on molecular modelling studies, the chiral bimetallic catalysts have the potential for high asymmetric induction.

The basis of this dissertation, therefore, is to:

1. develop techniques for the bulk separation of pure *racemic* and *meso*- et,ph-P4.
2. execute separate catalytic runs in order to determine the performance of the *meso*- and *racemic*- dirhodium catalysts.
3. isolate (*S,S*)- and (*R,R*)- enantiomers of *racemic*-et,ph-P4 for asymmetric catalysis.

Chapter 2 Synthesis, Separation, and Structures of *Racemic*- and *Meso*-et,ph-P4 Complexes of Nickel

2.1 Introduction

One ideal separation procedure to obtain pure *racemic* and *meso*-et,ph-P4 ligands would involve production of a metal complex in which one diastereomer would be soluble in a suitable solvent, while the other would precipitate out allowing simple isolation of each in high yields. The pure *racemic* and *meso*-et,ph-P4 ligands could then be released from the metal complex by some suitable reagent to give the pure ligand. Because nickel complexes had been successfully used to separate other diastereomeric mixtures in the past, we decided to concentrate our separation chemistry effort on nickel.[14]

Lippard and coworkers successfully separated diastereomers of an oxaphosphand ligand by treating the diastereomeric mixture in CH_2Cl_2 with $NiCl_2.6H_2O$, and the products were separated and then treated with KSCN in methanol. Performing flash chromatography of the thiocyanate complexes on a silica column precipitated one diastereomer.[15]

Using this general protocol, we developed a relatively straightforward route for the bulk separation and isolation of uncomplexed *racemic* and *meso*-et,ph-P4 ligands in very pure diastereomeric form.

2.2 *Racemic* and *Meso*-[Ni(NCS)(η^3-et,ph-P4)](NCS)

The reaction of et,ph-P4 with one equivalent of $Ni(NCS)_2$ in EtOH produces a mixture of *racemic*-[Ni(NCS)(η^3-et,ph-P4)](NCS) and *meso*-[Ni(NCS)(η^3-et,ph-P4)](NCS) in high yields. The *meso*-[Ni(NCS)(η^3-et,ph-P4)](NCS) is precipitated immediately and quantitatively as an air-stable, orange solid. Its structure was confirmed from a single crystal *X*-ray structure determination. Red-orange *meso*-[Ni(NCS)(η^3-et,ph-P4)](NCS) crystals are easily grown in a chloroform/ethanol solvent mixture or from dichloromethane.

An ORTEP diagram of *meso*-[Ni(NCS)(η^3-et,ph-P4)]$^+$ is shown in Figure **2**. The NCS^- counter anion is not shown. The geometry about the metal center is basically distorted square planar with the ligand forming fused five and seven-membered chelate rings. The distortion arises from the steric strain of having five-and seven-membered chelate rings fused in a square planar orientation. As a result, the cisoidal P2-Ni-P1 and P1-Ni-P4 bond angles are 85.63 (3)° and 96.21 (4)°. The P2-Ni-P4 and P-Ni-N bond angles are 160.84 (4)° and 170.9 (1)° respectively. Ni-P_{ext} bond distances are 2.2134 (9) Å and 2.2401 (9) Å which fall within normal Ni-P ranges. A shorter bond distance is observed for the internal phosphine (Ni-P_{int} bond distance of 2.1586 (9) Å).

Only one thiocyanate group is bonded to nickel through the nitrogen atom. The other thiocyanate counter anion appears to interact weakly with the metal through the sulfur with a Ni-S distance of 2.737 (1) Å. Selected bond lengths and bond angles are shown in Table **1** and Table **2** respectively. Based on elemental analyses and NMR, we believe that the monometallic *racemic*-Ni(NCS)(η^3-et,ph-P4)$^+$ complex has a similar structure.

The $^{31}P\{^1H\}$ NMR of *meso*-[Ni(NCS)(η^3-et,ph-P4)](NCS) in CD_2Cl_2 is illustrated in Figure **3**. It shows two triplets: the external phosphorus atoms resonate at 28.8 ppm (t, $J_{P\text{-}P}$ = 5.0 Hz) and the internal phosphorus atoms at 3.3 ppm (t, $J_{P\text{-}P}$ = 5.0 Hz). The presence of only two ^{31}P resonances points to the rapid equilibrium shown in Scheme **4**. This produces the average structure **b** and the two simple ^{31}P resonances.

The filtrate from the reaction of $Ni(NCS)_2$ and et,ph-P4 was slowly evaporated to give mainly wine-red *racemic*- [Ni(NCS)(η^3-et,ph-P4)](NCS). The *racemic*-[Ni(NCS)(η^3-et,ph-P4)](NCS) was characterized by $^{31}P\{^1H\}$ NMR (also shown in Figure **3**). There are two triplets: the external phosphorus resonates at δ = 52.5 ppm (t, $J_{P\text{-}P}$ = 18.6 Hz) and internal phosphorus atoms at 28.5 ppm (t, $J_{P\text{-}P}$ = 18.6 Hz).

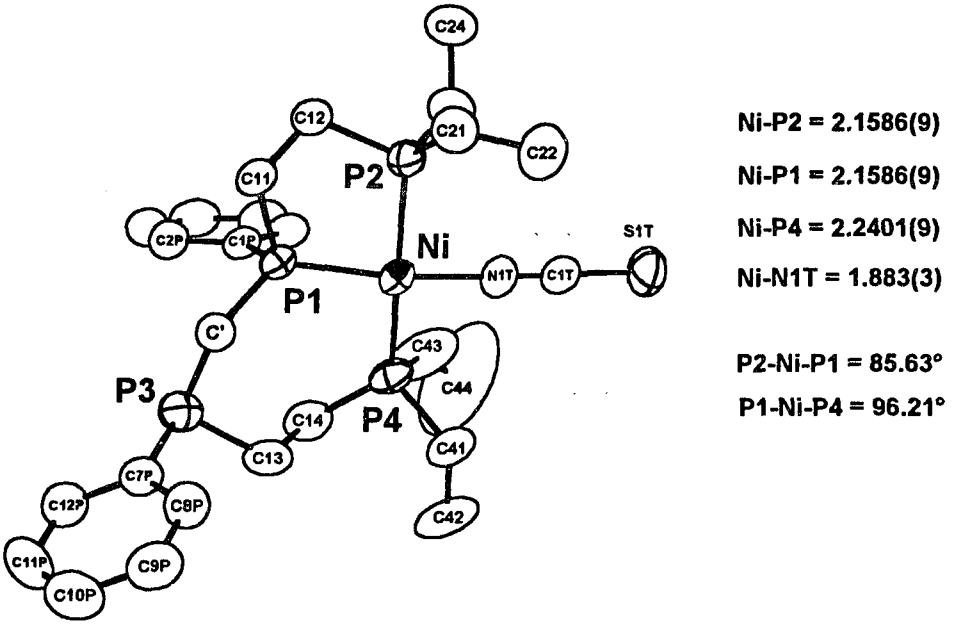

Figure 2. The ORTEP of *meso*-[Ni(NCS)(η^3-et,ph-P4)](NCS)

Table 1: Selected bond distances (Å) for *meso*-Ni(NCS)(η^3-et,ph-P4)]$^+$.[a]

Ni-P1	2.1586(9)	C23-C24	1.531(5)
Ni-P2	2.2134(9)	C41-C42	1.510(5)
Ni-P4	2.2401(9)	C43-C44	1.143(7)
Ni-N1T	1.883(3)	C1P-C2P	1.394(5)
Ni-S2T (calc)	2.7374(0.00122)	C1P-C6P	1.383(5)
P1-C'	1.823(3)	C2P-C3P	1.378(5)
P1-C11	1.828(3)	C3P-C4P	1.378(6)
P1-C1P	1.820(3)	C4P-C5P	1.371(5)
P2-C12	1.831(3)	C5P-C6P	1.385(5)
P2-C21	1.812(4)	C7P-C8P	1.393(5)
P2-C23	1.810(4)	C7P-C12P	1.384(5)
P3-C'	1.837(3)	C8P-C9P	1.373(6)
P3-C13	1.833(3)	C9P-C10P	1.369(6)
P3-C7P	1.836(4)	C10P-C11P	1.358(6)
P4-C14	1.819(4)	C11P-C12P	1.391(6)
P4-C41	1.827(4)	S1T-C1T	1.628(4)
P4-C43	1.843(5)	C1T-N1T	1.148(4)
C11-C12	1.523(5)	S2T-C2T	1.646(3)
C13-C14	1.531(6)	C2T-N2T	1.142(4)
C21-C22	1.525(5)		

[a]Numbers in parentheses are estimated standard deviations in the least significant digits.

Table **2:** Selected bond angles (°) for *meso*-Ni(NCS)(η^3-et,ph-P4)]$^+$.[a]

P1-Ni-P2	85.63(3)	Ni-P4-C14	122.0(1)
P1-Ni-P4	96.21(4)	Ni-P4-C41	110.3(3)
P1-Ni-N1T	170.9(1)	Ni-P4-C43	110.7(2)
P2-Ni-P4	160.84(4)	C14-P4-C41	104.7(2)
P2-Ni-N1T	88.57(8)	C14-P4-C43	102.1(2)
P4-Ni-N1T	87.01(8)	C41-P4-C43	105.8(2)
Ni-P1-C'	120.4(1)	P1-C'-P3	121.9(2)
Ni-P1-C11	108.6(1)	P1-C11-C12	108.1(2)
Ni-P1-C1P	112.3(1)	P2-C12-C11	107.1(2)
C'-P1-C11	100.6(1)	P3-C13-C14	113.0(2)
C'-P1-C1P	108.7(1)	P4-C14-C13	114.1(3)
C11-P1-C1P	104.5(1)	P2-C21-C22	1114.7(2)
Ni-P2-C12	110.2(1)	P2-C23-C24	115.1(3)
Ni-P2-C21	116.7(1)	P4-C41-C42	118.1(3)
Ni-P2-C23	113.3(1)	P4-C43-C44	135.4(7)
C12-P2-C21	104.1(1)	P1-C1P-C2P	121.5(2)
C12-P2-C23	105.2(2)	P1-C1P-C6P	119.6(2)
C21-P2-C23	106.4(2)	C2P-C1P-C6P	119.0(3)
C'-P3-C13	101.2(2)	S1T-C1T-N1T	179.2(3)
C'-P3-C7P	99.6(1)	Ni-N1T-C1T	178.0(2)
C13-P3-C7P	99.5(0)	S2T-C2T-N2T	179.4(4)

[a]Numbers in parentheses are estimated standard deviations in the least significant digits.

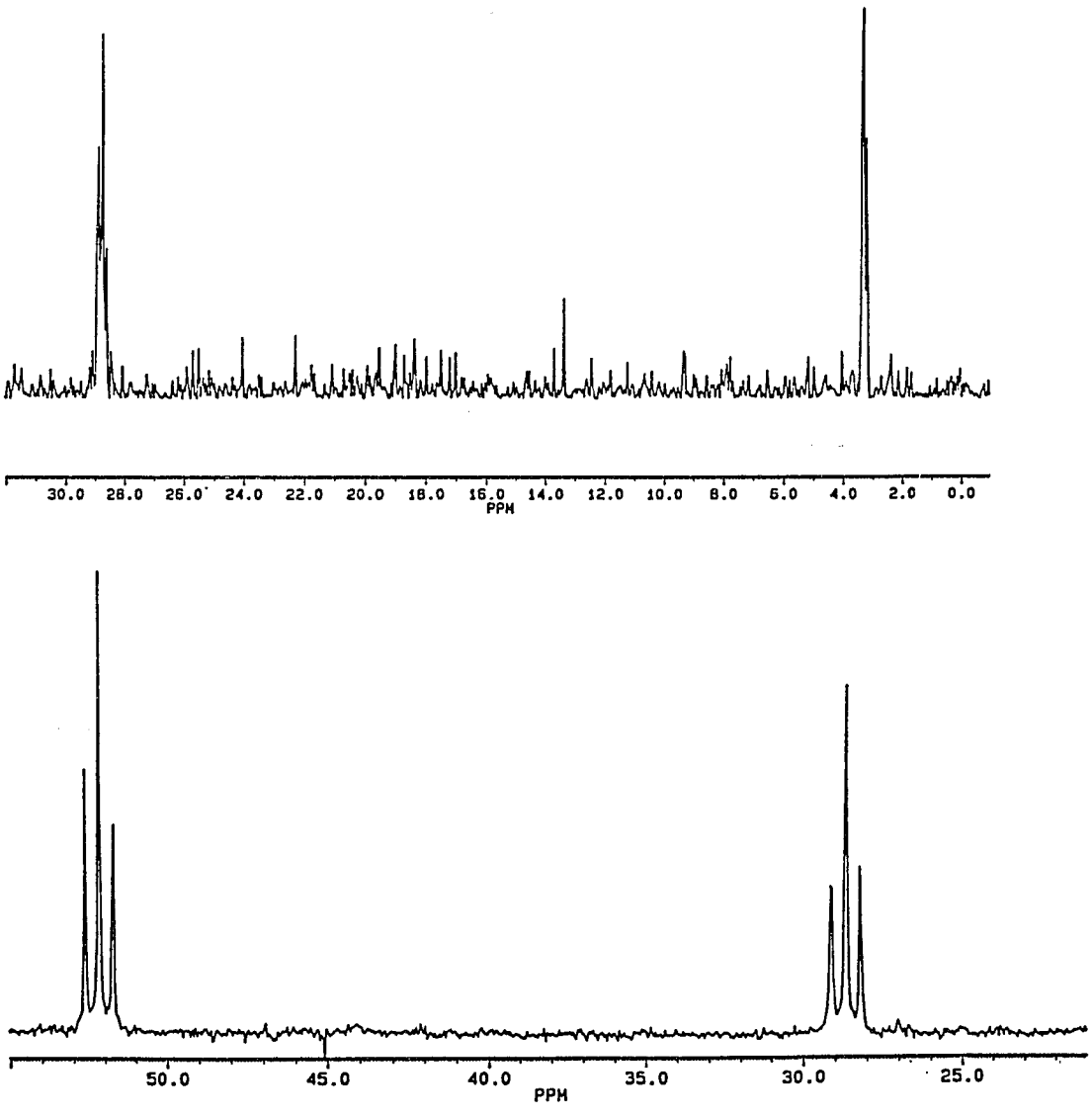

Figure 3. $^{31}P\{^{1}H\}$ NMR of *meso*-Ni(NCS)(η^3-et,ph-P4)](NCS) (top) and *racemic*-Ni(NCS)(η^3-et,ph-P4)](NCS) (bottom) in CD_2Cl_2 (40.48 MHz). Asterisked peaks are solvent impurities.

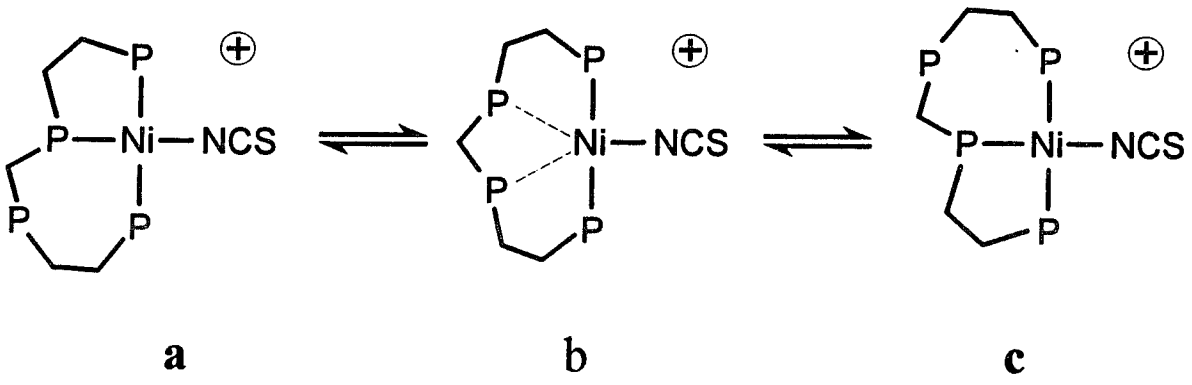

Scheme 4: The proposed behavior of Ni(NCS)(η^3-et,ph-P4)$^+$ in solution.

2.3 *Racemic* and *Meso*-[$Ni_2(NCS)_4$(et,ph-P4)]

The bimetallic complexes, *racemic*-and *meso*-[$Ni_2(NCS)_4$(et,ph-P4)], were synthesized to compare yields for each pure diastereomer of the bimetallic complex relative to the monometallic analogs.

The reaction of et,ph-P4 with two equivalents of $Ni(NCS)_2$ in EtOH produces a mixture of *racemic*-[$Ni_2(NCS)_4$(et,ph-P4)] and *meso*-[$Ni_2(NCS)_4$(et,ph-P4)] in nearly quantitative yields. The *meso*-nickel complex is precipitated immediately and quantitatively as an air-stable orange solid, whereas the wine-red *racemic* diastereomer remains in solution.

Orange needle-like crystals of the *meso*-[$Ni_2(NCS)_4$(et,ph-P4)] are easily grown in a chloroform/ethanol solvent mixture. The ORTEP diagram of the *meso*-$Ni_2(NCS)_4$(et,ph-P4) dimer is shown in Figure **4.** Each metal center is square planar with the tetraphosphine coordinating in a conventional chelating fashion at each nickel atom. There is no Ni-Ni bond; the Ni···Ni separation is quite large at 6.302 Å. The Ni-P···P-Ni torsion angle is158°. The bridging and chelating nature of the et,ph-P4 ligand can be clearly seen from the ORTEP. The structure is very similar to that observed for *meso*-Ni_2Cl_4(et,ph-P4).[16] Selected bond distances and angles are listed in Table **3** and Table **4** respectively. All the bond distances and angles in this complex are normal and will not be discussed further.

The $^{31}P\{^1H\}$ NMR of *meso*-[$Ni_2(NCS)_4$(et,ph-P4)] in CD_2Cl_2 shows doublets of triplets (Figure **5**) with external phosphorus atoms resonating at 75.4 ppm (d, $^2J_{P\text{-}P}$ = 79.3 Hz and virtual t, $^4J_{P\text{-}P}$ =10.5 Hz). Internal phosphorus atoms resonate at 57.4 ppm (d, $^2J_{P\text{-}P}$ = 79.3 Hz and virtual t, $^3J_{P\text{-}P}$ =10.5 Hz). External phosphorus atoms undergo a $^3J_{P\text{-}P}$ virtual coupling with the internal phosphorus atoms through the metal pathway generating the triplet pattern.

The filtrate was evaporated to dryness to give mainly wine-red air-stable *racemic*-[$Ni_2(NCS)_4$(et,ph-P4)]. $^{31}P\{^1H\}$ NMR of bimetallic

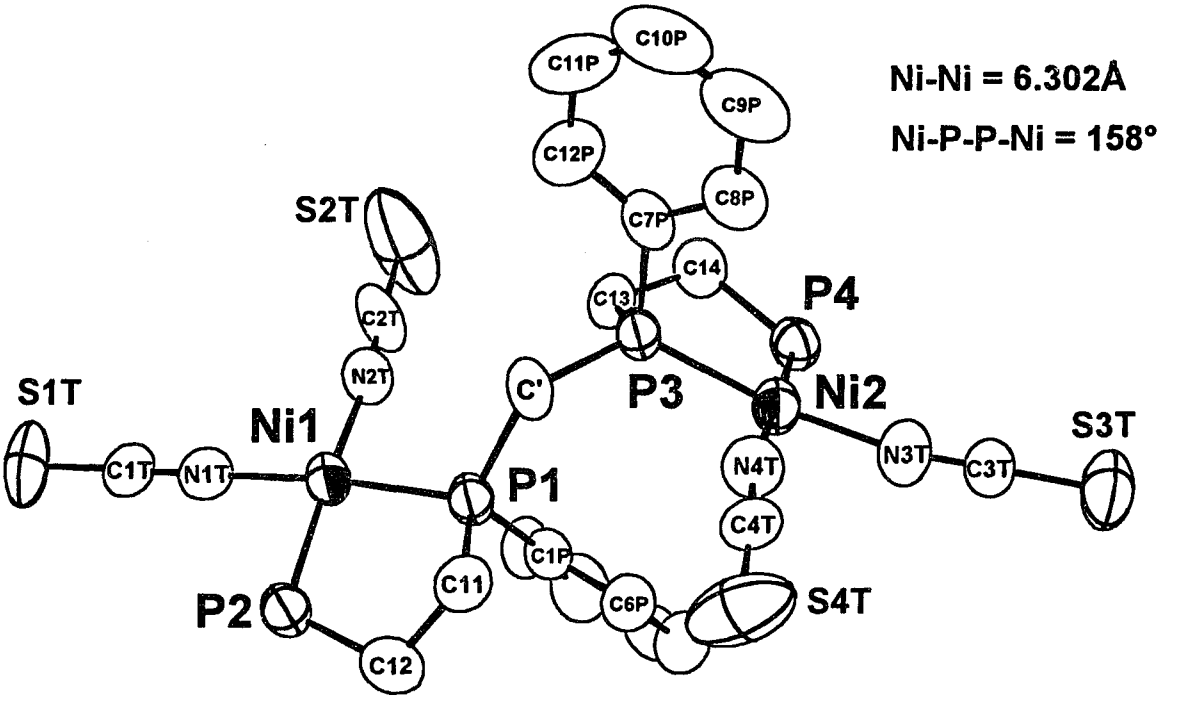

Figure 4. The ORTEP of *meso*-$Ni_2(NCS)_4$(et,ph-P4).

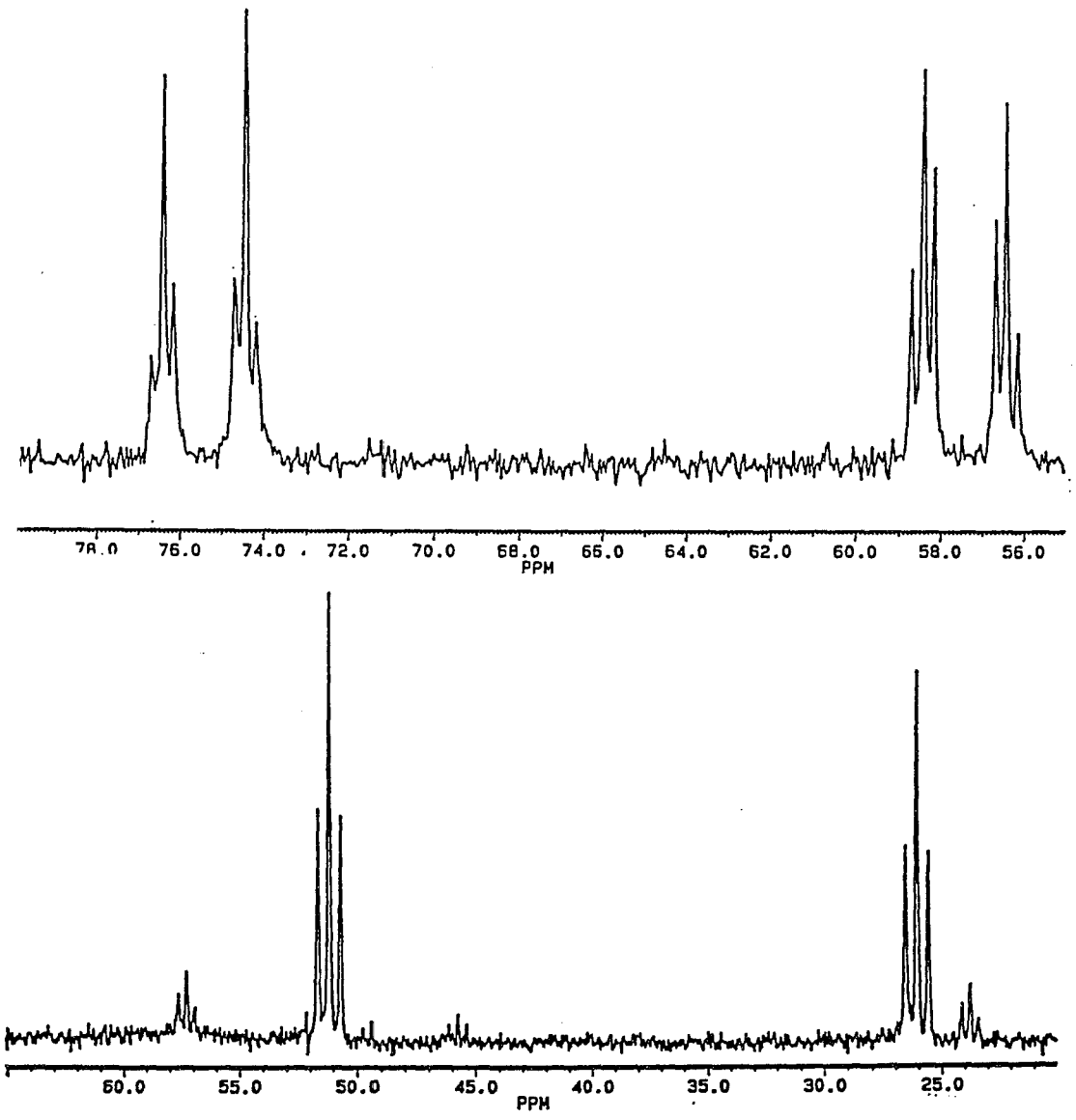

Figure 5. $^{31}P\{^{1}H\}$ NMR of *meso*-$[Ni_2(NCS)_4(et,ph\text{-}P4)]$ (top) and *racemic*-$[Ni_2(NCS)_4(et,ph\text{-}P4)]$ (bottom) in CD_2Cl_2 (40.48 MHz).

racemic-[$Ni_2(NCS)_4$(et,ph-P4)] is also shown in Figure 5. External phosphorus atoms resonate 51.1 ppm (t, J_{P_P} = 19.8 Hz), while the internal phosphorus atoms resonate at 26.1 ppm (t, J_{P_P} = 19.8 Hz). The peaks at 57.3 ppm (t, J_{P_P} = 14.4 Hz) and at 23.9 ppm (t, J_{P_P} = 13.9 Hz) are due nickel phosphine impurities. Based on the $^{31}P\{^1H\}$ NMR we believe that *racemic*-[$Ni_2(NCS)_4$(et,ph-P4)] has a structure similar to the *meso* isomer.

Table 3: Selected bond distances (Å) for *meso*-$Ni_2(NCS)_4$(et,ph-P4).[a]

Ni1-P1	2.152(2)	C23-C24	1.49(1)
Ni1-P2	2.148(3)	C41-C42	1.52(2)
Ni1-N1T	1.876(7)	C43-C44	1.51(1)
Ni1-N2T	1.874(7)	C1P-C2P	1.37(1)
Ni2-P3	2.135(2)	C1P-C6P	1.37(1)
Ni2-P4	2.161(3)	C2P-C3P	1.40(1)
Ni2-N3T	1.864(7)	C3P-C4P	1.35(1)
Ni2-N4T	1.879(7)	C4P-C5P	1.36(2)
P1-C'	1.816(9)	C5P-C6P	1.39(1)
P1-C11	1.819(9)	C7P-C8P	1.37(1)
P1-C1P	1.809(8)	C7P-C12P	1.40(1)
P2-C12	1.803(9)	C8P-C9P	1.39(1)
P2-C21	1.813(9)	C9P-C10P	1.35(1)
P2-C23	1.81(1)	C10P-C11P	1.35(2)
P3-C'	1.815(8)	C11P-C12P	1.38(2)
P3-C13	1.799(9)	S1T-C1T	1.600(8)
P3-C7P	1.815(9)	C1T-N1T	1.16(1)
P4-C14	1.817(9)	S2T-C2T	1.61(1)
P4-C41	1.812(9)	C2T-N2T	1.14(1)
P4-C43	1.80(1)	S3T-C3T	1.606(8)
C11-C12	1.52(1)	C3T-N3T	1.16(1)
C13-C14	1.51(1)	S4T-C4T	1.60(1)
C21-C22	1.48(2)	C4T-N4T	1.14(1)

[a]Numbers in parentheses are estimated standard deviations in the least significant digits.

Table 4: Selected bond angles (°) for *meso*-$Ni_2(NCS)_4$(et,ph-P4).[a]

P1-Ni1-P2	86.6(1)	C41-P4-C43	108.6(4)
P1-Ni1-N1T	174.3(2)	P1-C'-P3	126.2(5)
P1-Ni1-N2T	92.4(2)	P1-C11-C12	106.5(6)
P2-Ni1-N1T	87.7(2)	P2-C12-C11	108.8(6)
P2-Ni1-N2T	176.0(2)	P3-C13-C14	107.3(6)
N1T-Ni1-N2T	93.2(3)	P4-C14-C13	109.4(6)
P3-Ni2-P4	86.5(1)	P2-C21-C22	116.4(8)
P3-Ni2-N3T	172.2(3)	P2-C23-C24	112.9(7)
P3-Ni2-N4T	92.1(2)	P4-C41-C42	113.2(7)
P4-Ni2-N3T	88.8(3)	P4-C43-C44	116.2(7)
P4-Ni2-N4T	177.9(2)	P1-C1P-C2P	119.9(6)
N3T-Ni2-N4T	92.8(3)	P1-C1P-C6P	120.5(7)
Ni1-P1-C'	114.4(3)	C2P-C1P-C6P	119.6(7)
Ni-P1-C11	107.9(3)	C1P-C2P-C3P	120.3(8)
Ni1-P1-C1P	113.0(3)	C2P-C3P-C4P	119(1)
C'-P1-C11	104.8(4)	C3P-C4P-C5P	122.8(9)
C'-P1-C1P	109.5(4)	C4P-C5P-C6P	118.3(9)
C11-P1-C1P	106.6(4)	C1P-C6P-C5P	120.5(9)
Ni1-P2-C12	110.0(3)	P3-C7P-C8P	119.7(6)
Ni1-P2-C21	112.1(3)	P3-C7P-C12P	122.0(7)
Ni1-P2-C23	113.4(3)	C8P-C7P-C12P	118.2(9)
C12-P2-C21	108.0(4)	C7P-C8P-C9P	120.9(8)
C12-P2-C23	106.4(4)	C8P-C9P-C10P	119(1)
C21-P2-C23	106.6(4)	C9P-C10P-C11P	122.(1)
Ni2-P3-C'	120.4(3)	C10P-C11P-C12P	120.(1)
Ni2-P3-C13	110.1(3)	C7P-C12P-C11P	120.(1)
Ni2-P3-C7P	109.1(3)	S1T-C1T-N1T	178.0(8)
C'-P3-C13	109.9(4)	Ni1-N1T-C1T	175.6(7)
C'-P3-C7P	99.8(4)	S2T-C2T-N2T	178.(1)
C'13-P3-C7P	106.2(4)	Ni1-N2T-C2T	171.7(7)
Ni2-P4-C14	109.4(3)	S3T-C3T-N3T	179.1(9)
Ni2-P4-C41	113.7(3)	Ni2-N3T-C3T	170.0(8)
Ni2-P4-C43	112.1(3)	S4T-C4T-N4T	176.4(8)
C14-P4-C41	107.8(4)	Ni2-N4T-C4T	164.5(7)
C14-P4-C43	104.8(4)		

[a]Numbers in parentheses are estimated standard deviations in the least significant digits.

CHAPTER 3 Isolation of Individual Diastereomers of et,ph-P4

3.1 Introduction

The mixture of et,ph-P4 is easily separated as wine-red *racemic*-$[Ni_2(NCS)_4$(et,ph-P4)] and orange *meso*-$[Ni_2(NCS)_4$(et,ph-P4)] by taking advantage of their very different solubilities in ethanol. Decomplexing the metal complex by a suitable reagent would release diastereomerically pure *racemic* or *meso* et,ph-P4 ligands.

3.2 Racemic et,ph-P4

The diastereomerically pure *racemic*-et,ph-P4 ligand was decomplexed by refluxing the wine-red *racemic*-$[Ni_2(NCS)_4$(et,ph-P4)] complex in heptane/water (1:1 v/v) solvent mixture in the presence of ten-fold excess of NaCN (Ni:CN = 1:10) under inert atmosphere. The cyanide attacks the nickel center forming water soluble $Ni(CN)_4^{2-}$ and releasing et,ph-P4 which cleanly transfers into the organic phase.

The organic layer was transferred by cannula into another Schlenk flask and passed through a short alumina column to remove any solid impurities. The more volatile organic solvent was evaporated to produce oily *racemic*-et,ph-P4. This was dissolved again in heptane (or hexane) and passed through a second alumina column to improve the purity of product (>67% yield). The yield could be higher if not for the alumina-column cleaning necessary to remove yellowish impurities that result from the decomplexation. The separation route is summarized in Scheme 5. The *racemic*-et,ph-P4 ligand is a colorless, air-sensitive oily liquid and its identity was confirmed by $^{31}P\{^1H\}$ NMR and X-ray structures of metal complexes.

The monometallic *racemic*-$[Ni(NCS)(\eta^3$-et,ph-P4)]$^+$ complex undergoes similar decomplexation to release ligand. However, the bimetallic complex provided significantly higher yields of separated pure diastereomers compared to the monometallic analog. This was due to the fact that $Ni(NCS)_2$ was used as obtained without further purification and the use of two equivalents of $Ni(NCS)_2$ ensured that

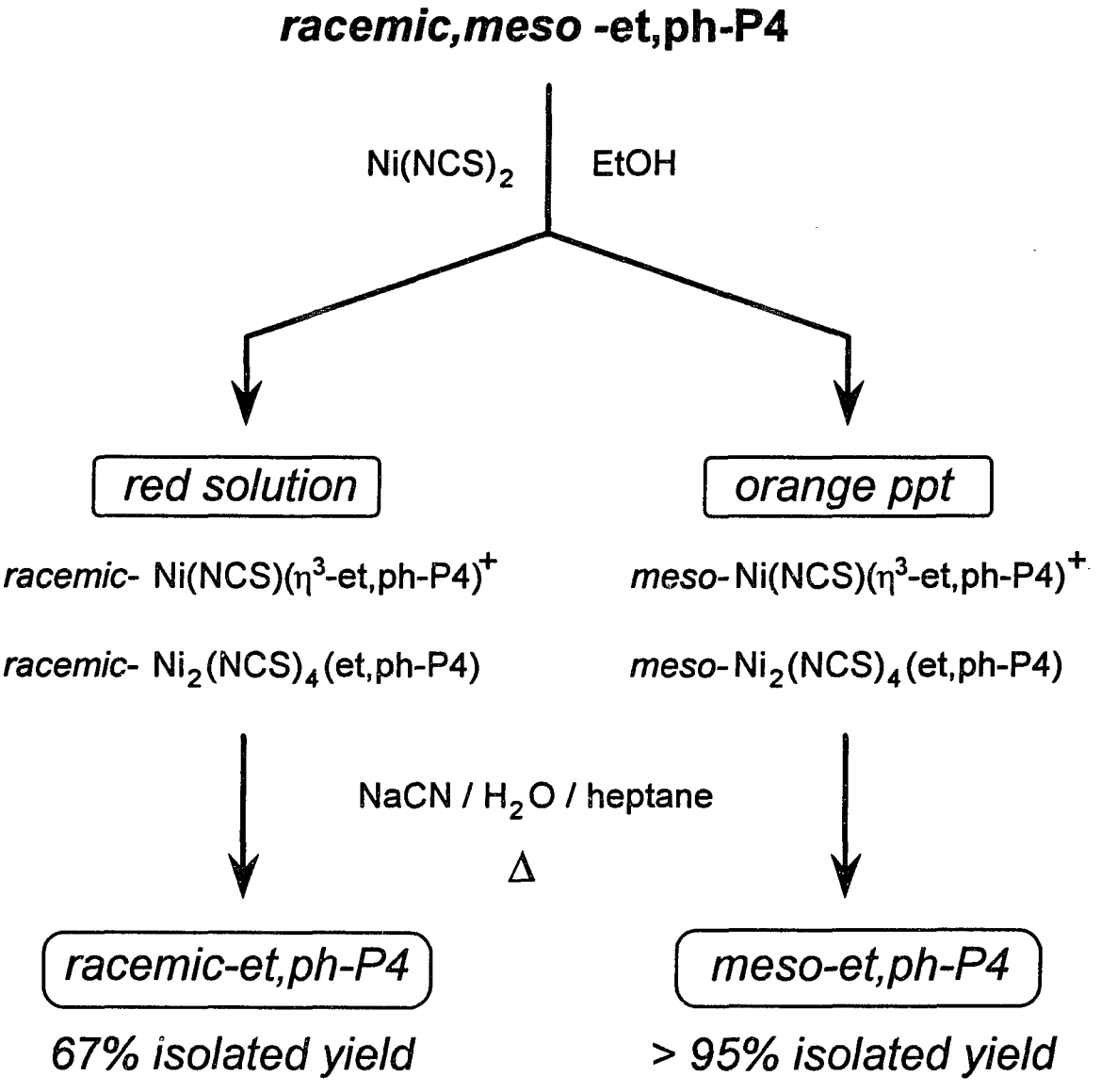

Scheme 5: Separation of diastereomers of et,ph-P4

et,ph-P4 was the limiting reagent. Therefore, for optimum separation and isolation of ligand, we routinely use the bimetallic route.

3.3 Meso et,ph-P4

The cyanolysis procedure above was repeated for orange *meso*-$[Ni_2(NCS)_4$(et,ph-P4)] to give *meso* et,ph-P4 as white air-stable solid. However, the *meso* ligand required additional cleaning. It was dissolved in a limited amount of hexane, precipitated at -32°C, and collected with a glass frit. This was washed with cold hexane and the solvent evaporated. Upwards of 95% isolated yield of pure *meso* diastereomer was obtained as compared to yields of 67% for *racemic* diastereomer.

Pure *meso* et,ph-P4 converts to a mixture of both diastereomers when heated close to 150 °C for 20 minutes. This can provide additional yields for the *racemic* diastereomer whenever desired by going through the previous separation procedure.

A diastereoisomeric mixture of et,ph-P4 at -32°C precipitates a white solid in hexane. This, at a glance, may appear to be clean *meso* et,ph-P4. Upon filtration, however, the white residue contains a mixture of both *racemic* and *meso* diastereomers. This was estimated from integration of the $^{31}P\{^1H\}$ NMR spectrum to contain approximately 75 % of crude *meso* ligand. As expected, the filtrate continued to have a mixture of diastereomers as identified from $^{31}P\{^1H\}$ NMR. So far, the nickel route is the best method for the separation.

Figure 6 shows $^{31}P\{^1H\}$NMR in C_6D_6 of the diastereoisomeric *mixture* of et,ph-P4 (1:1 *meso* to *racemic*) as contrasted with $^{31}P\{^1H\}$NMR spectra of pure *racemic*-et,ph-P4 and pure *meso*-et,ph-P4. The internal phosphorus atoms for *racemic* and *meso*-et,ph-P4 resonances are at -25.3 ppm (t, $J_{P\text{-}P}$ = 11.3 Hz) and -26.0 ppm (t, $J_{P\text{-}P}$ = 10.9 Hz), respectively. The internal phosphorus atoms resonate for *racemic*- and *meso*-et,ph-P4 at the same position -18.2 ppm (t, $J_{P\text{-}P}$ = 11.1 Hz).

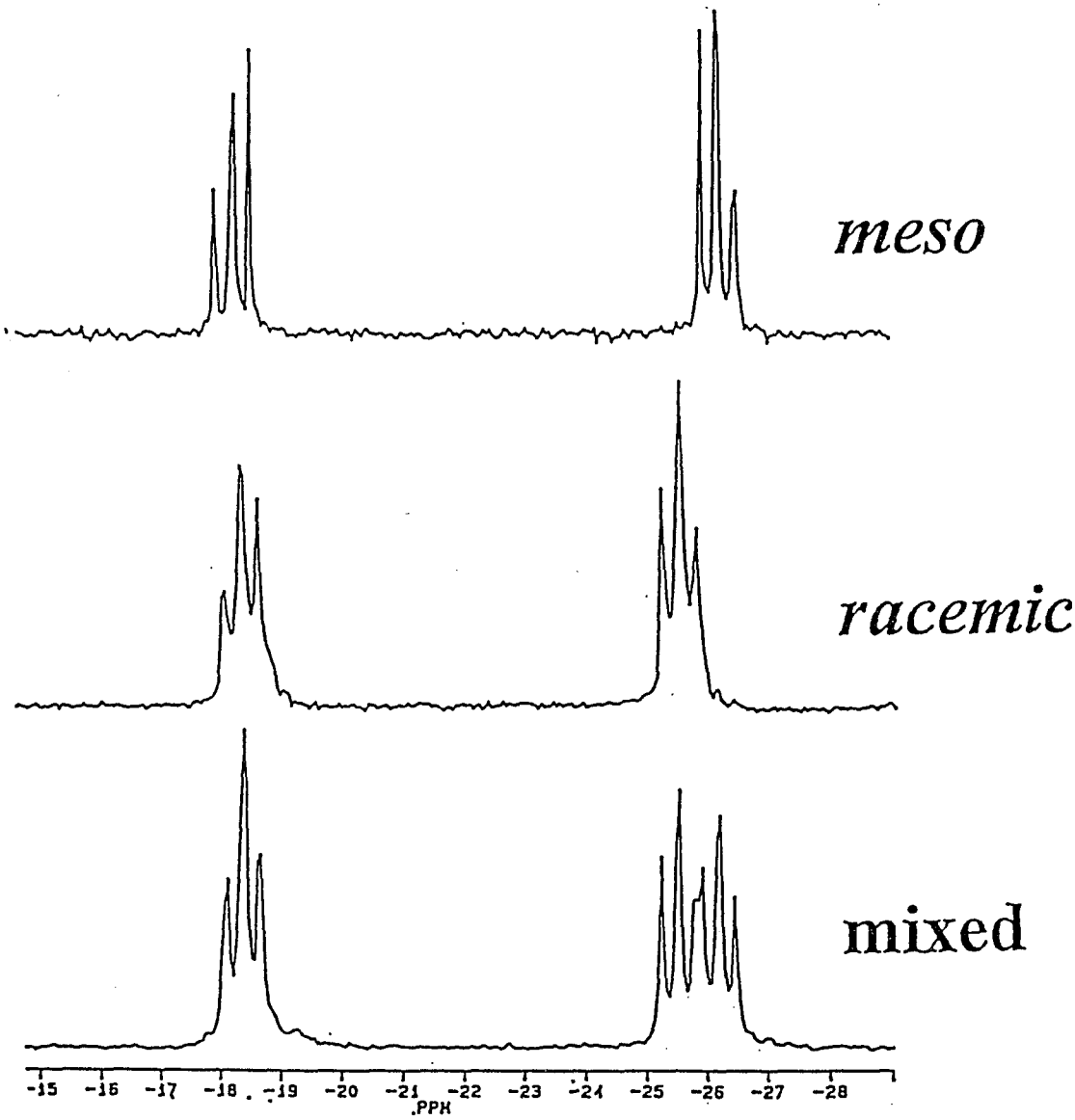

Figure 6. $^{31}P\{H\}$ NMR of *mixed*- et,ph-P4 as contrasted with $^{31}P\{H\}$ NMR of pure *meso* and *racemic*-et,ph-P4 in C_6D_6 (40.48 MHz).

The successful separation and isolation of diastereomerically *pure* et,ph-P4 ligand accomplished our first and primary goal. The diastereomeric mixture of et,ph-P4 was known to yield a good hydroformylation catalyst on complexation withrhodium.[13] However, it was not clear which diastereomer, *meso* or *racemic*, or both was the active catalytic species. By separating and isolating these diastereomers, individual hydroformylation performances could be evaluated.

The *racemic*-et,ph-P4 (**1r**) or *meso*-et,ph-P4 (**1m**) ligands were treated with two equivalents of $[Rh(nbd)_2](BF_4)$ (nbd = norbornadiene) to produce the bimetallic complex $[Rh_2(nbd)_2(et,ph\text{-}P4)](BF_4)$ (*racemic* **2r**, *meso* **2m**). Details on the synthetic procedures are discussed in the experimental section. Figure 7 illustrates an ORTEP of *racemic*-$[Rh_2(nbd)_2(et,ph\text{-}P4)](BF_4)_2$.[16] The two norbonadienes are syn to each other. The phenyl and ethyl groups have been removed for clarity. Once again, it is evident that et,ph-P4 is a good bridging and chelating ligand capable of keeping two metal centers in general proximity, a basic prerequisite for bimetallic cooperativity.

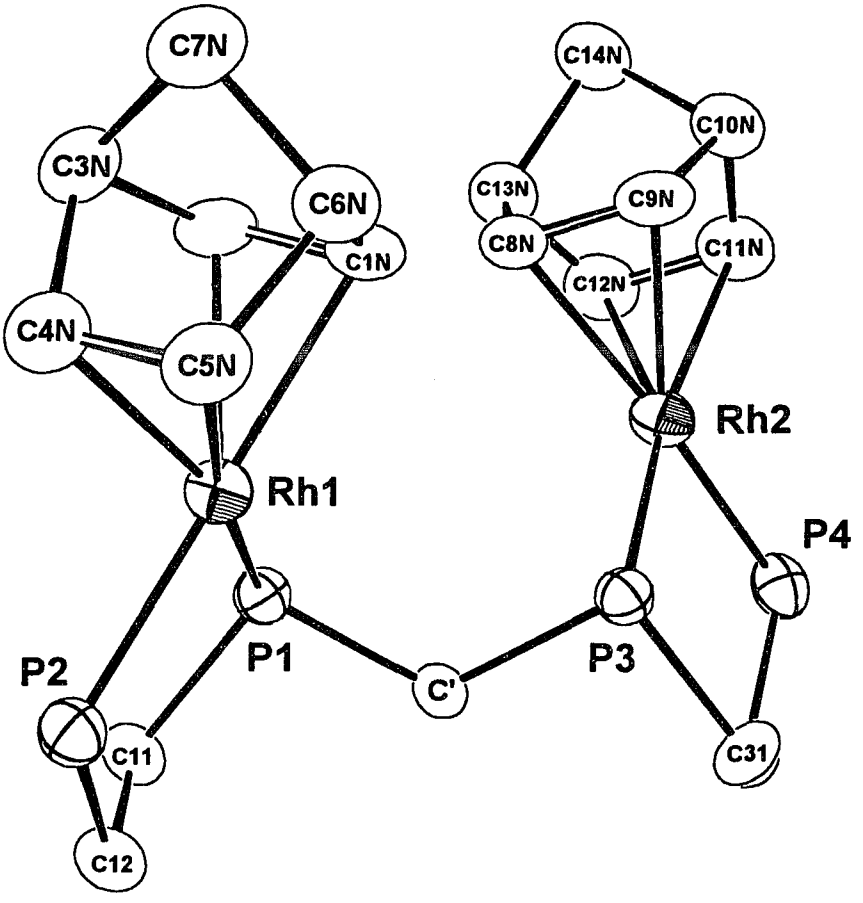

Figure 7: The ORTEP of *racemic*-$[Rh_2(nbd)_2(et,ph\text{-}P4)](BF_4)_2$. The phenyl groups on P1 and P3, as well as ethyl groups on P2 and P4 have been omitted for clarity

Chapter 4 Catalytic Hydroformylation of 1-Hexene

4.1 Introduction

The *meso*- and *racemic*-et,ph-P4 dirhodium catalyst systems (**2r** and **2m**) were evaluated to determine which one is the more active catalyst. The rates, selectivities (linear to branched aldehyde produced), and amount of side-products were investigated.[17]

4.2 Hydroformylation Runs

The hydroformylation of 1-hexene with individual *meso* and *racemic* catalyst precursors, $[Rh_2(nbd)_2(et,ph\text{-}P4)](BF_4)$, (*meso* **2m**, *racemic* **2r**) was studied alongside the commercial Rh/PPh_3 catalyst system using the apparatus illustrated in Figure **8**. Stainless steel high-pressure Parr autoclaves of 150 mL capacity were used for the reactions. These autoclaves can withstand high pressures up to 3000 psi.

Each autoclave was connected to a Parr 4850 computerized controller which controls and monitors the temperature and stirring rate (rpm's) within the autoclave. A regulator in-line with the gas reservoir cylinder delivers a constant pressure of the 1:1 mixture of H_2 and CO gas to the autoclave; any gas uptake and pressure decrease in the autoclave due to catalysis is offset via this regulator system and monitored by the Parr controller. All runs are done at constant pressure. The pressure decrease in the reservoir cylinder is monitored by electronic transducers and relayed to the controller. All data are stored internally on the controller by a RAM disk and eventually transferred for data workup to a personal computer.

A small addition cylinder is attached to the autoclave to add the olefin into the reaction vessel. At least four duplicate runs were made for each catalyst. The initial turnover rates were calculated by determining the initial slope of the aldehyde production curve plotted against time. The reaction products were characterized by ^1H NMR spectroscopy and by GC analysis. The **2r** or **2m** was weighed out in the glove box and brought out in a Schlenk line on the bench top. Dry acetone solvent was

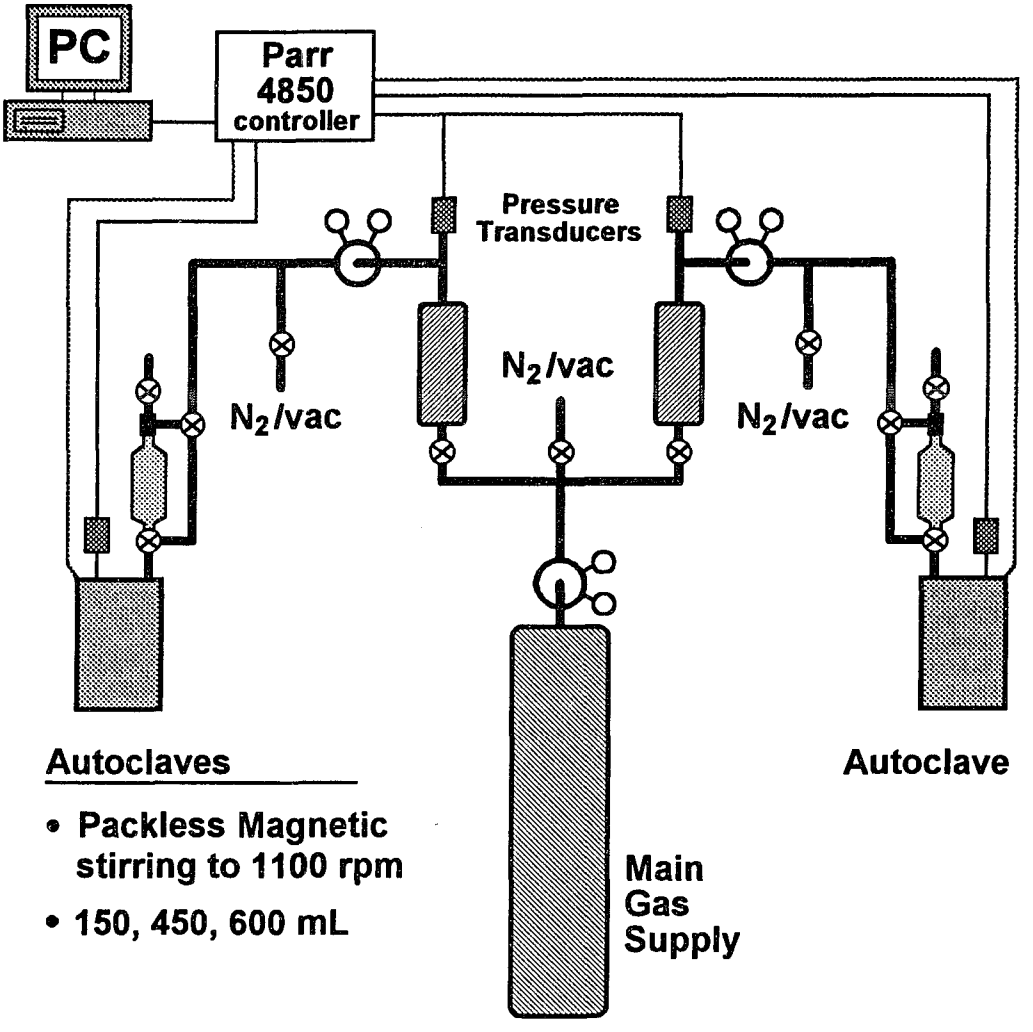

Figure 8. Schematic view of laboratory apparatus to perform hydroformylation reaction.

degassed and added to the flask via a cannula and the catalyst readily dissolved. This solution was then added to an evacuated autoclave system ready for pressurization and temperature ramp. The commercial catalyst Rh/PPh_3 [$Rh(CO)_2(acac)$ with 0.82 M PPh_3] was treated in a similar fashion.

4.3 Results of Hydroformylation of 1-Hexene

Figure 9 shows the number of equivalents of aldehyde[18] produced by hydroformylation catalysts employing Rh/PPh_3, *meso*-or *racemic*-$[Rh_2(nbd)_2(et,ph\text{-}P4)]^{2+}$ in the catalyst system. The turnover rates, selectivities of aldehydes produced, and amount of alkene isomerization of each catalyst system are compared in Table 5.

Based on the initial turnover rate, the *racemic* catalyst is 12 times faster than the *meso* catalyst, and 40% faster than the commercial Rh/PPh_3 catalyst based on the rate constant. This is remarkable since no catalyst exists today in the literature that is better from a rate and selectivity basis than the commercial Rh/PPh_3 catalyst. The *racemic* bimetallic catalyst is also more selective to linear aldehyde product than the *meso*.

The proposed catalyst, $Rh_2H_2(CO)_2(et,ph\text{-}P4)$ (**3r**), formed from addition of H_2 and CO to **2r** and overall bimetallic mechanism is shown in Scheme **6**. **3r** essentially acts as a conventional monometallic hydroformylation catalyst until it reaches the acyl intermediate via the following steps: a) coordination of alkene to **3r** makes **4r**; b) alkene insertion into the R-H bond gives the linear (or branched) alkyl species **5r**; c) coordination of CO, followed by CO insertion into the Rh-alkyl bond to yield the acyl complex **6r**. This is where the rotational flexibility of the et,ph-P4 ligand comes into play. The bimetallic acyl intermediate, *racemic*-Rh(acyl)(CO)(et,ph-P4)RhH(CO), can readily rotate about the central methylene bridge to form a doubly bridged intermediate species, **7r**; d) an *intra*molecular-hydride transfer from the carbonyl-bound rhodium to the acyl-bound rhodium is followed by reductive elimination of aldehyde and formation of **8r**. The isolation of **8r** has provided

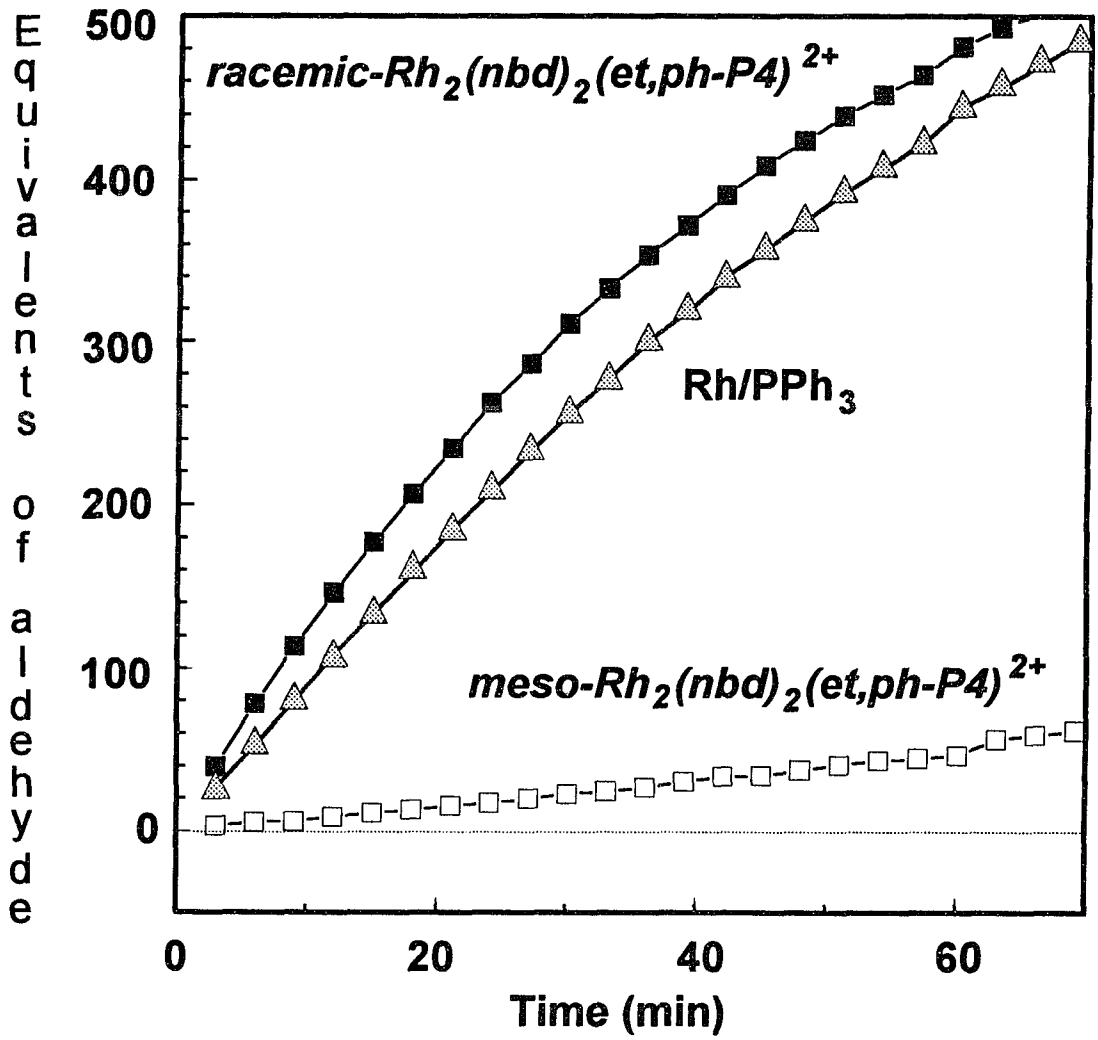

Rh/PPh_3 = $Rh(acac)(CO)_2$ with 0.82 M PPh_3

Figure 9: The hydroformylation of 1-hexene by Rh/PPh_3, *meso*- and *racemic*-$[Rh_2(nbd)_2(et,ph\text{-}P4)](BF_4)_2$ are grouped together by the number of equivalents of aldehyde produced per equivalent of catalyst versus time (/min) at 90°C, 90 psi, 1:1 H_2/CO

Table 5: Hydroformylation of 1-hexene in acetone at 90°C / 90 psi, 1:1 H_2/CO.

Catalyst precursor	Initial TO/(min)	k_{obs}† (min^{-1})	Aldehyde l:b ratio	% isom	% hydro
racemic-CAT	10.6(5)	0.0238(8)	27.5(8)	8(1)	3.4(3)
Rh/PPh_3#	9(1)	0.016(2)	17(2)	2.5(4)	2.8(3)
mixed-CAT*	4.1(1)	0.0102(11)	20.5(6)	9.8(2)	4.5(1)
meso-CAT	0.9(1)	--‡	14(2)	4.1(7)	2.3(3)

CAT = $Rh_2(nbd)_2(et,ph\text{-}P4)](BF_4)_2$
# Rh/PPh_3 = $Rh((acac)CO)_2$ with 0.82 M PPh_3
* *mixed* refers to approximately 1:1 mixture of *racemic* and *meso* in et,ph-P4 ligand.
† pseudo first order rate constant based on gas uptake; 1 mM catalyst concentration; average of at least The rates were obtained from the slope of a plot of *ln*(Δ pressure) versus time.4 runs.
‡ Rate constant for *meso*-catalyst could not be accurately calculated due to the slowness of the reactions and associated side reactions.

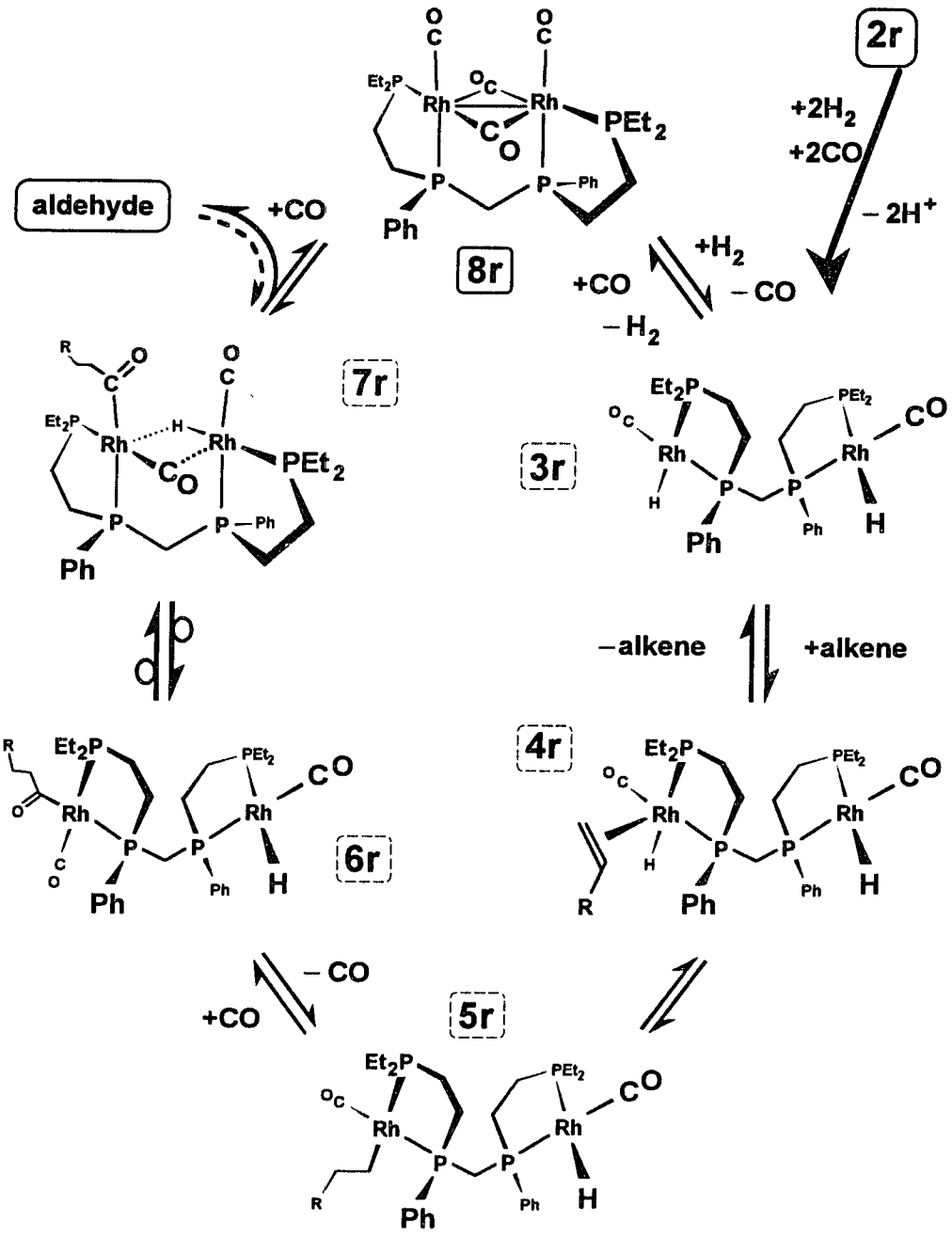

Scheme 6: Proposed mechanism for bimetallic hydroformylation

a key insight into the proposed mechanism;[19] Finally, e) addition of H_2 to **8r** generates **3r**.

Homobimetallic cooperativity, specifically, an *intra*molecular hydride transfer from one metal center to the other is a plausible explanation for the increased rate in our catalyst system. If we are to propose an intramolecular hydride transfer then the two rhodium centers in the bimetallic Rh_2(et,ph-P4) unit must be able to closely approach each another.

Stick models of the *racemic* and *meso* bimetallic species **7r** and **7m** are illustrated in Figure **10**. They are based on molecular modeling studies using the SYBYL program set[20,21] which help explain the differences in activity between **3r** and **3m**. The bimetallic acyl intermediate, *racemic*-Rh(acyl)(CO)(et,ph-P4)RhH(CO), **6r**, can readily rotate about the central methylene bridge to form a doubly bridged intermediate species, **7r**. The CO ligand on the acyl-bound rhodium can bridge to the hydride-bound rhodium, while the hydride bridges to the acyl-bound rhodium.

Only the *racemic* diastereomer can adopt this doubly-bridged intermediate species to facilitate the intramolecular hydride transfer step. The donation of π electron density from the bridging CO in **7r** will lower the energy of the formally 3-coordinate, high energy rhodium center remaining after the hydride is transferred to the acyl-bound rhodium.The *meso* analog, **7m**, however, can only form a single bridge via the hydride to the acyl-bound rhodium center. The CO ligand is oriented unfavorably to bridge to the acyl-bound rhodium. We believe that the second bridging interaction, present in the *racemic* complex, favors the intramolecular hydride transfer by stabilizing the Rh-H bond breaking step.

The second bridging interaction in **7r** has another important advantage. The subsequent reductive elimination step generates a relatively high energy Rh(-1) oxidation state on one metal center. The close proximity of the second rhodium atom

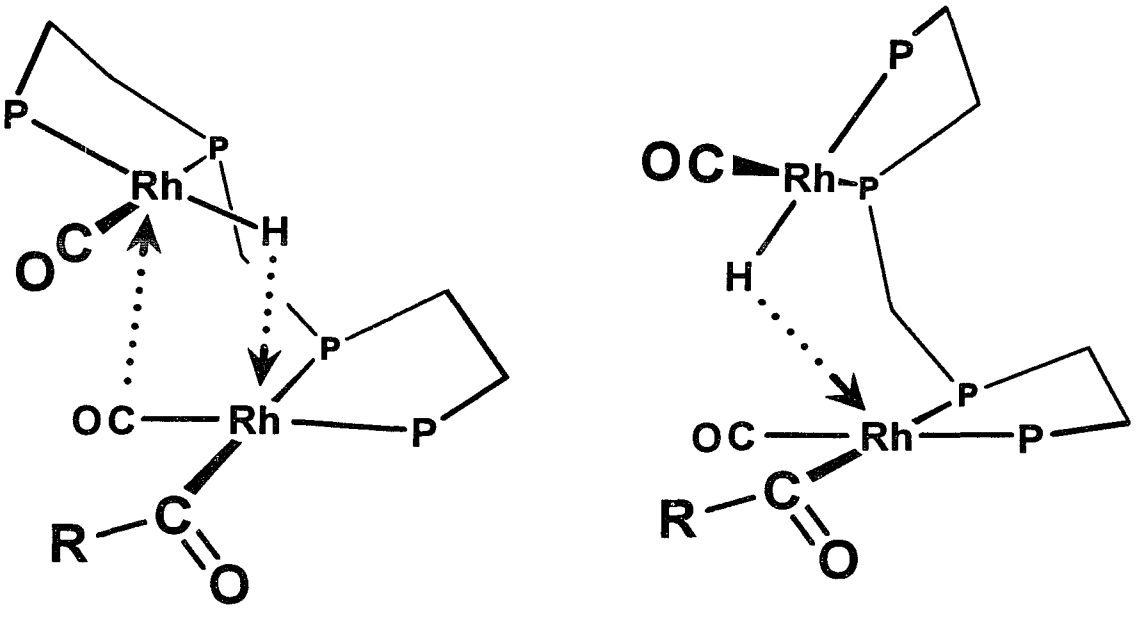

Figure 10. *Racemic*-$Rh_2H(acyl)(CO)_2$(et,ph-P4) and *meso*-$Rh_2H(acyl)(CO)_2$(et,ph-P4)

in a +1 oxidation state will favor electron transfer to give two Rh(0) centers with an energy lowering Rh-Rh bond to produce **8r**.

These results provide very strong, internally consistent evidence that our mechanism is fundamentally correct. The catalytic runs on each pure diastereomer confirm the molecular modeling predictions: *The racemic catalyst is the substantially more active species.*

4.4 Selectivity

Hydroformylation reactions produce a mixture of linear and branched aldehydes. However, linear aldehyde is the principal and most desired product of hydroformylation. Isomer control of hydroformylation (as is indicated by selectivity) is of great economic value and is the motivating force behind ligand, reaction parameters, pH and mechanism effects.

The 1-hexene converts to heptanal (linear) and 2-methylhexanal (branched) with a selectivity of 28:1 when catalyzed with the *racemic*-bimetallic catalyst, **2r**. Heptanal, the desired product can be converted to 1-heptanol which is mainly used to make plasticizers. The 2-methylhexanol, in contrast, has less industrial value than 1-heptanol. The *racemic*-$[Rh_2(nbd)_2(et,ph\text{-}P4)](BF_4)_2$ offers one of the highest linear selectivities for hexene hydroformylation reported to date.

Free energy calculations using Eyring equation,[22] [Eqn. (6)], indicate a 2.40 kcal/mole preference for the coordination of alkene to the rhodium center of **3r** to give the linear product.

$$\Delta G^{\ddagger}_{b} - \Delta G^{\ddagger}_{l} = RT\ln(k_l/k_b) \qquad (6)$$

The product regioselectivity has also been examined in more detail by performing molecular dynamics minimizations on a propylene molecule docked to **3r**. These docking studies estimate a 7.5 kcal/mol preference to give the linear product. This result is qualitative as molecular modeling only provides information on steric factors in the **3r**-propylene complex. Regioselectivity arises from energy differences in

transition states, where many steric and electronic effects operate. Attributing the origin of the aldehyde regioselectivity to the initial alkene coordination step (**3r** to **4r**) assumes that all (or most) regioselectivity arises from the alkene coordination and/or alkene insertion into the Rh-H bond.

4.5 Secondary Products

Two equivalents of HBF_4 are produced under the reaction conditions to generate the proposed active catalyst species, *racemic*-$Rh_2H_2(CO)_2$(et,ph-P4), **3r** from *racemic*-$[Rh_2(nbd)_2$(et,ph-P4)$](BF_4)_2$ as shown above in Scheme **6**. The presence of acid in the reaction mixture results in both alkene isomerization and hydrogenation.

Alkene isomerization is the major side product (8 %) of the hydroformylation of 1-hexene as shown in Table **9.** Indeed, alkene isomerization is well known to occur under hydroformylation conditions as a consequence of double bond shifts.[23] Scheme **7** illustrates the origin of our acid-catalyzed alkene isomerization side-reaction. The terminal double bond shifts position to an internal site, and the process is especially common in alkenes of higher chain lengths.

Hydrogenation is a side reaction also caused by the production of HBF_4. Scheme **8** shows a proposed acid catalyzed hydrogenation side-reaction for a typical rhodium-based catalyst system. The aldehyde product contains about 3-4 % alkanes formed by hydrogenation reactions.

Addition of 2 equivalents of a neutral base, such as Et_3N, resulted in a drop in the isomerization to 1.5%, and increased the product regioselectivity for **3r** to over 30:1. Unfortunately the amine bases used so far slow the catalyst somewhat due to what we believe is competitive binding to the rhodium centers.

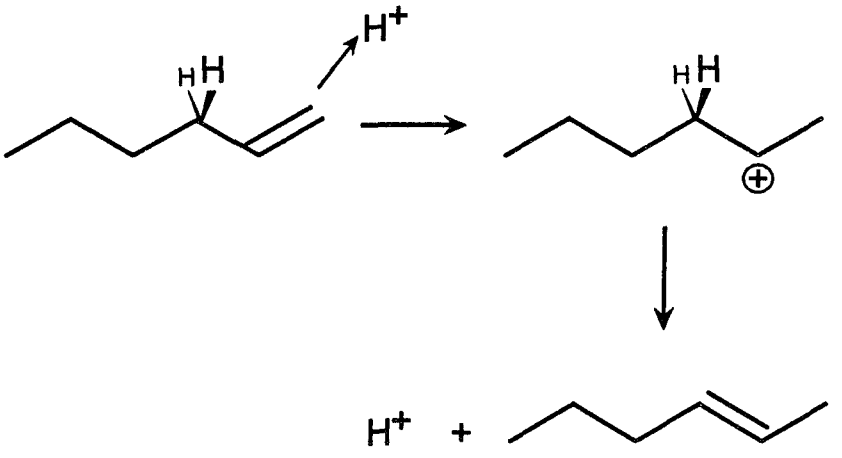

Scheme 7: Acid catalyzed alkene isomerization sidereaction.

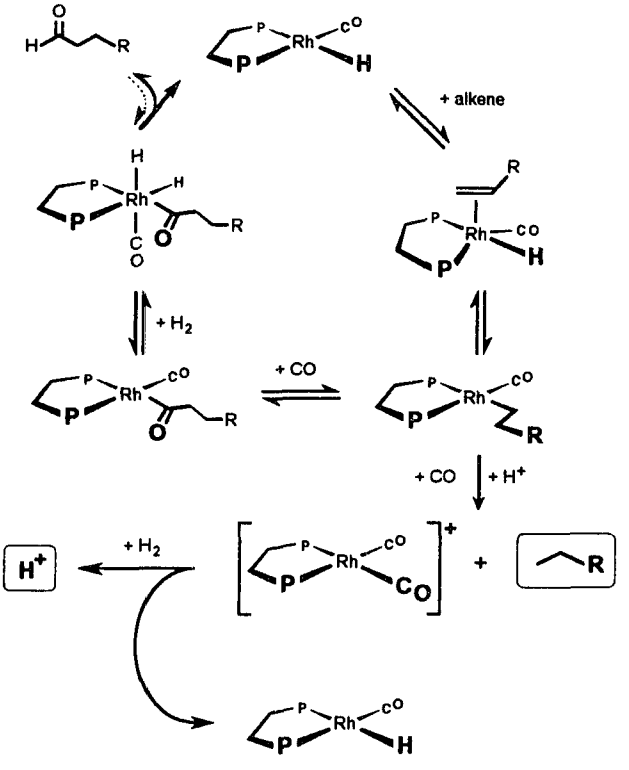

Scheme 8: Acid catalyzed hydrogenation sidereaction.

Chapter 5 Asymmetric Hydroformylation

5.1 Introduction

Our molecular modeling docking studies indicated that the *racemic*-$Rh_2H_2(CO)_2$(et,ph-P4) catalyst should have enough of an asymmetric environment sufficient to induce considerable enantioselectivity in the proper substrate. Docking the two different faces of propylene in the branched orientation to one exo face of our bimetallic catalyst gives a calculated energy difference of 2.5 kcal/mol. This corresponds to a hypothetical *ee* of ~ 98%. Hence, the rationale in separating *racemic et,ph-P4* into individual (*S,S*) and (*R,R*)-et,ph-P4 enantiomers. Separated and pure enantiomers of et,ph-P4 could then be used to prepare optically active (*S,S*) or (*R,R*)-$[Rh_2(nbd)_2$(et,ph-P4)$](BF_4)_2$ catalyst precursors.

Enantioselective catalytic synthesis promoted by chiral transition metal complexes has become more important and popular in recent years since the availability of enantiomerically pure compounds became necessary for the total synthesis of natural products. Today, with the heightened interest in stereochemistry in most branches of chemistry, biochemistry ,and pharmacology, there is even more urgent need for better methods of synthesizing pure enantiomers. One chiral catalyst molecule can potentially create millions of chiral product molecules, just as enzymes do in biological systems. Additionally, *catalytic* asymmetric synthesis has significant economic advantages over stoichiometric asymmetric synthesis in industrial scale production of optically active organic products.

Following success in achieving high efficiencies in asymmetric hydrogenation,[24] attention has turned to applying asymmetric catalysis to other reactions such as hydroformylation.[25] Enantioselectivity is expressed as *enantiomeric excess (ee)* which is defined as:

$$ee = \frac{|R-S|}{R+S} \times 100\%$$

There are a number of reports of asymmetric hydroformylation reactions of olefins with chiral catalysts, particularly those involving rhodium complexed to optically active phosphine ligands.[26] Reactions and applications of homogeneous catalysts that rely on their selectivity have become desirable and most challenging, some of which are discussed in the reviews by Parshall and Nugent.[27]

A practical application of asymmetric catalysis can be well illustrated by the proposed synthesis of (*S*)-ibuprofen and (*S*)-naproxen. The (*S*)-ibuprofen is a well known pain reliever in pharmaceutical products. It is, however, marketed as a *racemic* mixture since the (*R*)-ibuprofen has no proven adverse side effects. The (*S*)-naproxen is a very potent prescription pain reliever as well as a good antiinflamatory drug. (*R*)-naproxen, on the other hand, is a potent liver toxin. The need to use optically pure (*S*)-naproxen, therefore cannot be overemphasized. Presently it is recrystallized from the racemic mixture. By designing a suitable asymmetric hydroformylation catalyst, a more direct and efficient route to these pharmaceuticals can be established as shown in scheme **9**.

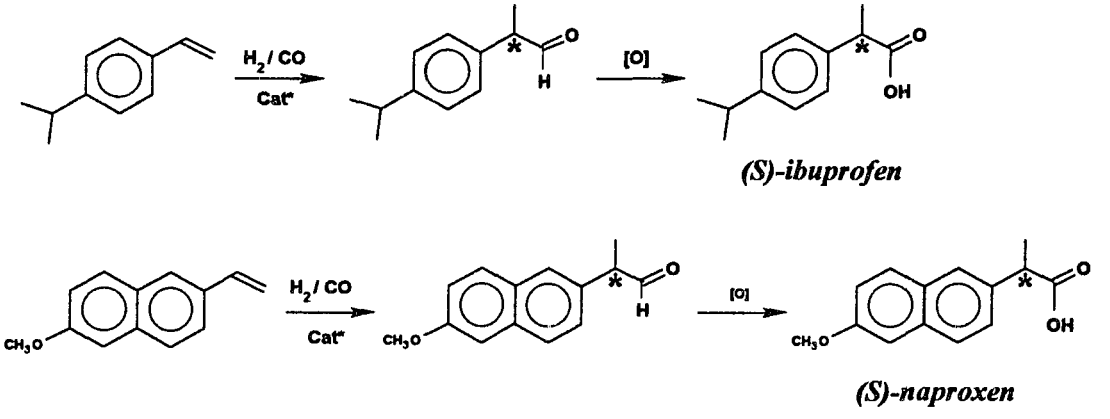

Scheme **9.** Asymmetric hydroformylation of vinylarenes.

Of particular interest to us is the production of chiral branched 2-acetoxypropanal, a precursor in the synthesis of the amino acid threonine (2-amino-3-hydroxybutanoic acid) by the Strecker Synthesis as shown in Scheme **10**. Of the four

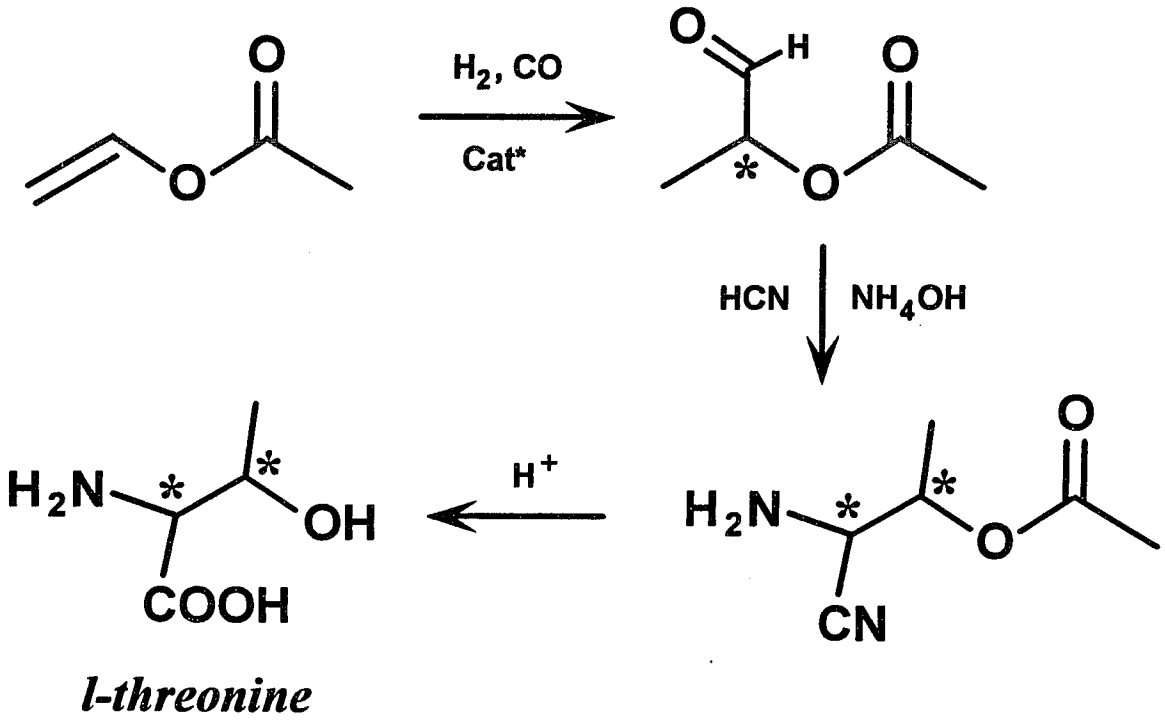

Scheme **10:** Asymmetric hydroformylation of vinyl acetate

stereoisomers of 2-amino-3-hydroxybutanoic acid, only *l*-threonine is an essential component in human nutrition and is not synthesized by the human body (it is commonly obtained from dairy products). Chiral rhodium catalysts of each et,ph-P4 enantiomer could potentially asymmetrically hydroformylate vinyl acetate to give the appropriate optically active 2-acetoxypropanal with high enantiomeric excess and regioselectivity.

5.2 Theory in Separation of Enantiomers

A high performance liquid chromatograph (HPLC) equipped with chiral column packing material was used to resolve the *racemic*-et,ph-P4 enantiomers on both analytical and semi-preparative scale. The first commercially available HPLC Chiral Stationary Phase (HPLC-CSP) was introduced by Pirkle in 1981 and it utilized a combination of π acidity, hydrogen bond receptor sites, hydrogen bond donor sites, and steric interactions for chiral differentiation purposes.[28]

Unlike conventional column packings, the stationary phase on the support material of these HPLC-CSPs column packings contains a chiral, optically pure residue. Chromatographic separation of enantiomeric molecules is made possible by virtue of their differential diastereomeric molecular interactions between each enantiomorph of the solute and the optically pure (chiral) selector bound to the chromatographic support (stationary phase). The stereochemical resolution of two enantiomeric solutes is, therefore, a reflection of the relative stabilities between the two diastereomeric complexes.[29]

5.3 Isolation of (*S,S*) and (*R,R*) enantiomers of *Racemic*-et,ph-P4

A commercially packed semi-preparatory chiral HPLC column was employed for bulk separations of the individual enantiomers of et,ph-P4. Sample concentration of 100 mg/mL in hexane was loaded directly onto the column from oxygen-free sealed vials at room temperature. The mobile phase was composed of 2-propanol/hexane solvent mixture (5/95 v/v). The eluted materials were collected in Schlenk flasks which

were continually purged with nitrogen. The resolution spectrum for the first eluate (enantiomer **1**) and the second eluate (enantiomer **2**) is shown in Figure **11**.

Figure **11:** Chiral HPLC resolution of enantiomers of *racemic*-et,ph-P4

The separated chiral ligands were then transferred into a glove-box and the solvents removed by vacuum evaporation. The overall purity of each enantiomer was determined by reinjection into the chiral HPLC column and by $^{31}P\{^{1}H\}$ NMR spectroscopy.

Specific optical rotation, [α], in angular degrees for the pure (*S,S*)) and (*R,R*)-et,ph-P4 ligands was determined by polarimetry techniques and calculated by using the formula:

$$[\alpha]_D^t = \frac{\alpha}{cl} \times 10000$$

where α is the angular rotation of sample, *c* is the sample concentration in g/100 mL and *l* is the length of sample cell, *D* represents the wavelength of sodium D lamp light (589 nm) and, *t* is the temperature in °C.

The sign and magnitude of optical rotation depends on temperature and solvent as well as the wavelength of the incident light. Whenever possible, specific rotations were measured in the same solvent, at the same wavelength and temperature, and at similar concentrations. In addition both measurements were made during the same general period of time.

Enantiomer **1** afforded a $[\alpha]_D^{21}$ of -71.0° (*c*1.9, hexane), and was identified as the (–)-et,ph-P4, whereas enantiomer **2** gave a $[\alpha]_D^{21}$ of + 87.6° (*c*1.9, hexane), and was identified as (+)-et,ph-P4 (the assignment as (*S,S*) or (*R,R*) could not be made directly but polarimeter properties of aldehyde products were compared with literature values for hydroformylation of vinyl acetate *vida infra*).[30]

Each enantiomer was treated with two equivalents of $Rh(nbd)_2(BF_4)_2$ in CH_2Cl_2 to give the optically active $[Rh_2(nbd)_2(et,ph\text{-}P4)](BF_4)_2$ catalytic system. The numerical optical rotation values obtained for these catalysts from polarimeter readings indicated the presence of impurities and, therefore, are not reported here. Figure **12** shows the $^{31}P\{^1H\}$ NMR for the chiral catalyst, (-)-$[Rh_2(nbd)_2(et,ph\text{-}P4)](BF_4)_2$, prepared using (-)-et,ph-P4 enantiomer. The external phosphorus centers resonate as dd at δ = 58.9 ppm ($J_{Rh\text{-}P}$ = 151.2 Hz, $^3J_{P\text{-}P}$ =23.0 Hz). Internal phosphorus centers resonate as dd at δ = 45.4 ppm ($J_{Rh\text{-}P}$ =164 Hz; $^3J_{P\text{-}P}$ = 20.5 Hz). The chemical shift of the internal phosphorus is unexpectedly more upfield by 3.6 ppm than those for $[Rh_2(nbd)_2(et,ph\text{-}P4)](BF_4)_2$ (with diastereomeric mixture of *meso* and *racemic* et,ph-P4), which are at 49.0 ppm (1P, dm, $J_{Rh\text{-}P}$ =158.1 Hz), and 49.7 ppm (1P, dm, $J_{Rh\text{-}P}$ = 153.8 Hz).[31]

The (+)-et,ph-P4 was similarly used to synthesize the chiral catalyst precursor (+)-$[Rh_2(nbd)_2(et,ph\text{-}P4)](BF_4)_2$. The $^{31}P\{^1H\}$ NMR spectrum of (+)-$[Rh_2(nbd)_2(et,ph\text{-}P4)](BF_4)_2$ is shown in Figure **13**. The chemical shifts and the $J_{P\text{-}P}$ coupling constants are very similar to those of (-)-$[Rh_2(nbd)_2(et,ph\text{-}P4)](BF_4)_2$ and the resonances in the $^{31}P\{^1H\}$ NMR are only shifted by a few tenths of a ppm. External

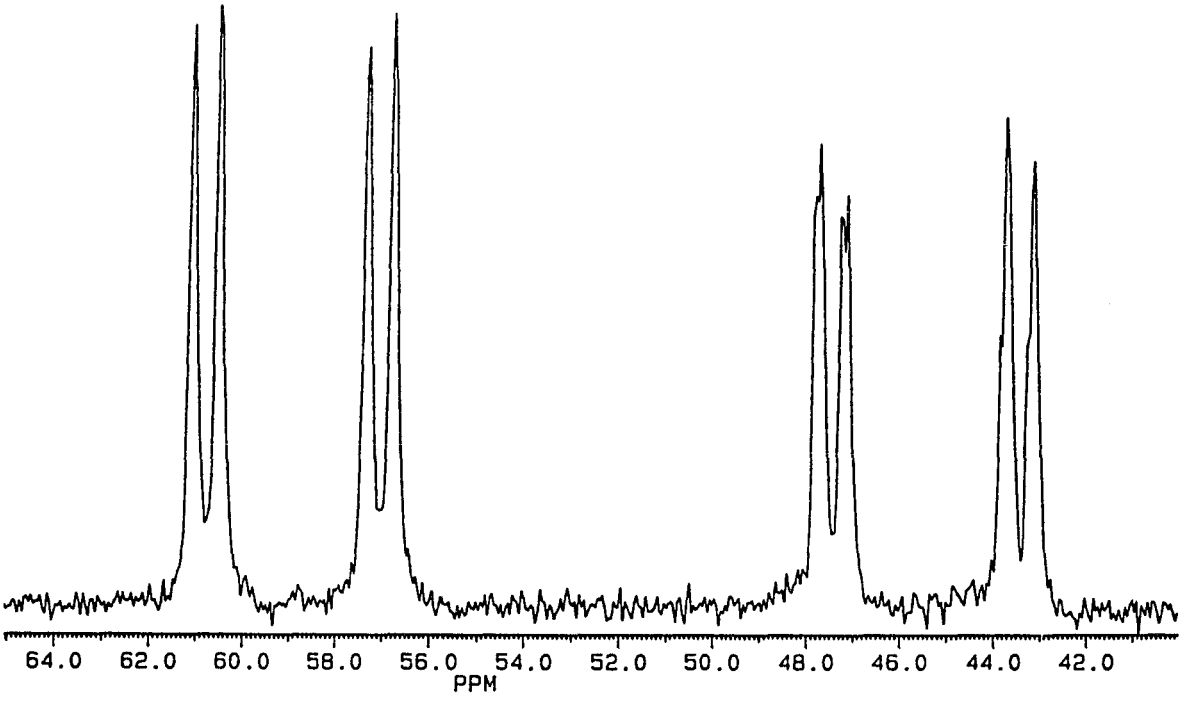

Figure 12: The $^{31}P\{^{1}H\}$ NMR of (-)-$[Rh_2(nbd)_2(et,ph\text{-}P4)](BF_4)_2$ in acetone-d_6 (40.48 MHz).

phosphorus atoms show a dd at 58.8 ppm ($J_{Rh\text{-}P}$ = 151.1 Hz, $^3J_{P\text{-}P}$ = 23.9 Hz), while the internal phosphorus centers show a dd at 45.4 ppm ($J_{Rh\text{-}P}$ = 166.1 Hz, $^3J_{P\text{-}P}$ = 23.5 Hz).

These chiral catalysts were used for the asymmetric hydroformylation of vinyl acetate. Optical rotations were measured in acetone using aldehyde product samples purified by trap-to-trap vacuum distillation. The aldehydes were initially identified by GC analysis and confirmed by NMR studies. (-)-2-acetoxypropanal was produced during hydroformylation with (-)-$[Rh_2(nbd)_2(et,ph\text{-}P4)](BF_4)_2$ catalyst system, whereas (+)-2-acetoxypropanal was produced with (+)-$[Rh_2(nbd)_2(et,ph\text{-}P4)](BF_4)_2$.

The (-)$[Rh_2(nbd)_2(et,ph\text{-}P4)](BF_4)_2$ catalyst gave branched/linear product aldehyde ratio of 9:1 with an *ee* of 90.6%. The presence of linear aldehyde product was suspected to be due to *meso-* catalyst impurities since pure *racemic* catalyst exhibits very high (>200:1) branched to linear regioselectivity (Figure 14). The hydroformylation was repeated with recrystallized (+)-$[Rh_2(nbd)_2(et,ph\text{-}P4)](BF_4)_2$ and afforded ~100% *ee* of the expected branched aldehyde (branched to linear regioselectivity >200:1) as shown in Figure 14. The reactions were carried out with small quantities of catalyst. These results are only preliminary since only a couple of runs were done and effort is being made to separate multi-gram quantities of ligand enantiomers to reproduce and confirm the data. These optical yields represent the highest regioselectivity and enantiomeric excess ever reported in the asymmetric hydroformylation of vinyl acetate.

To date the best enantioselective hydroformylation catalyst in the literature is a $PtCl_2$-$SnCl_2$ system developed by Stille and coworkers using the optically active chelating phosphine ligand BPPM.[32] A few of the prochiral substrates studied and *ee's* for the product aldehydes are given in Table 6. Stille could obtain higher *ee's* by using triethyl orthoformate as a trapping agent to remove the chemically reactive aldehyde. When this was done, > 96% *ee* for the asymmetric hydroformylation of styrene

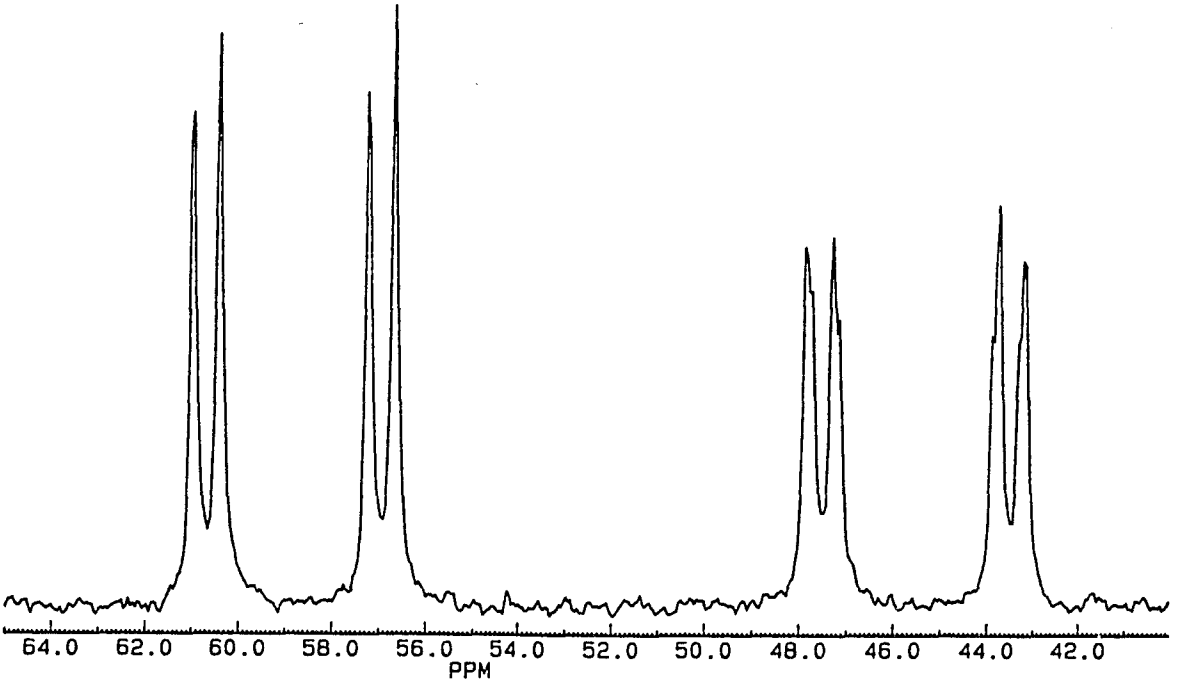

Figure 13: The $^{31}P\{^{1}H\}$ NMR of (+)-$[Rh_2(nbd)_2(et,ph\text{-}P4)](BF_4)_2$ in acetone-d_6 (40.48 MHz).

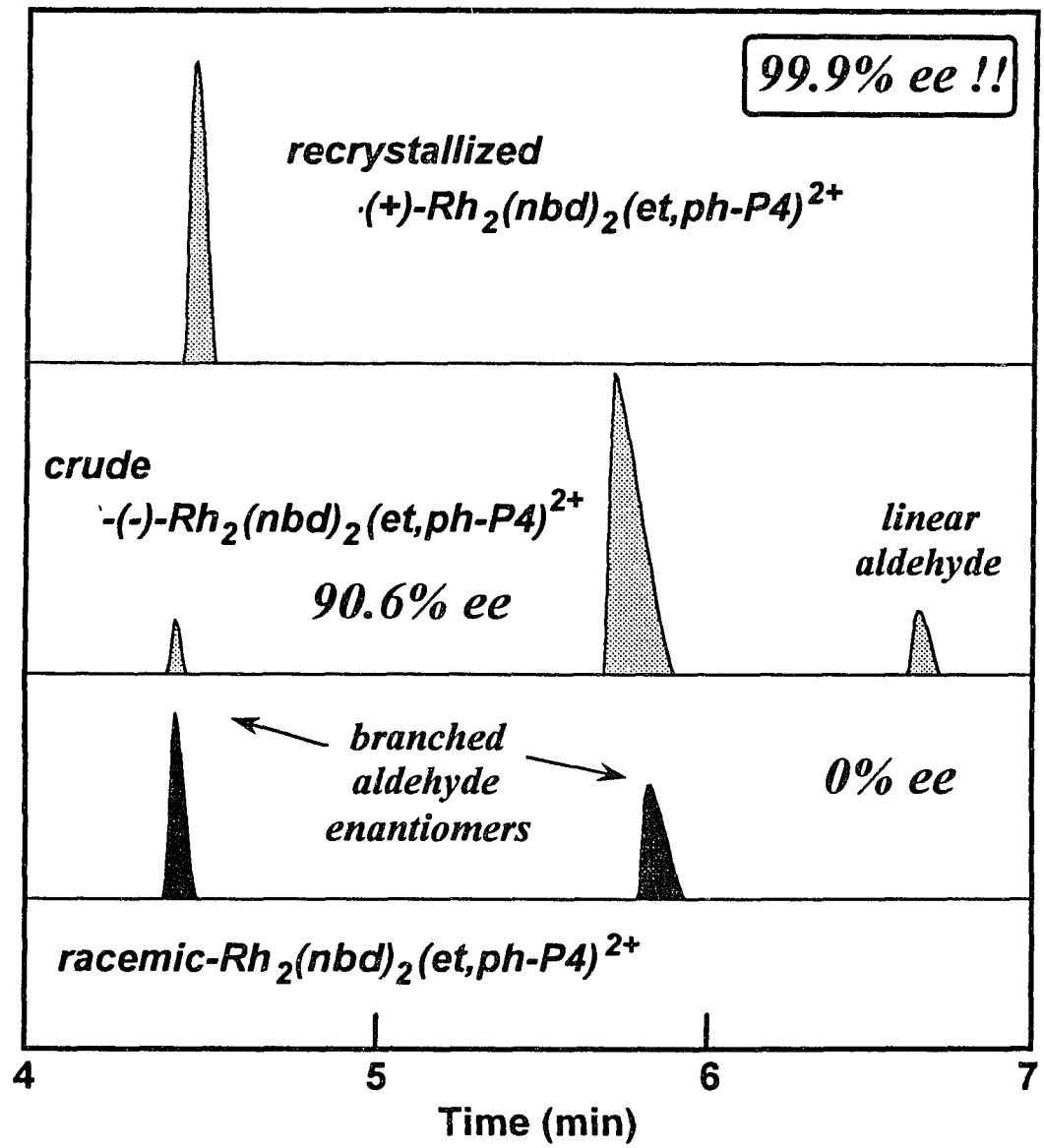

Figure 14: GC results of hydroformylation of vinyl acetate on chiraldex B-TA column at 90° C, 90 psig, 16 hours.

(or vinyl acetate) was found. There are, however, a number of practical problems with this system :

* *low branched to linear ratios (0.5:1)!*
* *a trapping agent was needed to obtain high ee's*
* *very low rates for $PtCl_2$-$SnCl_2$ catalysis*

Table 6: Enantiomeric excess results from Stille's catalyst

Substrate	*ee*
styrene	80%
2-vinylnaphthalene	77%
vinyl acetate	82%

Our catalyst shows far higher regioselectivity, higher catalytic rates and does not need any trapping agents relative to Stille's catalyst. On polymer-supported catalysts for similar reactions, values of 56-61% *ee* are, so far, the highest reported.[33]

Addition of base to the autoclave slows the reaction somewhat but eliminates side-reactions such as isomerization and hydrogenation. 1,4-Diazabicyclo[2.2.2]octane (DABCO) was the base used in these reactions.

Chapter 6 Synthesis, Solubility, and Structures of Model Nickel Phosphine Complexes

6.1. Introduction

Some of our initial work was done with monometallic complexes using ligands which essentially mimic et,ph-P4 in its chelating ability. These ligands will contain phosphorus atoms of similar electron basicities and/or steric bulk. The $Et_2PCH_2CH_2PPh_2$ (dedppe, 1-diethyldiphino-2-diphenylphosphinoethane) ligand was a reasonable bisphosphine model of our binucleating et,ph-P4 ligand system.

The monometallic complex $Ni(NCS)_2(Et_2PCH_2CH_2PPh_2)$ was synthesized by the reaction of one equivalent of $Ni(NCS)_2$ with $Et_2PCH_2CH_2PPh_2$ in EtOH. This was used as a simple model compound to study the chemistry needed to separate the two diasteromers of et,ph-P4.

Two products, $Ni(NCS)_2(Et_2PCH_2CH_2PPh_2)$ and $Ni(NCS)_2[Ph_2PCH_2CH_2P(Et)CH_2CH_2PPh_2)$ readily crystallized in solution. The former dissolved in heptane and acetone, yet remained insoluble in acetonitrile, whereas the latter dissolved only in acetonitrile. This allowed easy separation of the two products and provided a clue for using $Ni(NCS)_2$ as a route in separation of *meso* and *racemic* diastereomers of et,ph-P4. The coordinating properties of the common and similar bisphosphine ligand $Ph_2PCH_2CH_2PPh_2$, dppe, has been investigated by numerous workers.[34]

6.2 $Et_2PCH_2CH_2PPh_2$

$Et_2PCH_2CH_2PPh_2$, (dedppe), was synthesized by Meek's[35] free radical pathway from Ph_2PH and $Et_2PCH{=}CH_2$, using catalytic amounts of 2,2-azobis(isobutyronitrile) as the free radical initiator. In our hands, a 41% yield of dedppe was isolated. Characterization of the colorless dedppe was performed by $^{31}P\{^1H\}$ and ^1H NMR spectroscopy which indicated the presence of an additional phosphine product that could not be readily separated, but the simple $^{31}P\{^1H\}$ NMR

doublet-doublet pattern of dedppe clearly identified it as the major phosphine component.

6.3 $Ni(NCS)_2(Et_2PCH_2CH_2PPh_2)$ and $Ni(NCS)_2(\eta^3\text{-}Ph_2PCH_2CH_2P(Et)CH_2\text{-}CH_2PPh_2)$

The crude dedppe was allowed to react with one equivalent of $Ni(NCS)_2$ in EtOH under inert atmosphere conditions to produce yellow residue and red filtrate. On evaporating the EtOH solution, two air-stable crystal morphologies were produced: a mixture of yellow-brown plates and orange needles.

X-ray structure of the yellow-brown crystals identified them as the expected $Ni(NCS)_2(Et_2PCH_2CH_2PPh_2)$,[36] **1** with the diphosphine ligand coordinated to only one nickel atom. Compound **1** was soluble in heptane and acetone but insoluble in acetonitrile. Its $^{31}P\{^1H\}$ NMR shows two doublet resonances at 83.2 ppm (Et_2P-) and 66.9 ppm (Ph_2P-) which are consistent for chemical shifts for these type of phosphorus atoms. Each doublet has a coupling constant of $J_{P\text{-}P}$ = 77.3 Hz as a result of two inequivalent phosphorus nuclei of spin 1/2 interacting with each other.

The ORTEP plot of the structural determination of $Ni(NCS)_2(Et_2PCH_2CH_2PPh_2)$ is shown in Figure **15**. The thiocyanates are coordinated to the nickel atom through the nitrogen atoms. The Coordination geometry around the nickel(II) center is essentially square planar defined by the bidentate diphosphine ligand and two N-bonded thiocyanato groups. The Ni and the four coordinated atoms all lie within 0.034(2) Å of a common plane. The five-membered chelate ring is puckered with C3 0.406(3) Å and C4 0.130(3) Å out of the coordination plane. The two N-bonded thiocyanate groups are *cis* to each other and form an angle of 93.9 (1)° about Ni.

Thiocyanate coordination is nearly linear, with Ni-N-C angles 170.2 (2)° and 172.4 (3)°, and the P-Ni-P bite angle of the chelating $Ph_2P(CH_2)_2PEt_2$ ligand is 87.05 (3)°. The Ni-P (2.1413 (8), 2.145 (1) Å), and Ni-N (1.876 (3), 1.885 (2) Å), bond

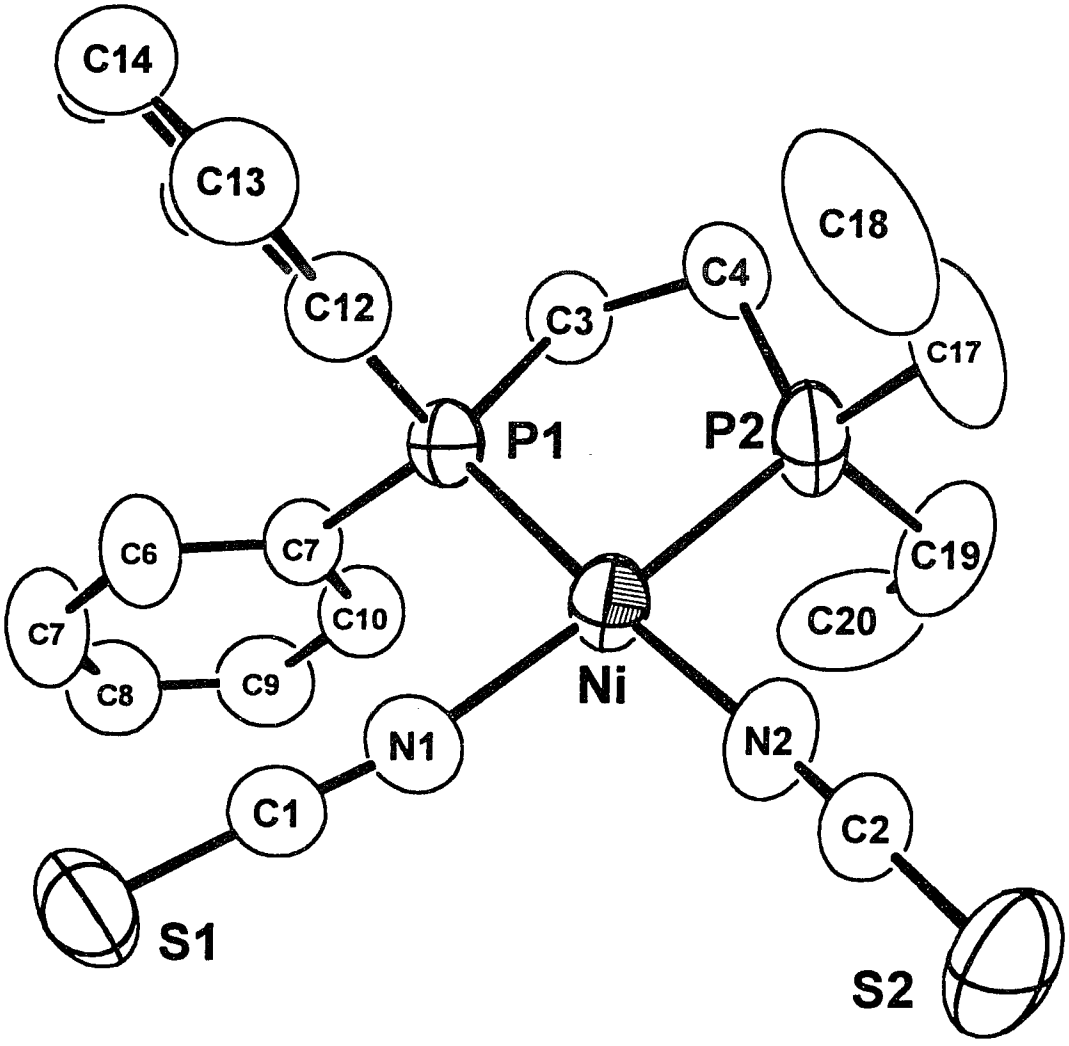

Figure 15: The ORTEP of $Ni(NCS)_2(Et_2PCH_2CH_2PPh_2)$.

distances agree reasonably well with corresponding values obtained for Ni-P (2.178 (3), 2.182 (4) Å), Ni-N (1.864 (12), 1.916 (10) Å) in $Ni(NO_2)_2dppe$[37] and $NiBr_2(dppe)$.[38] Selected bond distances are listed in Table 7. Bond angles are listed in Table 8.

To our surprise, the orange needles were identified by an X-ray crystal structure determination as $Ni(NCS)_2(\eta^3\text{-}Ph_2PCH_2CH_2P(Et)CH_2CH_2PPh_2)$, **2**, as shown in Figure **16**. The tridentate phosphine ligand $Ph_2PCH_2CH_2P(Et)CH_2CH_2PPh_2$ was formed as a rearrangement product in the free-radical ligand synthesis reaction.

The $^{31}P\{H\}$ NMR of **2** shows a triplet resonance at 117.0 ppm ($-CH_2P(Et)-CH_2-$) and a doublet at 53.9 ppm (Ph_2P-) which are as expected for these types of phosphorus atoms. The triplet has a coupling constant of $J_{P\text{-}P}$ = 53.2 Hz as a result of two equivalent phosphorus nuclei of spin 1/2 interacting with the central P atom. The doublet also has a coupling constant of $J_{P\text{-}P}$ = 53.2 Hz. Another doublet resonance observed at 56.7 ppm is probably due to an impurity. Unlike **1**, which is soluble in acetone and heptane, complex **2** is essentially insoluble in these solvents, but is soluble in acetonitrile. This allowed easy separation of the two compounds.

The structure of **2** is best described as a distorted square pyramid, although it could also be considered to be a distorted trigonal bipyramid with P2 and N1 axial. We favor the distorted square pyramid description because of the long Ni-N2 bond distance, 2.088 (7) Å, which is 0.192 Å longer than the Ni-N1 distance of 1.896 (6) Å. This fits well with a square pyramidal geometry and the corresponding electronic structure where the axial ligand should have the weakest metal-ligand bonding.

The Ni-P bond distances are in the normal bonding range with Ni-P1,2,3 = 2.223 (2), 2.150 (2), 2.189 (2) Å. The axial NCS ligand is bent quite substantially with a Ni-N2-C2 angle of 158.1 (6)°. This bending appears to be caused mainly by crystal packing forces since the only close intramolecular contact is between N2 and the

hydrogen atom on C26 with a calculated distance of 2.496 Å. Selected bond distances and angles are listed in Table **9** and Table **10** respectively.

Table 7: Selected bond distances (Å) for $Ni(NCS)_2(Et_2PCH_2CH_2PPh_2)$.[a]

Ni-P1	2.1413(8)	C5-C6	1.369(4)
Ni-P2	2.145(1)	C5-C10	1.390(4)
Ni-N1	1.885(2)	C6-C7	1.393(5)
Ni-N2	1.876(3)	C7-C8	1.362(4)
S1-C1	1.601(3)	C8-C9	1.365(5)
S2-C2	1.605(3)	C9-C10	1.381(4)
P1-C3	1.837(3)	C11-C12	1.384(4)
P1-C5	1.813(3)	C11-C16	1.384(4)
P1-C11	1.810(3)	C12-C13	1.384(5)
P2-C4	1.826(3)	C13-C14	1.366(6)
P2-C17	1.811(4)	C14-C15	1.376(5)
P2-C19	1.826(4)	C15-C16	1.380(5)
N1-C1	1.153(4)	C17-C18	1.510(7)
N2-C2	1.149(4)	C19-C20	1.524(7)
C3-C4	1.509(4)		

[a]Numbers in parentheses are estimated standard deviations in the least significant digits.

Table 8: Selected bond angles (°) for $Ni(NCS)_2(Et_2PCH_2CH_2PPh_2)$.[a]

P1-Ni-P2	87.05(3)	S2-C2-N2	178.5(3)
P1-Ni-N1	89.27(7)	P1-C3-C4	108.8(2)
P1-Ni-N2	175.49(9)	P2-C4-C3	110.5(2)
P2-Ni-N1	176.32(8)	P1-C5-C6	121.8(2)
P2-Ni-N2	89.75(9)	P1-C5-C10	119.3(2)
N1-Ni-N2	93.9(1)	C6-C5-C10	118.8(3)
Ni-P1-C3	110.23(9)	C5-C6-C7	119.9(3)
Ni-P1-C5	116.14(9)	C6-C7-C8	121.6(2)
Ni-P1-C11	109.45(8)	C7-C8-C9	119.3(3)
C3-P1-C5	106.5(1)	C8-C9-C10	120.6(3)
C3-P1-C11	106.7(1)	C5-C10-C9	120.3(3)
C5-P1-C11	107.3(1)	P1-C11-C12	119.5(2)
Ni-P2-C4	111.0(1)	P1-C11-C16	121.6(2)
Ni-P2-C17	115.9(1)	C12-C11-C16	118.9(3)
Ni-P2-C19	109.4(1)	C11-C12-C13	120.1(3)
C4-P2-C17	106.0(2)	C12-C13-C14	120.4(3)
C4-P2-C19	108.3(2)	C13-C14-C15	120.0(3)
C17-P2-C19	105.8(2)	C14-C15-C16	120.3(3)
Ni-N1-C1	170.2(2)	C11-C16-C15	120.5(3)
Ni-N2-C2	172.4(2)	P2-C17-C18	114.6(3)
S1-C1-N1	178.3(2)	P2-C19-C20	112.8(3)

[a]Numbers in parentheses are estimated standard deviations in the least significant digits.

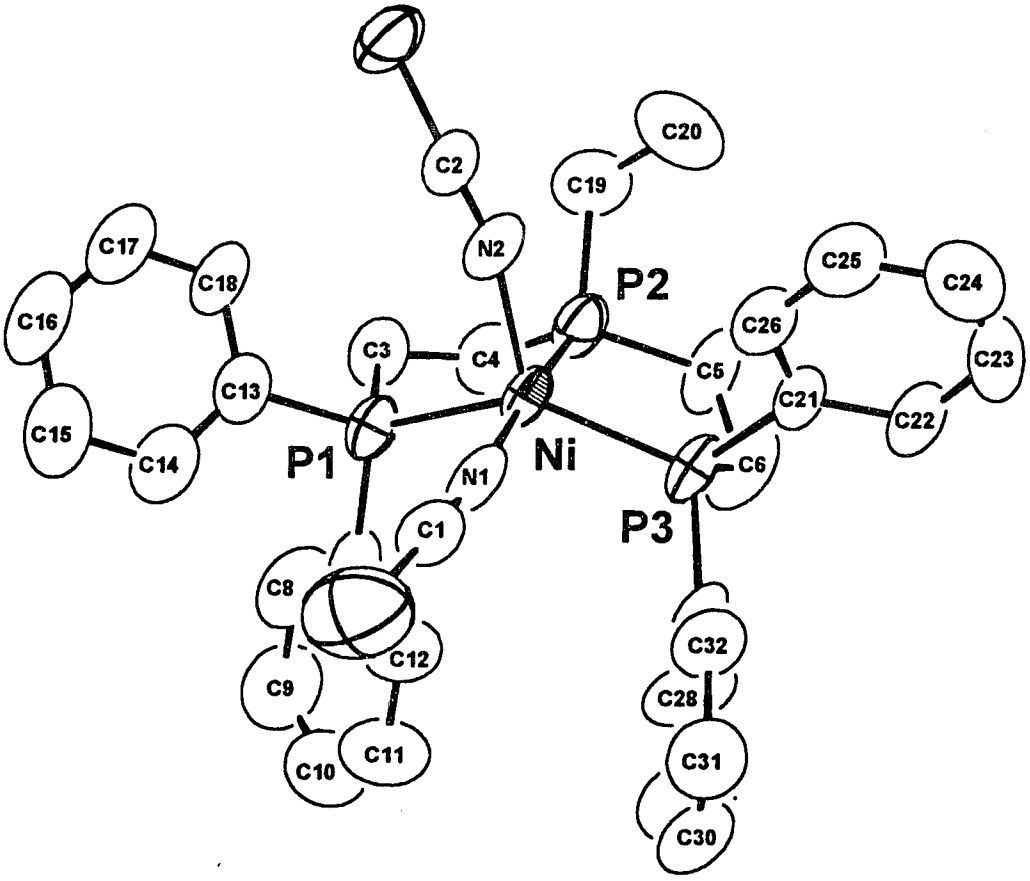

Figure 16. The ORTEP of $Ni(NCS)_2(Ph_2PCH_2CH_2P(Et)CH_2CH_2PPh_2)$

Table 9: Selected bond distances (Å) for $Ni(NCS)_2(Ph_2PCH_2CH_2P(Et)CH_2CH_2PPh_2)$[a]

Ni-P1	2.223(2)	C9-C10	1.37(2)
Ni-P2	2.150(2)	C10-C11	1.34(2)
Ni-P3	2.189(2)	C11-C12	1.38(1)
Ni-N1	1.896(6)	C13-C14	1.37(1)
Ni-N2	2.088(7)	C13-C18	1.39(1)
S1-C1	1.587(8)	C14-C15	1.41(1)
S2-C2	1.635(8)	C15-C16	1.38(1)
P1-C3	1.832(8)	C16-C17	1.36(1)
P1-C7	1.795(9)	C17-C18	1.36(1)
P1-C13	1.820(8)	C19-C20	1.53(1)
P2-C4	1.826(9)	C21-C22	1.40(1)
P2-C5	1.834(9)	C21-C26	1.37(1)
P2-C19	1.83(1)	C22-C23	1.38(1)
P3-C6	1.81(1)	C23-C24	1.34(2)
P3-C21	1.829(8)	C24-C25	1.38(1)
P3-C27	1.821(8)	C25-C26	1.38(1)
N1-C1	1.131(9)	C27-C28	1.36(2)
N2-C2	1.14(1)	C27-C32	1.35(1)
C3-C4	1.51(1)	C28-C29	1.36(2)
C5-C6	1.47(1)	C29-C30	1.37(2)
C7-C8	1.40(1)	C30-C31	1.35(2)
C7-C12	1.38(1)	C31-C32	1.39(2)
C8-C9	1.37(2)		

[a]Numbers in parentheses are estimated standard deviations in the least significant digits.

Table **10:** Selected bond angles (°) for $Ni(NCS)_2(Ph_2PCH_2CH_2P(Et)CH_2CH_2PPh_2)$[a]

P1-Ni-P2	86.20(9)	P3-C6-C5	111.4(7)
P1-Ni-P3	137.3(1)	P1-C7-C8	121.0(7)
P1-Ni-N1	91.2(2)	P1-C7-C12	122.2(7)
P1-Ni-N2	101.9(2)	C8-C7-C12	116.8(8)
P2-Ni-P3	85.53(9)	C7-C8-C9	121(1)
P2-Ni-N1	173.7(2)	C8-C9-C10	120.(1)
P2-Ni-N2	95.0(2)	C9-C10-C11	120.(1)
P3-Ni-N1	92.5(2)	C10-C11-C12	121.(1)
P3-Ni-N2	120.5(2)	C7-C12-C11	121.2(9)
N1-Ni-N2	91.2(3)	P1-C13-C14	122.3(7)
Ni-P1-C3	107.6(3)	P1-C13-C18	119.1(6)
Ni-P1-C7	113.6(3)	C14-C13-C18	118.5(8)
Ni-P1-C13	117.9(3)	C13-C14-C15	121.4(9)
C3-P1-C7	106.3(4)	C14-C15-C16	117.9(9)
C3-P1-C13	104.9(4)	C15-C16-C17	120.9(8)
C7-P1-C13	105.7(4)	C16-C17-C18	120.9(9)
Ni-P2-C4	110(2)	C13-C18-C17	120.4(8)
Ni-P2-C5	112.0(2)	P2-C19-C20	116.4(7)
Ni-P2-C19	116.1(3)	P3-C21-C22	122.1(7)
C4-P2-C5	107.8(4)	P3-C21-C26	118.5(6)
C4-P2-C19	105.6(4)	C22-C21-C26	119.4(7)
C5-P2-C19	104.7(4)	C21-C22-C23	118.1(8)
Ni-P3-C6	108.2(3)	C22-C23-C24	122.1(8)
Ni-P3-C21	115.6(3)	C23-C24-C25	120(1)
Ni-P3-C27	115.4(3)	C24-C25-C26	120(1)
C6-P3-C21	107.7(4)	C21-C26-C25	120.9(8)
C6-P3-C27	105.0(4)	P3-C27-C28	121.3(7)
C21-P3-C27	104.2(3)	P3-C27-C32	119.6(7)
Ni-N1-C1	169.9(6)	C28-C27-C32	119.0(8)
Ni-N2-C2	158.1(6)	C27-C28-C29	120.(1)
S1-C1-N1	177.6(8)	C28-C29-C30	121.(1)
S2-C2-N2	178.5(6)	C29-C30-C31	120(1)
P1-C3-C4	107.9(6)	C30-C31-C32	119.(1)
P2-C4-C3	107.3(6)	C27-C32-C31	121(1)
P2-C5-C6	110.4(6)		

[a]Numbers in parentheses are estimated standard deviations in the least significant digits.

Chapter 7 Dimethylammonium [hydrogen-μ-oxo-bis{phenylphosphinate}]

7.1 Introduction

As part of our interest to prepare and characterize bridging methylene phosphine complexes, dimethylammonium[hydrogen-μ-oxo-bis{phenylphosphinate}, compound was accidentally isolated fin an attempt to synthesize $Ph(H)PCH_2P(H)Ph$ by Stelzer's reaction[39] when the order of addition of DMF and water was reversed.

Two equivalents of phenyl phosphine was added to CH_2Cl_2 in an ice-cooled Schlenk flask and stirred. To this mixture was added degassed water. DMF was then syringed into the mixture and the solution turned cloudy. Degassed KOH solution (56%) was slowly added by canula and stirred for 10 hours. The organic layer was extracted three times with pentane. The pentane was vacuum distilled leaving two layers in the reaction flask: the upper layer was thin, less viscous, the lower layer was thick and very viscous.

Distillation of this reaction mixture provided the starting phenyl phosphine. The liquid residue was yellow when hot, and colorless on cooling with some white solid. This liquid residue was insoluble in both ether and hexane. Vacuum fractional distillation on the liquid residue gave first fraction at 30°C. The second fraction was collected in liquid nitrogen-cooled flask at 34°C as white fumes, which eventually turned into shiny white crystals. These crystals did not dissolve in ether or hexane and were stable in air.

7.2 Discussion

This ORTEP of this unusual hydrogen-bonded dimer is illustrated in Figure 17. The dimer consists of two O-P(O)(Ph)-O-P(O)(Ph)-O groups bridged by hydrogen bonds and crystallizes in the body-centered tetragonal space group $I4_1cd$. The $Me_2NH_2^+$ came from breakage of the DMF solvent. This H-bonded dimer lies on a 2-fold axis with an O···O distance of 2.40 (1)Å. The short oxygen-oxygen distances and the presence of one proton for each pair of oxygen atoms suggest that the dimer is held

together by cooperative O-H···O hydrogen bonding. These short hydrogen bonded O···O distances are very close to the 2.43 (3) Å reported for the diaquohydrogen ion, $H(H_2O)_2^+$ or $H_5O_2^+$ by Cotton and coworkers.[40]

Although other crystalline salts of hydrated hydronium ions have been characterized ($H_7O_3^+$[41],[42] $H_9O_4^+$,[43] and $H_{13}O_6^+$[44]), to our knowledge, the very short hydrogen bond we have reported here is the shortest observed for a non-metal complex system. A hydrogen-bonded oxygen-oxygen distance of 2.51 Å was reported by Bertrand as indicating fairly strong bonding sufficient to maintain the dimeric nature of a polynuclear complex of copper in solution.[45] A shorter O···O distance of 2.29 (2) Å has only been reported in the bihydroxide ($H_3O_2^-$) anion that occurs in a mixed salt of sodium and chromium.[46]

The O-H···O angles range from 160 (5)° to 175 (5)° and compare well with typical values observed for hydrogen bond geometries. Further hydrogen bonding holding this compound together is provided by the N-H···O linkage. The N···O distances average 2.76 (3) Å and the N-H···O angles range from 166.0 (3) Å to 1.65 (4) Å. Apart from the short O···O and N···O bond distances, the other bonds show differences that are not significant, especially the average values for sets of chemically equivalent bonds.

Bonds and angles that do not participate in hydrogen-bonded bridges compare well with corresponding values reported for dimethylammonium ion in the literature.[47] Similarities are also noted in bond lengths and bond angles obtained for the tetramethylformamidinium phosphonic anhydride.[48] Bond angles and distances for P_4O_{10} reported by Cruickshank[49] compare very well with those reported herein.

Selected bond distances are given in Table **11** and Table **12.** Bond angles are given in Table **13** and Table **14.**

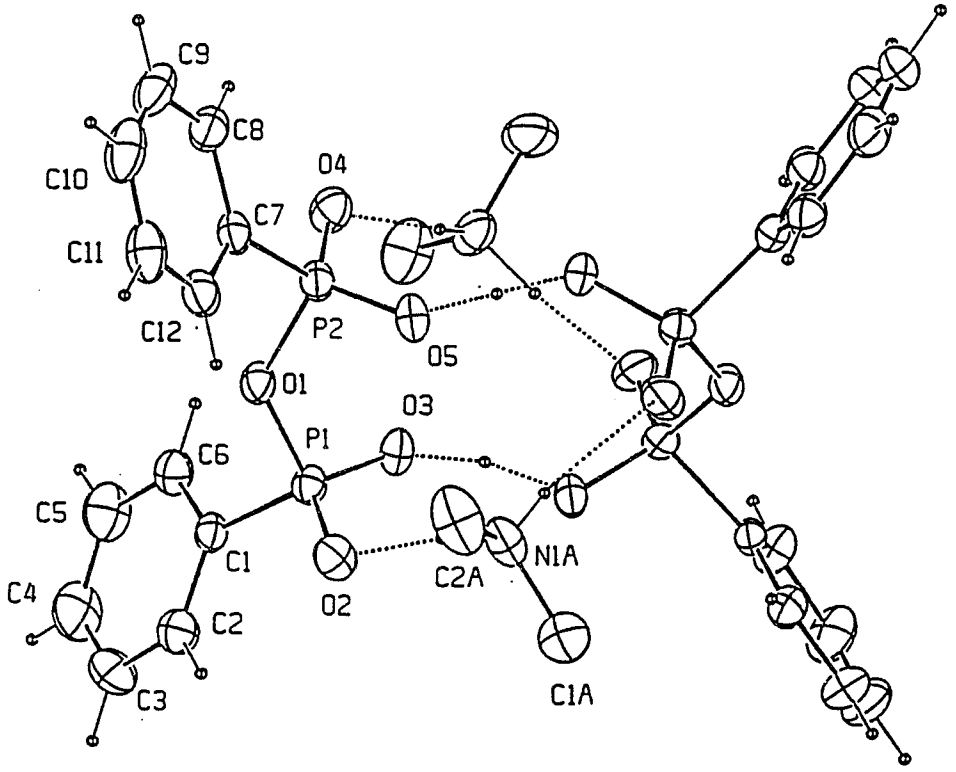

Figure 17: The ORTEP of dimethylammonium [hydrogen-μ-oxo-bis-{phenylphosphinate}]

Table **11:** Selected bond distances of (Å) of dimethylammonium [hydrogen-μ-oxo-bis-{phenylphosphinate}][a]

P1-O1	1.603(3)	C2-C3	1.395(7)
P1-02	1.485(3)	C3-C4	1.356(9)
P1-03	1.524(3)	C4-C5	1.359(8)
P1-C1	1.782(4)	C5-C6	1.371(7)
P2-01	1.618(3)	C7-C8	1.400(6)
P2-04	1.471(3)	C7-C12	1.379(6)
P2-05	1.516(3)	C8-C9	1.389(6)
P2-C7	1.763(4)	C9-C10	1.365(8)
03-H30	1.21(1)	C10-C11	1.353(7)
05-H50	1.205(3)	C11-C12	1.384(6)
C1-C2	1.366(6)	N1A-C1A	1.476(7)
C1-C6	1.391(6)	N1A-C2A	1.458(7)
		N1A-H1N	1.12(5)
		N1A-H2N	0.81(3)

Table **12:** Hydrogen bonding distances (Å) of dimethylammonium [hydrogen-μ-oxo-bis{phenylphosphinate}]

N1A-O2	2.764(5)	H1N-N1A	1.12(5)
N1A-O4	2.763(5)	H2N-O4	1.97(3)
H1N-O2	1.67(5)	H2N-N1A	0.81(3)
O3-O3	2.386(4)	O5-O5	2.409(3)

[a]Numbers in parentheses are estimated standard deviations in the least significant digits.

Table **13:** Selected bond angles (°) of dimethylammonium [hydrogen-μ-oxo-bis-{phenylphosphinate}].[a]

O1-P1-O2	111.8(2)	C3-C4-C5	120.0(5)
O1-P1-O3	106.5(1)	C4-C5-C6	120.6(5)
O1-P1-C1	101.7(2)	C1-C6-C5	120.1(4)
O2-P1-O3	116.6(2)	P2-C7-C8	120.3(3)
O2-P1-C1	112.1(2)	P2-C7-C12	121.1(3)
O3-P1-C1	106.9(2)	C8-C7-C12	118.2(4)
O1-P2-O4	111.3(2)	C7-C8-C9	119.4(4)
O1-P2-O5	105.2(1)	C8-C9-C10	121.2(5)
O1-P2-C7	101.6(2)	C9-C10-C11	119.5(5)
O4-P2-O5	117.1(2)	C10-C11-C12	120.9(5)
O4-P2-C7	112.8(2)	C7-C12-C11	120.8(4)
O5-P2-C7	107.3(2)	C1A-N1A-C2A	115.5(4)
P1-O1-P2	126.3(1)	C1A-N1A-H1N	112.(2)
P1-O3-H30	119.1(6)	C1A-N1A-H2N	110.(2)
P2-O5-H50	120.7(4)	C2A-N1A-H1N	106.(2)
P1-C1-C2	120.9(4)	C2A-N1A-H2N	103.(2)
P1-C1-C6	119.8(2)	H1N-N1A-H2N	109.(3)
C2-C1-C6	119.0(3)	O3-H30-O3	160.(5)
C1-C2-C3	119.8(4)	O5-H50-O5	176.(5)
C2-C3-C4	120.4(4)		

Table **14:** Hydrogen bond angles (°) of dimethylammonium [hydrogen-μ-oxo-bis{phenylphosphinate}].

O2-H1N-N1A	165(4)
O4-H2N-N1A	166(3)
O3-H30-O3	160(6)
O5-H5-O5	176(5)

[a]Numbers in parentheses are estimated standard deviations in the least significant digits.

Chapter 8 Conclusions

The separation of diastereomeric mixtures of et,ph-P4 can be achieved in 90-95 % yield for the *meso* diastereomer and 60-67% yield for *racemic* et,ph-P4, by refluxing the readily separated homobimetallic nickel complexes of et,ph-P4; *racemic*- and *meso*-$Ni_2(NCS)_4$(et,ph-P4) with excess NaCN in a heptane/water mixture. The monometallic *racemic*- and *meso*-$Ni(NCS)_2(\eta^3$-et,ph-P4) complexes give lower yields of et,ph-P4.

The *racemic*-$[Rh_2(nbd)_2$(et,ph-P4)$](BF_4)_2$ diastereomer in homogeneous hydroformylation catalysis provides high turnover rates (>10/min) and selectivities (28-30:1) of linear aldehyde product for 1-hexene substrate at 90 °C and 90 psi (H_2/CO). Based on the initial turnover rate, the *racemic* catalyst is 12 times faster than the *meso* bimetallic catalyst. These results provide very strong, internally consistent results that our proposed bimetallic cooperativity mechanism may be correct. The catalytic runs on each pure diastereomer support the molecular modeling predictions: *The racemic catalyst is the far more active species.*

The *racemic* diastereomer of et,ph-P4 can be separated by a commercially packed chiral HPLC column into (*S,S*) and (*R,R*) enantiomers. The separated pure enantiomers can then be used to prepare optically active $[Rh_2(nbd)_2$(et,ph-P4)$](BF_4)_2$ catalyst precursors for asymmetric hydroformylation reactions with vinyl acetate substrate.

The present study strongly supports bimetallic cooperativity in homogeneous catalysis. Another very important aspect of the present study is the discovery of asymmetric hydroformylation catalysis with extremely high regio- and enantioselectivity towards vinyl acetate to synthesize optically active products.

Chapter 9 Experimental

9.1 General Experimental Considerations

All manipulations were performed under inert atmosphere (argon or nitrogen) unless otherwise noted, with high vacuum, Schlenk, or glove box techniques. Proton and phosphorus NMR spectra were recorded at 100 MHz for ^{1}H and 40.48 MHz for $^{31}P\{^{1}H\}$ NMR on a Brucker AC/100 spectrometer. The $^{31}P\{^{1}H\}$ NMR spectra (referenced to 85% H_3PO_4) are especially suitable for characterization of these ligands and complexes. IR spectra were run on a Perkin Elmer 1760X FT-IR spectrometer. Elemental analyses were performed by Oneida Research Services, Inc., Whitesboro, NY. Semi-preparative scale HPLC was done on a Rainin Rabbit chromatograph using a 25 cm x 2 cm (I.D), substrate column (Chiralcel OD Cellulose tris(3,5-dimethylphenyl carbamate) on a 10 μm silicagel) supplied by J.T. Baker. Polarimeter measurements were made on a Jasco DIP-370 digital polarimeter. The enantiomeric excess for each asymmetric hydroformylation run of vinyl acetate was determined on the reaction mixture by the use of GC equipped with Chiraldex Capillary GC columns supplied by *Astec Inc.*

Solvents were dried and distilled under inert atmosphere from the appropriate drying agents as follows: tetrahydrofuran, diethyl ether, hexane (potassium/benzophenone); dichloromethane (calcium hydride); ethanol, methanol (magnesium), heptane was purchased under nitrogen from Aldrich. Distilled water was obtained from the chemistry building and degassed by purging with nitrogen gas for 20 minutes.

Reagents purchased were used without further purification. Ph_2PH, Et_2PCl, NaCN, $Ni(NCS)_2$, were purchased from Strem Chemicals. The $Ni(NCS)_2$ and NaCN were used without further purification, degassed and transferred into a glovebox. CH_2=CHMgBr, potassium, and cyclohexane were purchased from Aldrich.

9.2 Ligand Synthesis

9.2.1 $Et_2PCH_2CH_2PPh_2$

A 100-mL Schlenk flask was charged with 1.87 g (0.016 moles) of $Et_2PCH_2{=}CH_2$ (prepared according to published procedures)[50] and 3.002 g (0.016 moles) of Ph_2PH in cyclohexane. To this mixture was added 0.02 g of AIBN and refluxed for 16 hours. 3.03g of $Et_2PCH_2CH_2PPh_2$ was obtained as colorless viscous liquid in 62% yield (with 11% impurities) as characterized by ^1H NMR and $^{31}P\{^1H\}$ NMR.

Analysis: $^{31}P\{^1H\}$ NMR (C_6D_6, H_3PO_4 reference): Et_2P-, -18.11 ppm (1P, *d*, $J_{P\text{-}P}$ = 24.39 Hz); Ph_2P-, -12.10 ppm (1P, d, $J_{P\text{-}P}$ = 32.27 Hz). ^1H NMR (C_6D_6, TMS reference): 0.54-1.11 ppm and 1.68-1.92 ppm (m, CH_3CH_2P-); 6.53-6.82 and 6.95-7.20 ppm (m, -PCH_2CH_2P-).

9.2.2 et,ph-P4

Photolysis of the neat (H)PhPCH$_2$PPh(H) with two equivalents of $Et_2PCH_2{=}CH_2$ resulted in a quantitative synthesis of et,ph-P4.[51] (H)PhPCH$_2$PPh(H) was prepared according to published procedures.[16]

9.3 Nickel Complexes

9.3.1 $Ni(NCS)_2(Et_2PCH_2CH_2PPh_2)$

A solution of crude $Et_2PCH_2CH_2PPh_2$ (1.87 g,16 mmol) dissolved in 10 mL of EtOH was added dropwise to a 20 mL EtOH solution of $Ni(NCS)_2$ (0.542g, 32 mmol) and the resultant solution mixture stirred at glovebox temperature (23° C) overnight. Gravity filtration gave a yellow residue and a red filtrate. Two sets of crystals formed slowly from the filtrate: yellow and red needle-like crystals. The yellow crystals were identified by X-ray single crystal analysis as $Ni(NCS)_2(Et_2PCH_2CH_2PPh_2)$, whereas the red needle-like crystals were characterized as trisphosphine chelated $Ni(NCS)_2(Ph_2PCH_2CH_2P(Et)CH_2CH_2PPh_2)$. These were washed with anhydrous ethanol and ether.

Spectroscopic data on $Ni(NCS)_2(Et_2PCH_2CH_2PPh_2)$: $^{31}P\{^1H\}$ NMR (acetone d_6, δ in ppm, H_3PO_4 reference): Et_2P-, 83.2 (d, $^3J_{P-P}$ =77.3 Hz); -PPh_2, 66.9 (d, $^3J_{P-P}$=77.3 Hz); ^1H NMR (acetone d_6, δ in ppm, TMS reference):1.10-1.62 (m, CH_3CH_2P-); 1.88-1.92 (m, CH_3CH_2P-), 2.56-2.97 (m,-PCH_2CH_2P-);7.50-8.22 (m, -PPh_2).

Spectroscopic data on $Ni(NCS)_2(Ph_2PCH_2CH_2P(Et)CH_2CH_2PPh_2)$: $^{31}P\{H\}$ NMR (acetonitrile-d_3, δ in ppm, H_3PO_4 reference); -P(Et)-, 117.0 (t, $^3J_{P-P}$ = 53.2 Hz); -PPh_2, 53.9 (d, $^3J_{P-P}$=53.2 Hz).

9.3.2 *Racemic-* and *meso-*[Ni(NCS)(η^3-et,ph-P4)](NCS)

A 100 mL EtOH solution of mixed et,ph-P4 (25 g, 0.054 mol) was added to a stirred clear olive-green solution of $Ni(NCS)_2$ (9.4 g, 0.054 mol) in 100 mL EtOH. The solution turned orange, then finally to a deep brown at the end of the addition. The stirring was continued for two days resulting in a wine-red solution with an orange-brown precipitate. The orange-brown precipitate was collected by filtration and washed with three 50 mL portions of cold EtOH to give 16.8 g (97% yield) of orange-brown air-stable *meso*-[Ni(NCS)(η^3-et,ph-P4)](NCS). The filtrate was evaporated to dryness to give 16.1 g (93%) of mainly wine-red air-stable *racemic*-[Ni(NCS)(η^3-et,ph-P4)](NCS). This was characterized by $^{31}P\{^1H\}$ NMR spectroscopy and by elemental analysis.

Anal. calc.(%) for *meso*-[Ni(NCS)(η^3-et,ph-P4)](NCS) (Mw = 639.4): C, 50.72; H, 6.31; N, 4.38; S, 10.03; P, 19.38; Found C, 50.20; H, 6.38; N, 4.18; S, 10.07; P, 19.46; $^{31}P\{^1H\}$ NMR (CD_2Cl_2, δ in ppm, H_3PO_4 reference): external phosphorus, 28.8 (t, J_{P-P} = 5.0 Hz) ; internal phosphorus atoms, 3.3 (t, J_{P-P} = 5.0 Hz).

Anal. calc.(%) for *racemic*-[Ni(NCS)(η^3-et,ph-P4)](NCS) (Mw = 639.4): C, 50.72; H, 6.31; N, 4.38; S, 10.03; P, 19.38; Found C, 49.7; H, 6.13; N, 3.59; S, 7.45; P, 16.46. $^{31}P\{^1H\}$ NMR (CD_2Cl_2, δ in ppm, H_3PO_4 reference): external phosphorus, 52.5 (t, J_{P-P} = 18.6 Hz) ; internal phosphorus atoms, 28.5 (t, J_{P-P} = 18.6 Hz).

The IR (KBr) of *racemic*-[Ni(NCS)(η^3-et,ph-P4)](NCS) has a strong absorption at 2088 cm^{-1} characteristic of free NCS^- stretch.

9.3.3 *Racemic*- and *meso*-[$Ni_2(NCS)_4$(et,ph-P4)]

A 100 mL EtOH solution of mixed et,ph-P4 (25 g, 0.054 mol) was added to a stirred clear olive green solution of $Ni(NCS)_2$ (18.8 g, 0.108 mol) in 200 mL EtOH under inert atmosphere. The solution turned orange, then finally to a deep brown at the end of the addition. The stirring was continued for 2 days resulting in a wine-red solution with orange-brown precipitate. The orange-brown precipitate was collected by filtration and washed with 3 x 50 mL portions of cold EtOH to give 21.7 g (98% yield) of orange-brown air-stable *meso*-[$Ni_2(NCS)_4$(et,ph-P4)]. The metal complex crystallized in $CHCl_3$/EtOH mixture on slow evaporation to give yellow-orange crystals. This product was characterized by single X-ray structure determination and by $^{31}P\{^1H\}$ NMR spectroscopy.

The $^{31}P\{^1H\}$ NMR of *meso*-[$Ni_2(NCS)_4$(et,ph-P4)] (CD_2Cl_2, δ in ppm, H_3PO_4 reference): external phosphorus, 75.4 (d, $^2J_{P\text{-}P}$ = 79.3 Hz and virtual t, $^4J_{P\text{-}P}$ =10.5 Hz); internal phosphorus atoms, 57.4 ppm (d, $^2J_{P\text{-}P}$ = 79.3 Hz and virtual, t, $^3J_{P\text{-}P}$ =10.5 Hz). The water molecule in the crystal structure was apparently picked up from the solvent mixture in which the crystals formed.

The filtrate was evaporated to dryness to give 19.8 g (90%) of mainly wine-red air-stable *racemic*-[$Ni_2(NCS)_4$(et,ph-P4)]. $^{31}P\{^1H\}$ NMR of *racemic*-[$Ni_2(NCS)_4$(et,ph-P4)] (CD_2Cl_2, δ in ppm, H_3PO_4 reference): external phosphorus, 51.1 (t, $J_{P\text{-}P}$ = 19.8 Hz); internal phosphorus atoms, 26.1 (t, $J_{P\text{-}P}$ = 19.8 Hz).

9.4 *Racemic*-et,ph-P4

The diastereomerically pure free *racemic* ligand was decomplexed and isolated by refluxing *racemic*-[$Ni_2(NCS)_4$(et,ph-P4)] (10.57 g, 0.013 moles) with heptane/water (1:1 volume ratio) solvents in 500 mL Schlenk flask in the presence of ten-fold molar excess of NaCN (10 g, 13.0 moles) for 8 hours under inert atmosphere. The cyanide attacks the nickel center and forms water soluble $Ni(CN)_4^{2-}$ and releases et,ph-P4, which cleanly transfers into the organic phase. The organic layer was transferred by cannula into a 500 mL Schlenk flask and the aqueous layer extracted with 2 x 100 mL pentane. The pentane washings were combined with the heptane layer and passed through a short alumina column to remove any solid impurities. The solvent was removed by vacuum evaporation to give 4.1 g (68%) of colorless oily air-sensitive *racemic*-et,ph-P4 diastereomer in >98% purity. This was dissolved again in approximately 40 mL of heptane and passed through a second alumina column to improve purity of product. Its identity was conveniently confirmed by $^{31}P\{^1H\}$ NMR spectroscopy..

$^{31}P\{^1H\}$ NMR (C_6D_6, δ in ppm, H_3PO_4 reference): external phosphorus, -18.2 (t, J_{P-P} = 11.4 Hz); internal phosphorus atoms, -25.3 (t, J_{P-P} = 11.3 Hz). ^1H NMR on 400 MHz (acetone d_6, δ in ppm, TMS reference): 0.74-0.82 (m, CH_3CH_2P-); 1.11-1.19 (m, CH_3CH_2P-), 1.63-1.67, (m,-PCH_2CH_2P-); 2.11 (s, P-CH_2-P), 7.22-7.23 and 7.45-7.47 (m, Ph).

9.5 Meso-et,ph-P4

Pure *meso*-et,ph-P4 is an air-stable white solid and was obtained by repeating same procedure above with the orange residue, *meso*-[$Ni_2(NCS)_4$(et,ph-P4)] (16.3 g, 0.02 moles). However, the *meso* ligand required additional cleaning. Dissolution in a minimum amount of hexane, precipitation at -32°C, filtration, and washing with cold hexane gave 9.1 g (98%) of very clean white solid *meso*-et,ph-P4.

$^{31}P\{^{1}H\}$ NMR (C_6D_6, δ in ppm, H_3PO_4 reference): external phosphorus, -18.1 (t, J_{P_P} = 10.7 Hz); internal phosphorus atoms, -26.0 (t, J_{P_P} = 10.9 Hz). ^{1}H NMR on 400 MHz ($CDCl_3$, δ in ppm, TMS reference): 0.94-1.01 (m, CH_3CH_2P-); 1.30-1.35 (m, CH_3CH_2P-), 1.51-1.70, 1.75-1.89 (m,-PCH_2CH_2P-);2.10-2.12 (m, P-CH_2-P), 7.30-7.32 and 7.45-7.49 (m, Ph).

9.6 Isolation of (*S,S*) and (*R,R*) Enantiomers of *Racemic* et,ph-P4

A commercially packed chiral HPLC column (250 x 20 mm) (I.D.) of cellulose tris(3,5-dimethylphenyl carbamate) on a 10 μm silica-gel substrate was provided by J.T. Baker Chemical Co. This was sequentially treated, at a pumping flow rate of 6 mL/min, with 2-propanol/hexane mixture (5/95 v/v) until base line stabilized. This way, the mobile phase was composed of hexane modified with 2-propanol. 300 mg of *racemic* et,ph-P4 in 10 mL of hexane was then loaded onto the column. Sample and eluent solutions were filtered through a 0.45 μm membrane filter. This chiral column successfully resolved the racemate of et,ph-P4 at room temperature with retention time values of 13.2 and 14.8 minutes for the two diastereomers at 21°C. A semi-prep scale chiral HPLC column was employed for bulk separations of the individual enantiomers of et,ph-P4.

The eluted materials were collected in Schlenk flasks which were continually purged with nitrogen. The ligands were transferred into the glove-box and solvents removed by vacuum evaporation. Purity of each enantiomer was determined by $^{31}P\{^{1}H\}$ NMR spectroscopy for any phosphine contaminants. Optical rotations for the pure enantiomers were determined on a Jasco DIP-310 Digital Polarimeter.

9.7 $[Rh_2(nbd)_2(et,ph\text{-}P4)](BF_4)_2$

$[Rh(nbd)_2]BF_4$ (0.19 g, 0.51 mmole) was dissolved in 10 mL CH_2Cl_2 in a flask. Specific et,ph-P4 ligand (*meso*, *racemic*, as well as each enantiomer) (0.12 g, 0.25 mmole) was dissolved in 10 mL CH_2Cl_2. The ligand solution was added dropwise into the metal complex solution. The red-orange solution was vacuum evaporated to give

orange-yellow product which recrystallizes in acetone to give red-orange $[Rh_2(nbd)_2(et,ph\text{-}P4)](BF_4)_2$.

9.8 Hydroformylation Runs

Glass-lined Parr autoclaves of 150 mL capacity were used for the reactions. Each autoclave was connected to a Parr 4850 controller which controls and monitors the temperature and stirring rate (RPM's) within the autoclave. The $[Rh_2(nbd)_2(et,ph\text{-}P4)](BF_4)_2$ catalyst (0.090 g) of individual *meso*, *racemic* and mixed-et,ph-P4 was weighed into a pear-shaped Schlenk flask in the glove box and brought out to the Schlenk-line. Reactions were carried out in acetone solvent.

The degassed and dry acetone (80 mL) was added to the flask via a cannula and the catalyst readily dissolved in the acetone. This solution was added to an evacuated autoclave system ready for the temperature ramp and pressurizing. Pressure was raised to 44 psi. The substrate [1-hexene (density = 0.673g/mL) or vinyl acetate] was added (10 mL) via a small cylinder attached to the autoclave only after the temperature had reached 90°C. Pressure was then adjusted to 90 psi. In each experiment, therefore, the catalyst charged was 9.73×10^{-4} M of rhodium complex.

A regulator inline with the gas reservoir cylinder delivered a constant pressure of the 1:1 mixture of H_2 and CO gas to the autoclave; any gas uptake and pressure decrease being offset via this regulator system and monitored by the Parr controller. All data were stored internally on the controller in a RAM disk and eventually transferred for data workup on a personal computer.. Four to five runs were usually done for each catalyst studied. The asymmetric hydroformylation catalytic runs were limited to 1-2 runs due to the small amounts of chiral catalyst initially prepared.

The initial turnover rates were calculated by determining the slope of the curve when the number of equivalents of gas used is plotted versus time. The reaction products were analyzed by ^1H NMR spectroscopy and by GC.

9.9 Determination of Enantiomeric Excess in 2-Acetoxypropanal

Enantioselectivity is expressed as enantiomeric excess (ee) which is defined as:

$$ee = \frac{R-S}{R+S} \times 100\%$$

where R and S are the areas of GC peaks of the R and S enantiomers of 2-acetoxypropanal respectively. The enantiomeric excess for each hydroformylation run was determined on the reaction mixture by the use of GC equipped with Chiraldex Capillary GC columns supplied by *Astec Inc.*

9.10 Dimethylammonium [hydrogen-μ-oxo-bis{phenylphosphinate}]

Phenyl phosphine (19.75 g, 0.180 mole) was added to CH_2Cl_2 (7.63 g, 0.090 mole) in an ice-cooled Schlenk flask and stirred. To this mixture was added degassed water (150 mL). DMF (56 mL) was syringed into the mixture and the solution turned cloudy. Degassed 27 mL KOH solution (56%) was slowly added by canula for 20 minutes and stiring continued for 10 hours. The cloudiness decreased and two layers formed, organic and inorganic. The organic layer was extracted three times with 50 mL pentane. The pentane was vacuum distilled via a trap-to trap arrangement leaving two layers in the reaction flask: the upper layer was thin, less viscous, the lower layer was thick and very viscous.

Distillation of this reaction mixture provided the starting phenyl phosphine. The liquid residue was yellow when hot, and colorless on cooling with some white solid. This liquid residue was insoluble in both ether and hexane. Vacuum fractional distillation on the liquid residue gave first fraction at 30°C. The second fraction was collected in liquid nitrogen-cooled flask at 34°C as white fumes, which eventually turned into shiny white crystals. These crystals did not dissolve in ether or hexane and were stable in air. Due to the small quantities isolated, no spectroscopic or elemental data was obtained. Only an X-ray crystal structure was performed.

References

1. (a) Muetterties, E. L.;Krause, M. J. *Angew. Chem. Int. Ed. Engl.* **1983**, 22, 135. (b) Johnson, B. F. G. *"Transition Metal Clusters"* Wiley, New York, 1980.

2. Casey, C. P.; Whiteker, G. T.; Melville, M.G.; Petrovich, L. M.; Gavney, J. A.; Powell, D. R. *J. Am. Chem. Soc.* **1992**, *114*, 5535.

3. Heck, R. F.; Breslow, D. S. *J. Am. Chem. Soc.* **1961**, *83*, 4023. (b) Brelow, D. S.; Heck R.F. Chem. Ind. (London) P.467, 1960.

4. (a) Mirbach, M. F. *J. Organomet. Chem.* **1984**, *265*, 205. (b) Moser, W. R. In *Homogeneous Transition Metal Catalyzed Reactions*; Moser, W. R.; Slocum, D., Eds; *Advances in Chemistry*, (American Chemical Society, Washington, D.C, 1992), vol. 230, chap. 1.

5. (a) Jones, W. D.; Bergman, R. G. *J. Am. Chem. Soc.* **1979**, *101*, 5447. (b) Jones, W. D., Huggins, J. M.; Bergman, R. G. *J. Am. Chem. Soc.* **1981**, *103*, 4415.

6. Nappa, M. J.; Santi, R.; Halpern, J. *Organometallics* **1985**, *4*, 34.

7. Martin, B. D.; Warner, K. E.; Norton, J. R. *J. Am. Chem. Soc.* **1986**, *108*, 33.

8. Kovacs, I.; Hoff, C. D.; Ungvary, F.; Marko, L. *Organometallics* **1985**, *4*, 1347.

9. King, R. B. *"Catalytic Aspects of Metal Phosphine Complexes", ACS Symp. Ser.* **1982**, *196*, 312.

10. (a) Kubiak, C. P.; Eisenberg, R. *J. Am. Chem. Soc.* **1977**, *99*, 6129.(b) Sanger, A. R. *J. Chem. Soc., Dalton Trans.* **1977**, 1971.

11. Laneman, S. A.; Fronczek, F. R.; Stanley, G. G. *J. Am. Chem. Soc.* **1988**, *110*, 5585.

12. Broussard, M. Unpublished results.

13. Lanemann, S. A.; Stanley G. G., In *Homogeneous Transition Metal Catalyzed Reactions*; Moser, W. R.; Slocum, D., Eds; Advances in Chemistry, (American Chemical Society,Washington, D.C, 1992), vol. 230, chap. 24. Please note that all experimental rates in this reference are twice their correct values.

14. (a) Schlenk, T. G.; Downes, J. M.; Milne, C.R.C.; Mackenzie, P.B.; Boucher, H.; Whalen, J.; Bosnich, B. *Inorg. Chem.* **1985**, *24*, 2334. (b) Allen, D. L.; Gibson, V. C.; Green, M. L. H.; Skinner, J. F.; Baskin, J. Grebenik, P. D. *J. Chem. Soc., Chem. Commun.* **1983**, 895.

15. Liwen, W.; Bell, A.; Ahn, K.; Holl, M. M.; Warner, S.; Williams, I. D.; Lippard, S. J. *Inorg. Chem.* **1990**, *29*, 825.

16. Laneman, S. A.; Fronczek, F. R.; Stanley, G. G. *Inorg. Chem.* **1989**, *28*, 1872.

17. Catalytic runs were done in well-stirred computer controlled Parr autoclaves under constant pressure conditions. The solvents were free of oxygen and inert conditions maintained during loading. The autoclave is heated to 90°C and stirred at 1000 rpm with approximately half the desired operating pressure (approx. 45 psi) of 1:1 H_2/CO gas mixture. When the autoclave stabilizes at 90°C (apprx. 65 psi), the olefin addition cylinder is pressurized to 90 psi with H_2/CO and the release valve is opened to add the olefin into the autoclave. An initial sample is taken and the data collection begins. 1-2 mL samples from the autoclave are taken hourly and analysed by GC and NMR for product distributions. Catalyst concentration was 9.73 x 10^{-4} M, acetone was the solvent, and initial 1-hexene concentration (10mL, 6.73 g, 0.80 mole) in 80mL acetone solvent was 0.89 M.

18. Number of moles of aldehyde = 0.5 mole of gas since it is 1:1 H_2/CO.

19. Broussard, M. E.; Juma, B.; Train, S. G.; Peng, W. J.; Stanley, G. G. *Science*, in press.

20. TRIPOS Associates, Inc., 1699 S. Hanley Rd., Suite 303, St. Louis, MO 63144; Naruto, S.; Motoc, I.; Marshall, G. R.; Daniels, S. B.; Sofia, M. J.; Katzenellenbogen, J. A. *J. Am. Chem. Soc.* **1985**, *107*, 5262.

21. Stanley, G., SYBYL Users Meeting, May 1992, St. Louis, MO..

22. Glasstone's, S.; Laidler, K.J.; Eyring, H. The Theory of Rate Processes; McGraw-Hill 1941; p. 195.

23. Piacenti, F.; Pino, P; Lazzaroni, R.; Bianchi, M. *J. Chem. Soc.* C **1966**, 488.

24. (a) Vineyard, B. D.; Knowles, W. S.; Sabacky, M. J.; Bachman, G. L; Weinkauff, D. J. *J. Am. Soc.* **1977**, *99*, 5946. (b) Kitamura, M.; Hsiao, Y; Noyori, R.; and Takaya, *Tetrahedron Lett.* **1987** *28*, 4829 (c) Kawano, H.;Ishii, Y; Saburi, M. and Uchida, Y. *J. Chem. Soc., Chem. Commun.* **1988**, 87.

25. Brunner, H. *Synthesis* **1988**, 645. (d) Pino P.; Consiglio, G.; Boteteghi, C.; Salomon, C. *Adv. Chem. Ser.* **1974**, *132*, 295, and references therein.

26. (a) Consiglio, G.; Pino P. *Top. Curr. Chem.* **1982**, *105*, 77. (b) Bosnich, B., Ed. *Asymmetric Catalysis;* Martinus Nijhoff Publishers:Boston, **1986**; 43.

27. Parshall, G.; Nugent, W. *Chemtech* **1988**, *18*, 194.

28. Pirkle, W.H.; Finn, J.M.; Schriner,J.L.; Hamper, B.C. *J. Am. Chem. Soc.* **1981**, *103*, 3964.

29. Warner, I.V., *A Practical guide to the selection and Use of HPLC Chiral Stationary Phases.* J.T. Baker Inc.,1988.

30. Hobbs, C. F.; Knowles, W. S. *J. Org. Chem.* **1981**, *46*, 4422

31. Laneman, S. A. PhD Thesis, Louisiana State University, August 1990, 125.

32. (a) Parrinello G. and Stille, J.K. *J. Am. Chem. Soc.* **1987**, *109*, *23*, 7122.

33. Parrinello, G.; Stille, J. K. *Polym. Prepr.* (Am. Chem. Soc., Div. Polym. Chem.) **1986**, *27*, 9.

34. (a) Spek, A. L., Van Eijck, B. P., Jans, R. J. F., Van Koten, G. **1987,** *Acta Cryst.* **C43,** 1878-1880.(b) Rahn, J.A., Delian, A., Nelson, J.H. **!989**, *Inorg. Chem.* **28**, 215.

35. Dubois, D. L.; Hyers, W. H, & Meek, D. W. *J. Chem. Soc., Dalton Trans.*, **1975**, 1011.

36. Juma, B; Fronczek; F. R.; Stanley, G.G. *Acta Crystallogr., Sect.C.* in press.

37. Kriege-Simondsen, J.; Feltham, R. D., *Inorg. Chim. Acta*, **1983**, 71, 185.

38. Rahn, J. A., Delian, A.; Nelson, J. H. *Inorg. Chem.*, **1989**, *28*, 215.

39. Langhans, K. P.; Stelzer,O. *Chem.Ber.*, **1987**,*120*, 1707.

40. Cotton, F.A.; Fair, C.K.; Lewis, G.E.; Mott, G.N.; Ross, F.K.; Schultz, A.J., Williams, J.M. *J. Am. Chem. Soc.* **1984**, *106*, 5319.

41. Lundgren, J.-O; Ollovson, I. *J.Chem. Phys.* **1968**, *49*, 1068.

42. Almlof, J. *Acta Crystallogr., Sect. B* **1972**, *28*, 481.

43. Lundgren, J.-O. *Acta Crystallogr., Sect. B* **1978**, *23*, 3432

44. Bell, R.A.; Christoph, G.G.; Fronczek, F.R.; Marsh, R.E. *Science* **1975**, *190*, 151.

45. Bertrand, J.A.; Black,T.D.; Garry E.P.; Helm,F.T.; Mahmood, R. *Inorg. Chem.* **1976**, *15*, 2965.

46. Abu-Dari, K.; Raymond, K.N.; Freyberg, D.P. *J. Am. Chem. Soc.* **1979**, *101*, 3688.

47. (a) Knodler F., Ensinger,U., Schwarz,W. & Schmidt A., *Z. Anorg. All. Chem.*, **1988**, *557*, 208. (b) Thomas,J.O., *Acta. Cryst.*, **1977**, *B23*, 2867. (c) Wahlberg, A., *Acta. Cryst.*, **1978**, *B34*, 3392.

48. (a) Daly,J.J., & Sanz,F. , *J.Chem.Soc. Dalton*, **1972**, 2267. (b) Daly, J.J. *J.Chem. Soc, Dalton Trans.*, **1972**, 1048.

49. (a) Cruickshank, D.W.J., *J.Chem. Soc.* ,**1961**,5486.(b) Cruickshank, D.W.J., *Trans. Faraday Soc.*, ***1967*** ,63,836.

50. Askham, F.R.; Maverick, A.W.; Marques, E.C.*J. Am. Chem. Soc.* **1985**, *107*, 7428.

51. Peng, W.J. Unpublished results.

Appendix

Table **A-1:** Fractional atomic coordinates and equivalent isotropic displacement parameters (Å^2) for *meso*-Ni(NCS)(η^3-et,ph-P4)](NCS).

$$Beq = \left(\frac{8\pi^2}{3}\right)\sum_i \sum_j U_{ij} a_i^* a_j^* \mathbf{a}_i \cdot \mathbf{a}_j$$

Atom	x	y	z	B*eq*
Ni	0.21204(3)	0.51558(4)	0.44411(3)	3.63(1)
P1	0.31542(4)	0.40378(6)	0.45888(5)	3.19(1)
P2	0.26048(5)	0.53329(7)	0.58709(5)	3.72(2)
P3	0.34936(5)	0.33997(8)	0.28224(6)	4.31(2)
P4	0.13692(5)	0.45468(8)	0.31188(5)	4.20(2)
C'	0.3770(2)	0.4156(3)	0.3864(2)	3.73(6)
C11	0.3936(2)	0.4328(3)	0.5635(2)	3.84(6)
C12	0.3506(2)	0.4419(3)	0.6319(2)	4.35(7)
C13	0.2500(2)	0.4056(4)	0.2237(2)	5.05(8)
C14	0.1784(2)	0.3572(3)	0.2499(2)	5.11(8)
C21	0.2965(2)	0.6727(3)	0.6291(2)	4.77(8)
C22	0.2300(3)	0.7640(3)	0.6081(3)	6.7(1)
C23	0.1877(2)	0.4894(3)	0.6406(2)	5.13(8)
C24	0.2220(3)	0.4866(4)	0.7399(2)	6.5(1)
C41	0.0990(2)	0.5749(4)	0.2392(2)	5.47(9)
C42	0.0562(3)	0.5509(5)	0.1441(3)	8.2(1)
C43	0.0444(3)	0.3786(5)	0.3165(3)	10.3(1)
C44	-0.0241(3)	0.3799(8)	0.2770(7)	25.2(4)
C1P	0.2884(2)	0.2555(3)	0.4652(2)	3.50(6)
C2P	0.3436(2)	0.1687(3)	0.4650(2)	4.45(7)
C3P	0.3205(2)	0.0574(3)	0.4687(2)	5.19(9)
C4P	0.2436(3)	0.0305(3)	0.4728(2)	5.60(9)
C5P	0.1900(2)	0.1157(3)	0.4756(2)	5.22(8)
C6P	0.2123(2)	0.2280(3)	0.4721(2)	4.17(7)
C7P	0.4155(2)	0.4157(3)	0.2313(2)	4.07(7)
C8P	0.4135(2)	0.5327(3)	0.2191(2)	4.84(8)
C9P	0.4588(2)	0.5832(3)	0.1733(2)	5.48(9)
C10P	0.5080(2)	0.5180(4)	0.1405(2)	6.0(1)
C11P	0.5132(2)	0.4041(4)	0.1530(2)	5.97(9)
C12P	0.4663(2)	0.3521(3)	0.1980(2)	4.87(8)
S1T	-0.01501(6)	0.7268(1)	0.45260(7)	6.31(3)
C1T	0.0631(2)	0.6517(3)	0.4476(2)	4.28(7)
N1T	0.1186(2)	0.5990(3)	0.4450(2)	4.60(6)
S2T	0.28035(6)	0.69835(9)	0.38903(7)	5.71(2)
C2T	0.3764(2)	0.7090(3)	0.4533(2)	4.66(8)
N2T	0.4431(2)	0.7155(3)	0.4978(2)	6.34(9)

Table A-2: Crystallographic data for *meso*-Ni(NCS)(η^3-et,ph-P4)](NCS)

formula	$NiC_{27}H_{40}S_2P_4N_2$
fw	639.4
Fooo	1344
a, Å	17.127(2)
b, Å	11.798(1)
c, Å	16.266(2)
β, deg	108.76(1)
V, $Å^3$; Z	3112(1); 4
space group	$P2_1/c$
D_{calc}, g/ cm^3	1.365
μ, cm^{-1}	42.6
λ(Cu Kα), Å	1.54184
T °C	24
2θ range, deg	2 - 75
no. of unique data	6156
no. of data used	4614
no. of variables	326
Cutoff	$I > 3\sigma(I)$
R (obs. data)[a]	0.041
GOF[c]	2.018
R_W[b]	0.052
Max. Residual, $eÅ^{-3}$	0.62
Min. Residual, $eÅ^{-3}$	-0.61
Extinction coef.	$3.5(4) \times 10^{-7}$

[a]$R = \Sigma(|F_o| - |F_c|)/\Sigma|F_o|$; $R_W = \{\Sigma w(|F_o| - |F_c|)^2/\Sigma w(|F_o|^2\}^{1/2}$. $w = 4F_o^2[\sigma^2(I) + (0.02F_o^2)^2]^{-1}$. [c]Goodness of fit = $[\Sigma w (|F_o| - |F_c|)^2/(N_{obs}-N_{param})]^{1/2}$.

Data Collection and Refinement

difractometer	CAD4
scan method	ω/2θ
variable scan speed	0.61-3.30° min^{-1}

Table **A-3:** Fractional atomic coordinates and equivalent isotropic displacement parameters (Å^2) for *meso*-$Ni_2(NCS)_4$(et,ph-P4).0.78H_2O

$$Beq = \left(\frac{8\pi^2}{3}\right)\sum_i \sum_j U_{ij} a_i^* a_j^* \mathbf{a}_i \cdot \mathbf{a}_j$$

Atom	x	y	z	B*eq*
Ni1	0.41840(5)	0.0550(1)	0.35787(9)	4.22(3)
Ni2	0.13526(6)	0.1307(1)	0.25125(9)	4.45(3)
P1	0.33301(9)	0.1485(2)	0.3205(1)	4.03(5)
P2	0.46113(9)	0.2297(2)	0.3490(2)	4.46(6)
P3	0.20188(9)	0.0343(2)	0.3384(1)	4.02(5)
P4	0.1099(1)	-0.0457(2)	0.1949(2)	4.58(6)
C	0.2744(3)	0.1055(9)	0.3803(5)	4.9(2)
C11	0.3459(4)	0.3110(8)	0.3418(5)	4.9(2)
C12	0.4043(4)	0.3437(8)	0.3113(6)	5.4(2)
C13	0.2143(4)	-0.1156(8)	0.2982(5)	4.8(2)
C14	0.1528(4)	-0.1652(8)	0.2576(6)	5.4(2)
C21	0.5027(4)	0.2808(9)	0.4499(6)	6.7(3)
C22	0.5425(6)	0.389(1)	0.4483(8)	12.5(4)
C23	0.5145(4)	0.2305(9)	0.2768(6)	6.0(3)
C24	0.4922(4)	0.161(1)	0.1977(6)	7.2(3)
C41	0.0297(4)	-0.0809(9)	0.1864(6)	6.2(3)
C42	0.0135(5)	-0.209(1)	0.1541(7)	9.6(4)
C43	0.1304(4)	-0.0605(9)	0.0920(6)	6.2(3)
C44	0.0995(4)	0.027(1)	0.0251(6)	8.2(3)
C1P	0.3033(3)	0.1348(8)	0.2091(5)	4.4(2)
C2P	0.3218(4)	0.0400(9)	0.1641(6)	5.8(3)
C3P	0.2999(4)	0.030(1)	0.0774(6)	7.2(3)
C4P	0.2602(4)	0.115(1)	0.0400(6)	7.4(3)
C5P	0.2408(4)	0.210(1)	0.0827(6)	7.4(3)
C6P	0.2633(4)	0.2204(9)	0.1688(5)	5.8(3)
C7P	0.1729(3)	0.0102(8)	0.4356(5)	4.7(2)
C8P	0.1201(4)	0.0665(9)	0.4470(6)	5.9(3)
C9P	0.0985(4)	0.054(1)	0.5222(6)	8.3(3)
C10P	0.1317(5)	-0.009(1)	0.5863(7)	9.8(4)
C11P	0.1841(6)	-0.065(1)	0.5782(6)	10.1(4)
C12P	0.2051(5)	-0.058(1)	0.5024(7)	8.3(3)
S1T	0.6125(1)	-0.1033(3)	0.4409(2)	8.41(9)
C1T	0.5456(4)	-0.0490(8)	0.4114(5)	4.8(2)
N1T	0.4966(3)	-0.0121(6)	0.3881(4)	4.9(2)
S2T	0.3393(2)	-0.3360(3)	0.3527(4)	17.7(2)
C2T	0.3638(4)	-0.1970(9)	0.3572(8)	7.9(3)
N2T	0.3802(3)	-0.0980(7)	0.3574(5)	5.4(2)
S3T	-0.0401(1)	0.2781(3)	0.0862(2)	7.74(8)
C3T	0.0232(4)	0.2325(9)	0.1407(5)	5.2(2)

Table **A-3** (cont.): Fractional atomic coordinates and equivalent isotropic displacement parameters ($Å^2$) for *meso*-$Ni_2(NCS)_4$(et,ph-P4).$0.78H_2O$.

N3T	0.0694(3)	0.1998(7)	0.1792(5)	6.4(2)
S4T	0.1914(2)	0.5234(3)	0.3288(2)	9.8(1)
C4T	0.1714(4)	0.3838(9)	0.3119(5)	5.0(2)
N4T	0.1603(3)	0.2826(7)	0.3002(5)	6.0(2)
O1W	0.680(1)	0.186(3)	0.353(2)	42(2)*

Table A-4:. Crystallographic data for *meso*-$Ni_2(NCS)_4$(et,ph-P4).0.78H_2O.

formula	$Ni_2S_4P_4C_{29}H_{40}N_4$
fw	832.3
Fooo	1728
a, Å	22.304(4)
b, Å	10.913(2)
c, Å	16.125(5)
β, deg	100.10(2)
V, $Å^3$; Z	3864(3); 4
crystal system	monoclinic
space group	$P2_1/c$
D_{calc}, g/ cm^3	1.431
λ(Cu Kα), Å	1.54184
μ, cm^{-1}	50.3
T °C	26
2θ range, deg	2 - 60
no. of unique data	5690
no. of data used	3236
no. of variables	394
Cutoff	$I > 3\sigma(I)$
R (obs. data)[a]	0.064
R_w[b]	0.067
GOF[c]	2.197
Max. Residual, $eÅ^{-3}$	0.77(near Ni)
Min. Residual, $eÅ^{-3}$	-0.15
Crystal size	0.1 x 0.23 x 0.70

[a]$R = \Sigma(|F_o| - |F_c|)/\Sigma|F_o|$; $R_w = \{\Sigma w(|F_o| - |F_c|)^2/\Sigma w(|F_o|^2\}^{1/2}$. $w = 4F_o^2[\sigma^2(I) + (0.02F_o^2)^2]^{-1}$. [c]Goodness of fit = $[\Sigma w (|F_o| - |F_c|)^2/(N_{obs}-N_{param})]^{1/2}$.

Hydrogens were not refined. The 1.0 $e/Å^3$ peak in isolated position (3.29(4) Å from nearest non-hydrogen atom S2T) was interpreted as water molecule. Refinement of population and B_{iso} led to: pop = 0.78(2), B_{iso} = 42(2) $Å^2$. Values of density, etc. above are for monohydrate, x = 1.

Data Collection and Refinement

difractometer	CAD4
scan method	ω/2θ

Table **A-5:** Fractional atomic coordinates and equivalent isotropic displacement parameters (Å^2) for $Ni(NCS)_2(Et_2PCH_2CH_2PPh_2)$.

$$B_{eq} = \left(\frac{8\pi^2}{3}\right)\sum_i \sum_j U_{ij} a_i^* a_j^* \mathbf{a}_i \cdot \mathbf{a}_j$$

atom	x	y	z	B_{eq}
Ni	0.28547 (5)	0.25823 (2)	0.24948 (3)	3.969 (9)
S1	0.3130 (1)	0.42543 (5)	0.47975 (6)	6.43 (2)
S2	0.6906 (1)	0.11116 (5)	0.37181 (8)	7.46 (2)
P1	0.11882 (7)	0.33396 (3)	0.18668 (4)	3.47 (1)
P2	0.2611 (1)	0.19461 (4)	0.13020 (6)	5.30 (2)
N1	0.2976 (3)	0.3185 (1)	0.3508 (2)	4.61 (5)
N2	0.4396 (3)	0.1917 (1)	0.2962 (2)	5.87 (6)
C1	0.3018 (3)	0.3636 (2)	0.4044 (2)	4.08 (5)
C2	0.5446 (3)	0.1577 (2)	0.3267 (2)	4.59 (6)
C3	0.0163 (3)	0.2913 (2)	0.0888 (2)	4.28 (6)
C4	0.1318 (4)	0.2410 (2)	0.0462 (2)	4.73 (6)
C5	-0.0357 (3)	0.3680 (1)	0.2540 (2)	3.67 (5)
C6	-0.0306 (3)	0.4375 (2)	0.2888 (2)	5.25 (6)
C7	-0.1496 (4)	0.4608 (2)	0.3421 (2)	6.25 (7)
C8	-0.2725 (3)	0.4156 (2)	0.3601 (2)	5.39 (7)
C9	-0.2762 (3)	0.3456 (2)	0.3273 (2)	5.29 (7)
C10	-0.1591 (3)	0.3214 (2)	0.2745 (2)	4.77 (6)
C11	0.2250 (3)	0.4131 (1)	0.1480 (2)	3.80 (5)
C12	0.3891 (3)	0.4167 (2)	0.1627 (2)	4.65 (6)
C13	0.4722 (4)	0.4762 (2)	0.1322 (2)	6.04 (8)
C14	0.3929 (4)	0.5326 (2)	0.0890 (2)	6.31 (8)
C15	0.2294 (4)	0.5302 (2)	0.0752 (2)	6.06 (8)
C16	0.1459 (4)	0.4704 (2)	0.1040 (2)	5.18 (7)
C17	0.4445 (5)	0.1744 (2)	0.0786 (3)	9.1 (1)
C18	0.5409 (5)	0.2414 (3)	0.0567 (4)	11.9 (1)
C19	0.1727 (6)	0.1055 (2)	0.1534 (3)	8.8 (1)
C20	0.0140 (7)	0.1124 (2)	0.1959 (3)	10.7 (1)

Table **A-6:** Crystallographic Data for $Ni(NCS)_2(Et_2PCH_2CH_2PPh_2)$

formula	$NiP_2S_2C_{20}H_{24}N_2$
crystal system	monoclinic
crystal color	yellow brown
fw	477.2
Fooo	992
a, Å	8.4008 (7)
b, Å	18.178 (2)
c, Å	15.1640 (14)
β, deg	93.803 (7)
V, $Å^3$; Z	2310.6 (4); 4
space group	$P2_1/n$
D_{calc}, g/ cm^3	1.372
μ, cm^{-1}	42.6
λ(Cu Kα), Å	1.54184
crystal size	0.05 x 0.18 x 0.30 mm
Temp, °C	24
2θ range, deg	2 - 75
no. of observed reflcns	3717
no. of unique reflcns	4738
no. of variables	245
Cutoff	$I > 3\sigma(I)$
R (obs. data)[a]	0.039
R_w[b]	0.054
GOF[c]	2.154
Max. Residual	0.47
Min. Residual	0.48
Max. Transmission, $eÅ^{-3}$	99.62
Min. Transmission, $eÅ^{-3}$	67.05
Average transmission, (%)	88.76
Extinction coef.	$4.2\ (2) \times 10^{-7}$

[a] $R = \Sigma(|F_o| - |F_c|)/\Sigma|F_o|$; [b] $R_w = \{\Sigma w(|F_o| - |F_c|)^2/\Sigma w(|F_o|^2\}^{1/2}$; $w = 4F_o^2[\sigma^2(I) + (0.02F_o^2)^2]^{-1}$. [c] Goodness of fit = $[\Sigma w\ (|F_o| - |F_c|)^2/(N_{obs} - N_{param})]^{1/2}$.

Data Collection and Refinement

difractometer	CAD4
scan method	ω/2θ

Table A-7.: Fractional atomic coordinates and equivalent isotropic displacement parameters (Å^2) for $Ni(NCS)_2(\eta^3\text{-}Ph_2PCH_2CH_2P(Et)CH_2\text{-}CH_2PPh_2)$.

$$B_{eq} = \left(\frac{8\pi^2}{3}\right)\sum_i \sum_j U_{ij} a_i^* a_j^* \mathbf{a}_i \cdot \mathbf{a}_j$$

atom	x	y	z	B_{eq}
Ni	0.1752 (2)	0.08042 (5)	0.26659 (6)	4.11 (3)
S1	-0.3394 (4)	0.0339 (2)	0.1308 (2)	10.7 (1)
S2	-0.0849 (3)	0.2314 (1)	0.4007 (1)	6.24 (6)
P1	0.2063 (3)	0.1588 (1)	0.1952 (1)	4.46 (5)
P2	0.4346 (3)	0.1080 (1)	0.3135 (1)	4.92 (5)
P3	0.2667 (3)	-0.01957(9)	0.2845 (1)	4.67 (5)
N1	-0.0411 (8)	0.0531 (3)	0.2174 (3)	4.9 (2)
N2	0.0382 (9)	0.1282 (3)	0.3333 (3)	5.5 (2)
C1	-0.166 (1)	0.0441 (4)	0.1821 (4)	4.9 (2)
C2	-0.014 (1)	0.1706 (3)	0.3604 (4)	4.4 (2)
C3	0.399 (1)	0.2077 (4)	0.2284 (4)	5.6 (2)
C4	0.541 (1)	0.1621 (4)	0.2607 (4)	5.9 (2)
C5	0.580 (1)	0.0375 (4)	0.3322 (5)	7.3 (3)
C6	0.507 (1)	-0.0197 (5)	0.2951 (5)	7.8 (3)
C7	0.251 (1)	0.1292 (4)	0.1176 (4)	5.4 (2)
C8	0.343 (2)	0.1674 (5)	0.0774 (5)	9.9 (3)
C9	0.375 (2)	0.1453 (6)	0.0178 (5)	12.0 (4)
C10	0.319 (2)	0.0849 (7)	-0.0033 (5)	10.4 (4)
C11	0.230 (1)	0.0474 (6)	0.0341 (5)	8.3 (3)
C12	0.198 (1)	0.0684 (5)	0.0948 (4)	6.6 (2)
C13	0.026 (1)	0.2169 (4)	0.1771 (4)	5.0 (2)
C14	-0.081 (1)	0.2185 (4)	0.1179 (5)	6.6 (3)
C15	-0.220 (1)	0.2635 (5)	0.1051 (5)	7.4 (3)
C16	-0.252 (1)	0.3043 (4)	0.1549 (5)	7.0 (3)
C17	-0.150 (1)	0.3017 (4)	0.2143 (5)	6.6 (2)
C18	-0.011 (1)	0.2597 (4)	0.2256 (4)	5.6 (2)
C19	0.442 (1)	0.1510 (5)	0.3913 (4)	6.7 (2)
C20	0.383 (1)	0.1125 (6)	0.4477 (5)	9.1 (3)
C21	0.196 (1)	-0.0589 (3)	0.3559 (4)	4.7 (2)
C22	0.275 (1)	-0.1165 (4)	0.3822 (4)	6.4 (2)
C23	0.215 (1)	-0.1424 (5)	0.4368 (4)	8.0 (3)
C24	0.083 (1)	-0.1149 (5)	0.4640 (5)	8.3 (3)
C25	0.005 (1)	-0.0586 (5)	0.4380 (5)	7.7 (3)
C26	0.061 (1)	-0.0315 (4)	0.3836 (4)	5.6 (2)
C27	0.201 (1)	-0.0763 (4)	0.2182 (4)	4.9 (2)

Table A-7 (cont.): Fractional atomic coordinates and equivalent isotropic displacement parameters ($Å^2$) for $Ni(NCS)_2(\eta^3\text{-}Ph_2PCH_2CH_2P(Et)CH_2\text{-}CH_2PPh_2)$

C28	0.305 (2)	-0.0867 (5)	0.1707 (5)	9.0 (3)
C29	0.248 (2)	-0.1255 (7)	0.1191 (6)	11.0 (4)
C30	0.087 (2)	-0.1559 (5)	0.1144 (5)	9.5 (3)
C31	-0.018 (1)	-0.1465 (5)	0.1612 (5)	8.3 (3)
C32	0.041 (1)	-0.1061 (4)	0.2136 (4)	6.5 (2)

Table A-8: Crystallographic Data for $Ni(NCS)_2(\eta^3\text{-}Ph_2PCH_2CH_2P(Et)\text{-}CH_2CH_2PPh_2)$

formula	$NiP_3S_2C_{32}H_{33}N_2$
crystal system	monoclinic
crystal color	Orange
fw	661.4
Fooo	1376
a, Å	7.602(2)
b, Å	20.599(2)
c, Å	20.712 (4)
β, deg	97.98 (1)
V, $Å^3$; Z	3212 (2); 4
space group	$P2_1/n$
D_{calc}, g/ cm^3	1.368
μ, cm^{-1}	36.8
λ(Cu Kα), Å	1.54184
crystal size	0.08 x 0.12 x 0.32 mm
Temp, °C	25
2θ range, deg	2 - 70
no. of observed reflcns	3417
no. of unique reflcns	5947
no. of variables	362
Cutoff	$I > 3\sigma(I)$
R (obs. data)[a]	0.081
R_W[b]	0.089
GOF[c]	3.230
Max. Residual, $eÅ^{-3}$	1.03
Min. Residual, $eÅ^{-3}$	-0.94
Max. Transmission, $eÅ^{-3}$	99.44
Min. Transmission, $eÅ^{-3}$	49.33
Average transmission (%)	62.73
Extinction coef.	4.2 (2) x 10^{-7}

[a] $R = \Sigma(|F_o| - |F_c|)/\Sigma|F_o|$; [b] $R_W = \{\Sigma w(|F_o| - |F_c|)^2/\Sigma w(|F_o|^2\}^{1/2}$; $w = 4F_o^2[\sigma^2(I) + (0.02F_o^2)^2]^{-1}$. [c] Goodness of fit = $[\Sigma w (|F_o| - |F_c|)^2/(N_{obs}\text{-}N_{param})]^{1/2}$.
Hydrogens were not refined

Data Collection and Refinement

difractometer	CAD4
scan method	ω/2θ

Table **A-9:** Fractional atomic coordinates and equivalent isotropic displacement parameters (Å^2) for dimethylammonium [hydrogen-μ-oxo-bis-{phenylphosphinate}].

$$Beq = \left(\frac{8\pi^2}{3}\right)\sum_i \sum_j U_{ij} a_i^* a_j^* \mathbf{a}_i \cdot \mathbf{a}_j$$

Atom	x	y	z	B*eq*
P1	0.82387(8)	0.02489(7)	0.000	3.69(2)
P2	0.82791(7)	-0.04507(8)	-0.07035(3)	3.91(2)
O1	0.7712(2)	-0.0132(2)	-0.03494(9)	4.49(5)
O2	0.8371(2)	0.1359(2)	0.00029(7)	4.97(7)
O3	0.9187(2)	-0.0383(2)	0.00457(7)	4.52(7)
O4	0.8536(2)	-0.1528(2)	-0.07042(7)	5.17(7)
O5	0.9141(2)	0.0291(2)	-0.07413(7)	4.65(7)
C1	0.7363(3)	-0.0163(3)	0.03192(8)	3.54(8)
C2	0.7012(3)	0.0485(3)	0.0566(1)	5.4(1)
C3	0.6443(4)	0.0116(5)	0.0842(1)	7.2(1)
C4	0.6206(4)	-0.0876(5)	0.0860(1)	7.7(2)
C5	0.6521(4)	-0.1517(4)	0.0608(1)	6.8(1)
C6	0.7109(3)	-0.1177(3)	0.0341(1)	4.7(1)
C7	0.7369(3)	-0.0136(3)	-0.10173(9)	3.97(9)
C8	0.7146(3)	-0.0807(3)	-0.1286(1)	5.0(1)
C9	0.6532(4)	-0.0494(5)	-0.1556(1)	7.0(1)
C10	0.6134(4)	0.0454(4)	-0.1563(1)	7.1(1)
C11	0.6319(4)	0.1092(4)	-0.1297(1)	6.5(1)
C12	0.6936(3)	0.0808(4)	-0.1026(1)	5.0(1)
N1A	0.9888(3)	0.2377(2)	-0.0340(1)	5.43(7)
C1A	1.0440(4)	0.3001(5)	-0.0087(1)	8.5(2)
C2A	0.9322(4)	0.2933(4)	-0.0600(1)	8.3(2)

Table **A-10:** Crystallographic data for dimethylammonium [hydrogen-μ-oxo-bis-{phenylphosphinate}].

formula	$C_{28}H_{38}N_2O_{10}P_4$
fw	686.5
Fooo	2880
a, Å	13.2771(12)
c, Å	38.664(3)
color	colorless
$Å^3$; Z	6815.7(12); 8
crystal system	tetragonal
space group	$I4_1cd$
D_{calc}, g/ cm^3	1.338
λ(Cu Kα), Å	1.54184
T °C	23
2θ range, deg	2 - 75
no. of unique data	1790
no. of data used	
no. of variables	
Cutoff	$I > 1\sigma(I)$
R (obs. data)[a]	0.0363
R_w[b]	0.0351
Max. Residual density, $eÅ^{-3}$	0.20
Min. Residual, $eÅ^{-3}$	-0.23
Extinction coef.	$5(1)x\ 10^{-8}$

[a] $R = \Sigma(|F_o| - |F_c|)/\Sigma|F_o|$; $R_W = \{\Sigma w(|F_o| - |F_c|)^2/\Sigma w(|F_o|^2\}^{1/2}$.
$w = 4F_o^2[\sigma^2(I) + (0.02F_o^2)^2]^{-1}$.

Data Collection and Refinement

difractometer	CAD4
scan method	ω/2θ
variable scan speed	0.92-3.30 deg. min^{-1}

Vita

Booker Washington Ochieng' Juma was born in Maseno, Kenya on July 7, 1962. He graduated from Maseno High School in Maseno, in November, 1981. In January of 1982 he joined Kenya Power and Lighting Co. Ltd as Technician Trainee and attended Kenya Power & Lighting Training School, Nairobi. In January of 1983 he attended Mombasa Polytechnic as an employee of the Kenya Power and Lighting Co where he graduated with Electrical Installation Technicians Certificate Part I in August 1983.

He then enrolled at the University of Nairobi in October of 1983 where he graduated with a Bachelor of Science (1^{st} Class Honors) degree in Chemistry in June, 1986. During his studies at the University of Nairobi he was awarded IAESTE scholarship to study water-based cellulose amines at Chalmers University and the Colloid Division of Berol Kemi AB, Gothenborg, Sweden in 1985.

In October of 1986, he joined Kenya Marine and Fisheries Research Institute as Assistant Research Officer until November,1987 when he joined The Chemistry Department of Moi University as Graduate Assistant on staff-development program. In August of 1988, he enrolled at Louisiana State University, U.S.A., to pursue his Doctor of Philosophy, where he is now a candidate for the degree of Doctor of Philosophy in the department of chemistry. He married Linda Adhiambo in December 1990 and has a son, Fayez "Thuon" Juma.

DOCTORAL EXAMINATION AND DISSERTATION REPORT

Candidate: Booker Washington Ochieng Juma

Major Field: Chemistry

Title of Dissertation: Synthesis, Isolation, Characterization and Homogeneous Catalytic Reactions of Racemic - and Meso-Metal Binucleating Tetraphospine Complexes

Approved:

Major Professor and Chairman

Dean of the Graduate School

EXAMINING COMMITTEE:

Date of Examination:

April 5, 1993